

Light Harvesting and Photoprotection in Cyanobacteria

Lijin Tian

Thesis committee

Promotor

Prof. dr. H. van Amerongen

Professor of Biophysics

Wageningen University

Other members

Prof. dr. ir. P.C. Struik Wageningen University

Dr. ing. J.W. Borst Wageningen University

Prof. dr. R. Croce VU Amsterdam, The Netherlands

Prof. dr. T. Renger Johannes Kepler Universität Linz,
Germany

This research was conducted under the auspices of the
Graduate School of Experimental Plant Sciences

Light Harvesting and Photoprotection in Cyanobacteria

Lijin Tian

Thesis

submitted in fulfillment of the requirements for the

degree of doctor

at Wageningen University

by the authority of the Rector Magnificus

Prof. Dr M.J. Kropff,

in the presence of the

Thesis Committee appointed by the Academic

Board

to be defended in public

on Wednesday 8 May 2013

at 4 p.m. in the Aula.

© Lijin Tian

Light Harvesting and Photoprotection in Cyanobacteria 168
pages.

PhD thesis, Wageningen University, Wageningen, NL (© 2013)

With references, with summaries in Dutch and English

ISBN 978-94-6173-529-4

The research described in this thesis was financially supported by Graduate School Experimental Plant Sciences (EPS) and the Laboratory of Biophysics.

Financial support from Wageningen University for printing this thesis is gratefully acknowledged

CONTENTS

CHAPTER 1	7
INTRODUCTION	7
CHAPTER 2	35
PROBING THE PICOSECOND KINETICS OF THE PHOTOSYSTEM II CORE COMPLEX IN VIVO	35
CHAPTER 3	61
SITE, RATE AND MECHANISM OF PHOTOPROTECTIVE QUENCHING IN CYANOBACTERIA	61
CHAPTER 4	97
PICOSECOND KINETICS OF LIGHT HARVESTING AND PHOTOPROTECTIVE QUENCHING IN WT AND MUTANT PHYCOBILISOMES ISOLATED FROM THE CYANOBACTERIUM <i>SYNECHOCYSTIS</i> PCC 6803	97
CHAPTER 5	127
LIGHT HARVESTING AND BLUE-GREEN LIGHT INDUCED NON- PHOTOCHEMICAL QUENCHING IN TWO DIFFERENT C-PHYCOCYANIN MUTANTS OF <i>SYNECHOCYSTIS</i> PCC 6803	127
CHAPTER 6	149
SUMMARY AND DISCUSSION	149
PUBLICATIONS	163
ACKNOWLEDGEMENTS.....	165
CURRICULUM VITAE	167

Chapter 1

Introduction

The purpose of this thesis is to obtain an in-depth understanding of the early steps of photosynthesis of cyanobacteria at the molecular level *in vivo* by using picosecond time-resolved fluorescence techniques. These steps include sunlight energy-harvesting process, energy trapping and nonphotochemical quenching (NPQ). More precisely, one NPQ process, called blue-green light-induced NPQ, has been studied intensively, thereby becoming the focus of this thesis.

1.1 Photosynthesis

Photosynthesis is the process by which sunlight energy is captured and converted into chemical energy (see for instance ^{1,2,3}) by many living organisms. It is responsible for feeding nearly all life on Earth, providing oxygen and most of the natural energy. Because of its great potential in the development of renewable energy sources it is also regarded as a good candidate to partly solve the global energy problem and to develop a green sustainable life^{4,5}. Sunlight is an abundant and inexhaustible source of energy; to be more precise, the amount of sunlight energy reaching the Earth within one hour is more or less equal to the global energy consumption of 2002. A theoretical upper limit of ~10 %, in the sense of overall sunlight energy conversion efficiency, was estimated^{6,7,8}, but in reality it is far lower than that. For example, crops growing in the field, have an efficiency of biomass production lower than 1%^{9,10}, while algae can have a higher efficiency when growing in the lab, ~5%¹¹. Therefore, there still seems to be room for improvement referring to the overall solar energy conversion. To better utilize the energy from sunlight, we must understand the natural photosynthetic process at the molecular level, elucidate the bottlenecks of the low-efficiency processes of the natural systems and then hopefully remove these bottlenecks in existing systems or develop completely new artificial systems.

In this section, I will briefly introduce how photosynthesis works. Figure 1.1 illustrates schematically the locations of the main machineries of oxygenic photosynthesis in the thylakoid membrane and the electron and proton flows. All

Introduction

complexes involved, apart from the ATP synthase, function in series to transfer electrons from water to NADPH, and pump protons from the stroma to the lumen. The protons move back to the stroma via the ATP synthase, thereby producing ATP.

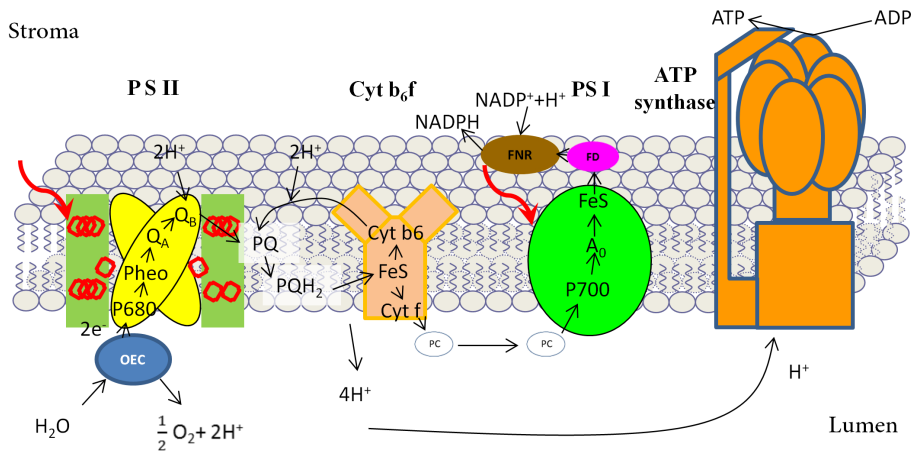


Figure 1.1: Schematic diagram of the electron transfer pathway in oxygenic photosynthesis. Simplified main photosynthetic complexes, including Photosystem II (PSII), Photosystem I (PSI), Cytochrome (Cyt b_6f), ATP synthase, the Oxygen evolving complex (OEC), Plastocyanin (PC), Ferredoxin (FD) and Ferredoxin-NADP reductase (FNR) are shown.

In general, photosynthesis can be separated into two stages, the light reactions and the dark reactions. In the light reactions of photosynthesis, as mainly described in Figure 1.1, firstly, sunlight is captured by the pigment-proteins (see section 1.2) and funnelled to the reaction centers (RCs) of PSI and PSII, where charge separation (CS) takes place. Secondly, in PSII RCs, after CS, the electron is rapidly transferred away via an electron transfer chain as shown in Figure 1.1. Meanwhile, electrons are extracted from water, which takes place in the OEC. In this process, both O_2 and protons are produced, the former one is released as a by-product, and the latter ones are accumulating on the luminal side thereby contributing to a proton gradient between the stroma and lumen that drives the ATP synthase to synthesize ATP. The electron from PSII re-reduces the primary donor of the PSI RC which is continuously being oxidised due to the light-driven CS in PSI. The electrons that are released by the PSI RC eventually are used to reduce

NQDP⁺ into NADPH. In the dark reactions of photosynthesis, ATP and NADPH are further used to reduce CO₂ into sugars via the so-called Calvin cycle¹².

In addition to photosynthesis, organisms also need the reverse process, respiration, in which sugar is converted into CO₂ and water and energy is released to support other life activities¹³.

1.2 Cyanobacteria

Cyanobacteria, often called “blue-green algae”, are oxygenic photosynthetic prokaryotes (for details see the book of Bryant D.A. 1994¹⁴), generally existing anywhere where there is water, ranging from hot springs to polar environments¹⁵. The oldest known fossils of cyanobacteria, ~3.5 billion years old, are from Archaean rocks of Western Australia. Actually, cyanobacteria probably have participated and contributed to the formation of the earth as we know it now, by participating in the creation of an oxygen-rich atmosphere, the formation of rocks and also most of the oterozoic oil deposits. Besides, some cyanobacteria can fix nitrogen from the air, which also has become a broad and important research field. More information about their evolution and the biochemistry and molecular biology of cyanobacteria is provided in the following books: (the Ecology of Cyanobacteria: their Diversity in time and space¹⁶; the Molecular Biology of Cyanobacteria¹⁴; The Cyanobacteria: Molecular Biology, Genomics, and Evolution¹⁷).

Studying photosynthetic behaviour of cyanobacteria is of great importance, not only because it extends our understanding of the photosynthesis in other species, such as plants, green algae and diatoms, but also because cyanobacteria are believed to be good candidates for producing biofuels, since they are easily growing, grow faster in general than plants and they are relatively easy to be genetically engineered as compared to algae^{18,19}.

As well as in other photosynthetic organisms, photosynthesis in cyanobacteria relies on pigment-proteins complexes, which are employed to capture light and perform charge separation. At the same time, photosynthesis needs effective photoprotection mechanisms. In the following paragraphs I will introduce the main photosynthetic complexes, and explain how they harvest light, why they

need to protect themselves from high light and how they manage to do so from a molecular level point of view.

1.2.1 Main photosynthetic complexes in *Synechocystis* sp PCC 6803

Like all other photosynthetic organisms, cyanobacteria rely on pigment-proteins; *Synechocystis* sp PCC 6803 (hereafter called *Synechocystis*) serves as a model system, similar to *Arabidopsis* in plant research. Its genome has been fully determined in 1996²⁰ and since then many mutants have been constructed, which greatly facilitates our studies.

Synechocystis contains a number of photosynthetic protein complexes. Besides the membrane-embedded complexes listed in Figure 1.1, namely photosystem I (PSI), photosystem II (PSII), the cytochrome b_6f complex, and the ATP synthase²¹, it also contains water-soluble antenna complexes, called phycobilisomes (PBs). All complexes work together to ultimately transform sunlight energy into chemical energy.

1.2.1.1 Photosystems

PSI and PSII are obviously the two most important photosynthetic machineries. They work in series to perform photosynthesis as discussed above.

The two photosystems are both large pigment-protein complexes. The PSI core complex from thermophilic cyanobacterium, of which the structure was determined at 2.5 Å by Jordan et al. and Fromme et al. in 2001^{22,23}, contains 12 protein subunits and 127 cofactors. In total, there are 96 chlorophylls (Chls), and 22 β -carotenoids (Cars) per P700 (see the structural model of PSI in Figure 1.2).

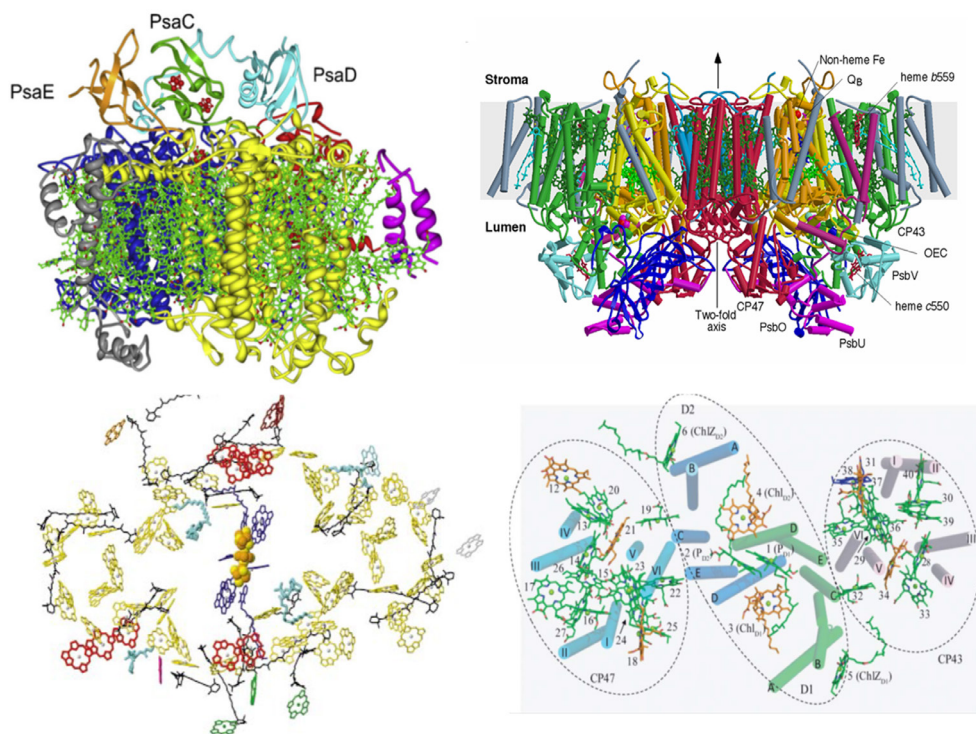


Figure 1.2: Protein structure. PSI monomer (side view from within the membrane, top left), PSII dimer (side view, top right), and their pigment arrangements (PSI, bottom left and PSII, bottom right). Figures are adapted from ref^{22,24,25,26} with permissions.

The PSII core complex contains ~35 Chls and ~12 Cars per monomer, and its structure has been determined at 1.9 Å by Umena et al²⁶(see Figure 1.2). The PSII core complex contains the reaction center (RC) associated with two Chl-binding polypeptides, CP43 and CP47, that function as core antennae²⁷. The PSII RC, consisting of the D1 and D2 polypeptides, cytochrome b559, and some other proteins encoded by the photosystem b (Psb) genes, binds six Chls, two pheophytin molecules and several other cofactors.

Note that both the structure and function of PSI and PSII core complexes are thought to be very similar for cyanobacteria and plant species with minor differences on the stromal side²⁸⁻³¹. In general, the photosystems in cyanobacteria can be considered as the core systems of the two photosystems in plants.

1.2.1.2 Phycobilisome

The use of phycobilisomes (PBs) as light-harvesting system for PSI and PSII, makes the cyanobacteria very different from plants and green algae, which only use membrane-embedded antennae. PB is a giant water-soluble protein-complex, associated to the photosystems at the cytoplasmic side of the thylakoid membrane³². Its structure was summarized in detail in several reviews³³⁻³⁵ (see Figure 1.3). In *Synechocystis* it is composed of phycocyanobilin-containing subunits, c_Phycocyanin (c_PC) rods and allophycocyanin (APC) cores, and of non-pigmented polypeptides that have been named linkers and connect the different subunits to each other. Although an X-ray structure of the whole PB is not available yet, the structures of most of its subunits have been determined^{36,37} (see Figure 1.3).

Both C_PC and APC contain phycocyanobilins that extend the wavelength range of light harvesting for the photosystems, see section 1.2.2. More details about their compositions and the excitation energy transfer (EET) processes will be presented in Chapter 4.

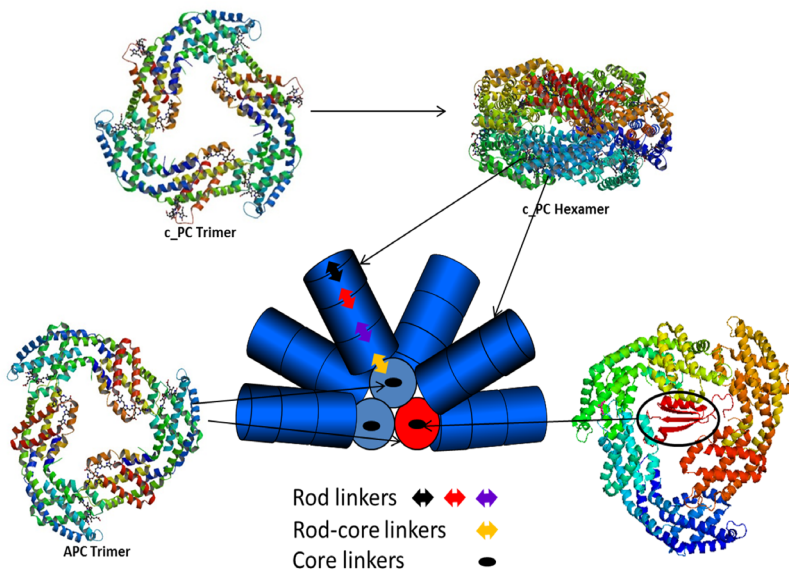


Figure 1.3: A cartoon of the whole phycobilisome of *Synechocystis* (center) and X-ray structures of the c_phycocyanin trimer (top left_PDB: 3018). C_phycocyanin hexamer

(top right, PDB: 1I7Y); allophycocyanin trimer (low left, PDB: 3DBJ); and allophycocyanin trimer with core linkers (low right, PDB: 1B33).

Note that the main function of a PB is harvesting light but it also plays a very important role in photoprotection of cyanobacteria and serves as a nutrient reservoir when needed. Moreover, it is interesting that PBs can be truncated in different light conditions for optimising light harvesting and the capacities of the photosystems.^{34,38,39}

1.2.1.3 Other important photosynthetic complexes:

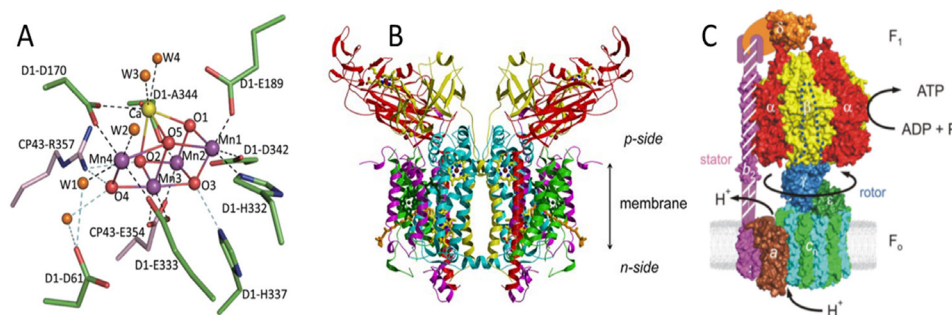


Figure 1.4: three photosynthetic complexes. A) The structure of the OEC, adapted from Umena et al 2011²⁵, B) Cytochrome b₆, adapted from Baniulis et al 2009⁴⁰. C) A Model of Escherichia coli ATP synthase -adapted from Joachim Weber et al 2007⁴¹.

The Oxygen-Evolving Complex

The Oxygen-evolving complex (OEC) is the complex where the oxidation of water into molecular oxygen and protons takes place; it contains a Mn₄Ca cluster (for a review see ^{42,43}). Its structure with atomic resolution was recently obtained by Umina et al. (Figure 1.4). However, the catalytic mechanism is still elusive.

ATP synthase

As its name suggests, ATP synthase can synthesize ATP from ADP and inorganic phosphate (Pi) driven by the transmembrane proton gradient³⁹. The ATP synthases of all species are similarly structured, comprising two major

components, F_0 and F_1 ^{44,45}. See Figure 1.4 for a cartoon model of ATP synthase that is taken from Ref.⁴⁶.

Cytochrome b_6f

The cytochrome b_6f complex functions as an interchange station in oxygenic photosynthesis to facilitate the electron transfer from PSII to PSI in the linear electron transfer pathway. The structure of cytochrome b_6f of *Mastigocladus laminosus* is shown in Figure 1.4⁴⁷. Interestingly, each cytochrome b_6f monomer contains one chlorophyll a and one β -carotene, but the functional role of these pigments is still under discussion⁴⁸.

All of the complexes discussed above are indispensable for the photosynthesis process. However, only two photosystems, together with the PBs, are covered in detail in this thesis. Note that to build a systems biology model for photosynthetic processes in cyanobacteria, other complexes should be considered as well in the future⁴⁹.

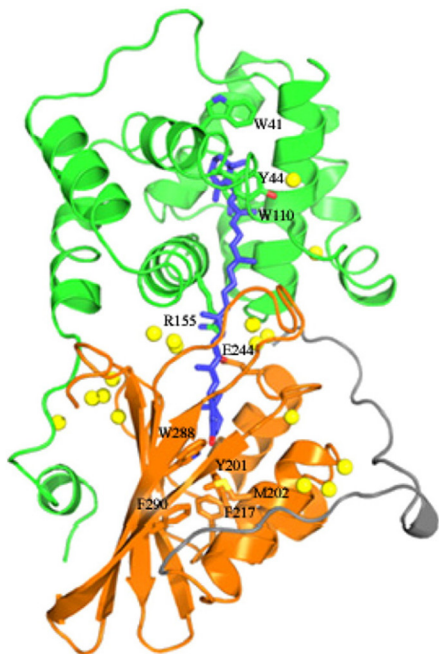


Figure 1.5: protein structure of OCP in *Synechocystis*, taken from ref⁵⁶

1.2.1.4 Orange Carotenoid Protein /Fluorescence Recovery Protein

We now turn to a special carotenoid protein, called orange carotenoid protein (OCP). In photosynthetic organisms, carotenoid proteins are well-known for their protective roles in balancing the energy consumption for photosynthesis with the energy released through heat dissipation via a process called non-photochemical quenching (NPQ)⁵⁰. In cyanobacteria, OCP (encoded by gene Slr1963 in *Synechocystis*), is a 35-kDa water-

soluble protein that is essential for triggering the blue-green light induced NPQ, and most likely functions as a quencher molecule⁵¹.

OCP was first identified in cyanobacteria in 1981⁵²; later it was found that it actually exists in most of the cyanobacteria. For quite a long time, the biological function of OCP was not known until the discovery of blue-green light induced NPQ, see section 1.2.4. Its structure has been determined and is shown in Figure 1.5^{53,54}. It binds a single pigment, the carotenoid 3'-hydroxyechinenone (hECN) of which the optical properties will be introduced in section 1.2.2.

The Fluorescence Recovery Protein (FRP), encoded by gene Slr1964 in *Synechocystis*, also plays a key role in the blue-green light induced NPQ of cyanobacteria. It can dramatically accelerate the recovery speed of the cells from their quenched state. The molecular weight of FRP is 15 kDa, while its crystal structure is unknown yet⁵⁵.

1.2.2 Pigments and their electronic transitions:

Synechocystis, like most of the cyanobacteria, contains chlorophylls *a*, phycocyanobilins and carotenoids as the main photosynthetic pigments. However, there are also cyanobacteria species that are able to produce chlorophyll *d* and chlorophyll *f*, which can catch near-IR light as well^{57,58}.

In a general way, the absorption and emission of light by a pigment can be illustrated by the Jablonski diagram, as shown in Figure 1.6. However, since there are other ways of relaxation especially when there are other pigments present or when the excitation can lead to a chemical reaction, we have added one extra depopulation pathway indicated by the blue arrow and lines from the S_1 state. Similarly, energy transfer is also possible from its triplet state, for instance, to molecular oxygen, which creates singlet oxygen, and via triplet-triplet Dexter energy transfer (see section 1.2.3), etc. (see also Figure 1.6).

Introduction

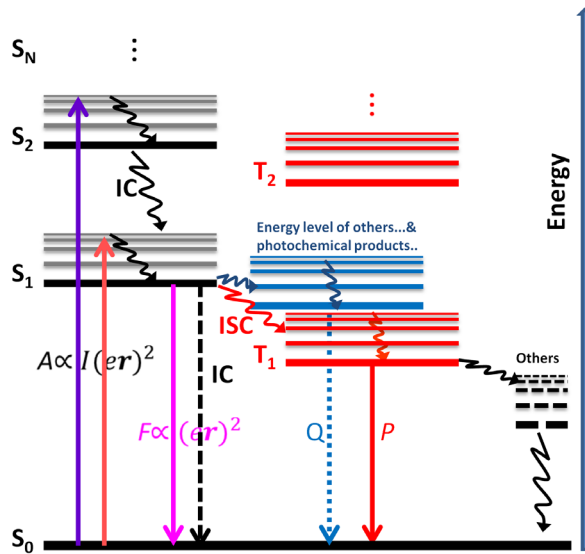
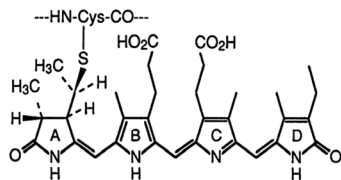
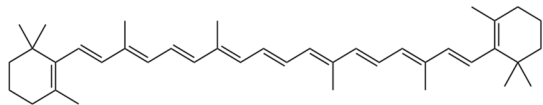


Figure 1.6: Jablonski diagram of the energy levels of a pigment and the possible transitions between them. er is the transition dipole moment of the pigment and I is the intensity of the excitation beam. Electron population on S_1 can either be transferred further to the triplet state T_1 (red lines) or to the blue lines that represent the energy levels of other pigments, from which the excitation might be used to drive charge separation of photosynthesis or simply

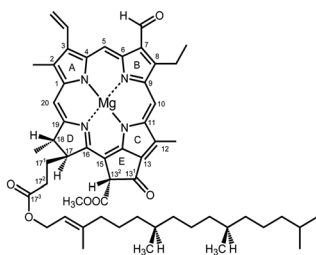
be dissipated as heat via NPQ. Black dash lines on the right indicate the low-lying states of the T_1 -quenchers such as O_2 or carotenoids.



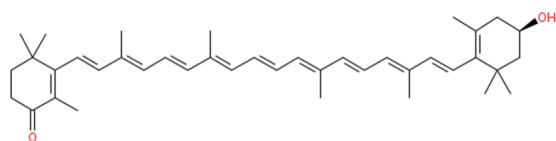
Peptide-linked phycocyanobilin



β -carotene



Chlorophyll a



3'-Hydroxyechinenone

Figure 1.7: Chemical structures of the photosynthetic pigments in *Synechocystis*.

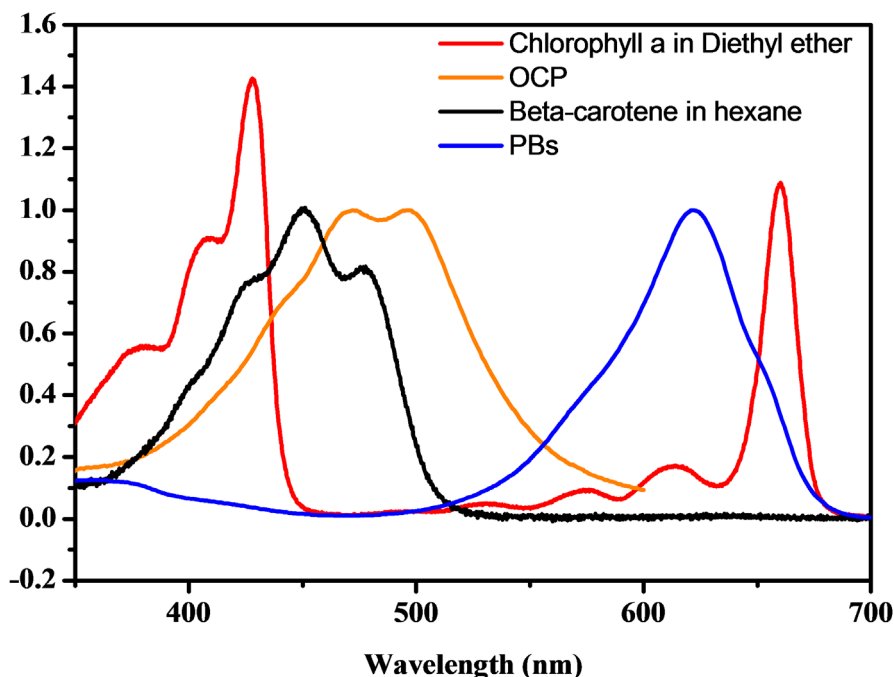


Figure 1.8: Absorption spectra of the pigments Chl *a*, β -carotene, and of OCP and the PB of *Synechocystis*.

Chlorophyll *a* is the most abundant pigment within photosynthetic organisms. Its chemical structure is shown in Figure 1.7, consisting of a N-ring with a Mg center, side chains, and a hydrocarbon tail. The absorption spectrum of Chl *a* in diethyl ether is shown in Figure 1.8, which exhibits characteristic absorption bands of metalloporphyrins, namely, Soret transition bands (300-450 nm) and Q bands (500-700 nm). These bands can be attributed to several $S_0 \rightarrow S_2$ and $S_0 \rightarrow S_1$ transitions, respectively.

Phycocyanobilin is used as a second kind of pigment that harvests light between 550 nm and 670 nm, which greatly enhances the wavelength range for light absorption and thus broadens the absorption cross section of the photosystems. As shown in Figure 1.7, phycocyanobilin has an open-chain tetrapyrrole structure, which is flexible, leading to different spectral properties. Moreover, its spectral properties depend on the protein environment as well⁵⁹, therefore, this group of

pigments can show different energy levels in C_PC and APC, the subunits of PBs. In C_PC, the central absorption wavelength is ~ 590 nm, while it is 650 nm for APC, and even longer (around 670 nm) for low-energy species in APC (see Figure 1.3 and chapter 4 in this thesis for details). This “funnel” shape design of the PBs greatly increases the EET efficiency, which is over 90%³⁴.

β -carotene commonly exists in PSI and PSII of plants, algae and cyanobacteria. The functions of β -carotene include light harvesting in the 300-500 nm range and photoprotection (*vide infra*). Its structure, shown in Figure 1.7, is characterized by a linear polyene chain with 11 conjugated double bonds. The $S_0 \rightarrow S_1$ transition of carotenoid is optically forbidden for single photon excitation, therefore, only a broad absorption peak of $S_0 \rightarrow S_2$ can be observed. Hardly any fluorescence can be detected of carotenoids, since the excitations in S_2 rapidly relax to S_1 and the $S_1 \rightarrow S_0$ transition is optically forbidden. Although the $S_1 \rightarrow S_0$ transition is forbidden, the lifetime of S_1 is extremely short due to fast non-radiative decay. The lifetime of S_1 is determined by the conjugation length of carotenoids and varies from 300 ps to several ps (for more details see e.g. Polivka and Sundstrom 2004⁵⁰).

OCP contains the carotenoid hECN, of which the structure is very similar to that of β -carotene (see Figure 1.7). When compared to β -carotene, hECN contains one carbonyl group and one hydroxyl group extra at each terminus. The absorption of OCP mainly covers the blue-green region around 500 nm (Figure 1.8). Interestingly, in cyanobacteria OCP can be converted into its active-red form OCP^r from its inactive-orange form OCP^o during the NPQ process⁵⁷. Spectral properties of OCP were first studied by Tomas et al in 2005⁶¹, and two S_1 /ICT states with lifetime of 0.9 ps and 3.3 ps were reported, which later were assigned to OCP^o and OCP^r , respectively, based on the near-IR transient absorption results in ref ⁶². The S_1 energy levels of OCP^o and OCP^r were determined in ref ⁶² as well, namely, ~ 14700 cm^{-1} in the former, but ~ 650 cm^{-1} lower in the latter one. Berera et al in 2012⁶³ have studied OCP in both forms (i.e. OCP^o and OCP^r) using pump-probe spectroscopy. They have reported that the ICT character of the excited state is more pronounced in OCP^r than in OCP^o . This might be related to its potential role as a quencher in the blue-green light induced quenching process.

1.2.3 Interaction Mechanisms between Pigments: Energy transfer and charge separation

In this paragraph I will discuss very briefly a few types of interactions between chromophores that may apply to photosynthetic pigment-protein complexes, such as Förster-Dexter energy transfer, exciton coupling and charge separation. These processes are happening all the time in photosynthesis and lie at the basis of the model-based data analysis (see section 1.3), although neither of them is directly studied in this work they underlie the observed picosecond fluorescence kinetics.

When considering two separated chromophores, various processes can take place upon excitation. Of course, in the extreme case that the chromophores are so well separated that there is no interaction between them, the excited molecule just relaxes to its own ground state. However, under some conditions, the chromophores can influence each other, which may correspond to different types of interactions. Here we use the simplest system (“dimer”), which is also extensively illustrated in the book of van Amerongen et al.³, to illustrate the possible interactions that can take place.

1) When the coupling strength between two pigments (V_{DA}) is dominated by Coulombic interaction and when this interaction is much smaller than the spectral broadening (homogenous and inhomogeneous), it can be treated as a perturbation. In this case, we say that the excitation is localized on one chromophore and energy transfer or excitation hopping from one chromophore to the other can be described by the Förster equation. Use is made of Fermi’s golden rule (second-order perturbation theory), and the transfer rate is given as a function of frequency (ν) by:

$$k_{DA} = C_1 \cdot |V_{DA}|^2 \cdot k_r^D \cdot \int \frac{\varepsilon_A(\nu) \cdot f_D(\nu)}{\nu^4} d\nu \quad (1.1)$$

where the integral reflects the overlap between donor emission ($f_D(\nu)$) and acceptor absorption ($\varepsilon_A(\nu)$) as presented as molar extinction coefficient. k_r^D is proportional to the square of the transition dipole moments of the donor (μ_D)⁶⁴. It is used here to normalize the fluorescence spectrum of the donor and to facilitate the calculation. In the dipole-dipole approximation,

$$V_{DA} = \frac{C_2 \cdot \kappa}{R^3} \quad (1.2)$$

where $\kappa = (\boldsymbol{\mu}_D \cdot \boldsymbol{\mu}_A) - 3(\boldsymbol{\mu}_D \cdot \mathbf{R})(\boldsymbol{\mu}_A \cdot \mathbf{R})$, $\boldsymbol{\mu}_A$ is the transition dipole moments of acceptor, and \mathbf{R} is the vector from the center of the donor to the center of the acceptor. Thus one obtains the famous Förster equation:

$$k_{DA} = C_3 \cdot \frac{k_r^D}{n^4} \cdot \frac{\kappa^2}{R^6} \cdot \int \frac{\varepsilon_A(\nu) \cdot f_D(\nu)}{\nu^4} d\nu \quad (1.3)$$

where n is the refractive index and C_3 together with C_1 and C_2 shown above are different constants, for details, I refer to the book of van Amerongen et al.³

2) When two chromophores approach each other very closely, we also need to include higher order terms of the multipole transition moments and also the exchange effect that can take place in case of overlapping molecular orbitals should be taken into account^{3, 65,66}. The transfer rate constant for the Dexter exchange mechanism, k_{DA} , is given by:

$$k_{DA} = K \cdot J \cdot \exp\left(\frac{-2R_{DA}}{L}\right) \quad (1.4)$$

where R_{DA} is the distance between donor (D) and acceptor (A), K is an experimental factor, L is the sum of van der Waals Radius of D and A, and J is the normalized spectral overlap integral. This mechanism is important for triplet transfer but can in most cases be ignored for singlet transfer.

3) When the coupling between the two interacting molecules becomes strong, i.e. the coupling strength is comparable to or larger than the spectral broadening, the molecules start to behave like one single molecule with two different excited energy levels and the corresponding transition dipole moments are linear combinations of the original ones. A few examples are shown in Figure 1.9. In A), the two dipole moments of the individual chromophores are oriented in a sandwich manner. For the transition to the highest energy state (highest exciton level) the transition dipole moment is a weighted sum of the parallel individual transition dipole moments, leading to a doubling of the dipole strength. The transition dipole strength corresponding to the lowest exciton level scales with the difference between the individual dipole moments and becomes zero; therefore, the transition to the lowest exciton state is forbidden in this particular case. In contrast, in C) the two dipole moments are oriented in a head-to-tail

manner, and the situation is reversed. The allowed transition is now the one to the lowest exciton state. Strictly speaking this description is only correct when the coupling strength is much larger than the spectral broadening; when the broadening is comparable, the forbidden transition becomes partly allowed (for details see van Amerongen et al 2000³).

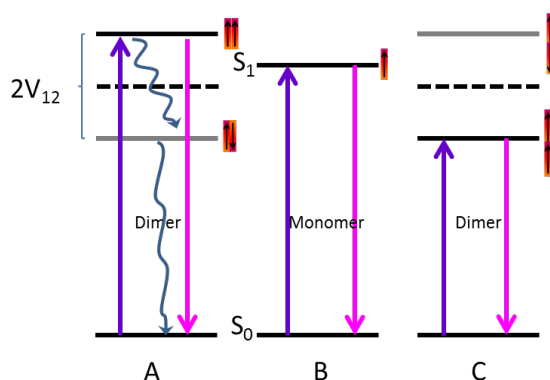


Figure 1.9: Energy levels of excitonic coupled dimer. A) a dimer in sandwich manner B) a monomer C) a “head to tail” dimer.

The excitations are not localized anymore on individual chromophores and the relaxation of an exciton is often treated in the literature by Bloch-Redfield

theory or modified Redfield theory⁶⁷. Other approaches for solving the quantum (coherence) dynamics of the excitations also exist, like the path integral approach⁶⁸, time-dependent self-consistent field approximation (TDSCF)⁶⁹, and so on. Note that an acceptable general model that can describe all conditions (weak, intermediate and strong coupling, and coupling between exciton and environment) still needs to be developed (see for instance refs⁷⁰⁻⁷²).

4) When two molecules interact with each other with one being in the excited state, also electron transfer between them can take place. The well-known Marcus nonadiabatic theory is often employed to determine the electron transfer rate:

$$k_{DA} = \frac{2\pi}{\hbar} \cdot |V_{DA}|^2 \cdot \frac{1}{(4\pi\lambda RT)^{\frac{1}{2}}} \cdot \exp\left(\frac{-(\Delta G + \lambda)^2}{4\pi RT}\right) \quad (1.5)$$

Here V_{DA} is the electronic coupling, λ is the reorganization energy and ΔG is the free energy difference between states before and after electron transfer.

Photosynthetic complexes do not just contain tens to hundreds of randomly packed pigments, but they can be considered as highly efficient pieces of equipment in a well-organized superstructure. They work together to harvest

sunlight and perform photosynthesis with high efficiency. It still remains a mystery how photosynthetic cells manage to manipulate these complexes precisely although little by little pieces of this mystery are being revealed. Studies that have been performed over the past decades have led to theoretical descriptions of the processes involved and have to a large extent explained the high efficiency within single complexes. For instance, for isolated complexes of *Synechocystis* PCC 6803, quantum coherence was reported to occur, both in C_PC and APC^{73,74} and most likely within part of the pigment-protein subunits excitations are delocalized, while between subunits, the energy transfer is dominated by Förster energy transfer. Somehow the cells are probably taking advantage of such a design⁷⁵.

1.2.4 NPQ in cyanobacteria

Sunlight is a relatively dilute light energy source¹, and therefore plants, algae and cyanobacteria must be very efficient in capturing light and transferring energy to its reaction centers. On the other hand, sunlight intensity can fluctuate a lot, even in a short period of time while it changes continuously during the day. In high light intensity, the absorbed light energy may exceed the capacity of the RCs, and thus generate oxygen species that are harmful to the cell. To diminish the amount of photodamage, photosynthetic organisms have evolved photoprotective mechanisms that dissipate excess harvested energy into harmless heat before it reaches the RCs. The resulting quenching of excited states is in general called non-photochemical quenching (NPQ).

1.2.4.1 A short summary of blue-green light induced NPQ in cyanobacteria

For a long time it was assumed that cyanobacteria were not capable of performing NPQ until a new NPQ mechanism was reported in 2000 by El Bissati et al.⁷⁶. The action spectrum of this light-induced quenching covers mainly the blue-green wavelength region of 450–550 nm, and the spectral shape suggests that this NPQ is triggered by a carotenoid⁷⁷. Later, Wilson et al demonstrated that OCP (see section 1.2.1 of this chapter) is responsible for this protection process, and that during NPQ the fluorescence of PBs is strongly quenched. But the site of quenching was not known yet, although in that work C_PC rods were excluded as

potential quenching sites by studying several mutant cells. Only recently, we demonstrated that APC₆₆₀ is the species that is directly quenched and not APC₆₈₀, both *in vivo* and *in vitro* (see chapters 2 & 3). This conclusion is strongly supported by later work on isolated PBs from APC mutants, missing specific low-energy pigments (APC₆₈₀), and it was confirmed that ApcD, ApcF and ApcE, three special subunits of APC core complex that are termed as APC₆₈₀ (see chapter 4), are not required for NPQ⁷⁸.

1.2.4.2 Physical models of NPQ

The molecular mechanisms underlying the NPQ protection of plants are still being discussed. Nevertheless, several models have been used successfully to interpret how excess excited state energy of Chl *a* can be quenched. This has recently been summarized by Polivka et al in 2012⁶² and schematically this is given in Figure 1.10.

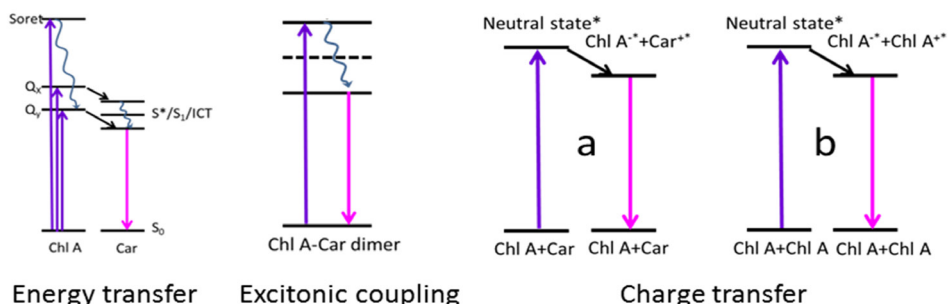


Figure 1.10: possible physical mechanisms responsible for NPQ in plants.

In one mechanism, proposed to occur in NPQ of plants by Ruban et al.⁷⁹, NPQ is caused by energy transfer from Chls to the carotenoid S₁ state. In that work, Ruban et al. have studied light-harvesting complex II (LHCII) both in the quenched and unquenched state.

A second possible quenching mechanism involves carotenoid-Chl exciton coupling^{80,81}. The authors in Ref 80 have pointed out that excitonic mixing of a Car S₁ and a Chl Q_y state can lead to drastic quenching of the fluorescence of Chl, while in ref 81, strong experimental evidence was given for the existence of this mechanism in plants and the close link with NPQ *in vivo*.

A third mechanism, as proposed by Holt et al.⁸², involves electron transfer from Chl to zeaxanthin (a carotenoid). Charge transfer within the formed Chl-Zea excited state results in a Chl-*a* anion and a carotenoid cation. This process takes places on a time scale of the order of 0.1 to 1 ps, while Zea+* is being quenched further in ~150 ps. This charge transfer mechanism was initially predicted by Dreuw et al in 2003 by means of quantum chemical methods⁸³.

A fourth mechanism is similar to the third one except that the interacting carotenoid molecule is replaced by another Chl. This idea is triggered by the existence of long-wavelength fluorescence in LHClI oligomers⁸⁴. In 2009, Müller et al. have suggested that a Chl/Chl charge transfer state serves as a pathway for Chl excited-state quenching. Clearly, this quenching mechanism is independent of carotenoids⁸⁵.

In principle, similar mechanisms might also apply to NPQ in cyanobacteria, replacing the Chls by allophycocyan bilins⁸⁶. A detailed analysis of the possible NPQ mechanisms in cyanobacteria is given in Chapter 3.

1.2.4.3 Other NPQ mechanisms evolved by cyanobacteria

Also other NPQ mechanisms have evolved in cyanobacteria, both for short-term and longer-term protection. Many short-term protection mechanisms exist, like HLIPs (high-light-inducible proteins)-related protection⁸⁷ or scytonemin-related protection against uv-B light.⁸⁸; In addition, state transitions, a mechanism that balances the light absorption by PSI and PSII is believed to be another important protection strategy for cyanobacteria⁸⁹. More recently, Zhang et al. have reported a hitherto unknown protection mechanism that is related to the *flv4-flv2* operon⁹⁰. So far, all mechanisms mentioned above are related to short-term protection, which typically happen in a few seconds to minutes. However, there are also protection mechanisms that start to function after relatively longer periods of time, say hours or even days. One is CP43'-related. Some freshwater cyanobacteria can overexpress the gene *isiA* in low-iron stress conditions, thereby producing a chlorophyll-binding antenna system around photosystem I, which is called CP43'^{91,92}. A protection mechanism including the formation of large aggregates of CP43' is reported in ref⁹³ and was studied by Berera et al in 2009⁹⁴.

Some other examples of long-term protection are: the adjustable stoichiometries of photosynthetic complexes^{95,96}, the yes/no expression of certain pigment- (C_Phycoerythrin) containing proteins, and the regulation of size and number of light-harvesting antennae⁹⁷ and so on. All these protection mechanisms will not be addressed in this thesis and we will focus on the OCP-related form of NPQ.

1.3 Experimental methods used in this work

The light-harvesting process in photosynthesis is competing with other relaxation pathways, like fluorescence. Therefore, to maintain a high efficiency, energy transfer has to be fast: It is not surprising that capturing of sunlight energy by photosynthetic complexes, transfer of the energy to the reaction centers, and subsequent charge separation take only a few hundreds of picoseconds (note that light can only travel a few centimeters in such a short period of time). To study these extremely fast processes, one needs time-resolved spectroscopy with at least picosecond time resolution and compatible data analysis methods.

1.3.1 Time-resolved fluorescence

One way to gain information about the dynamics of relaxation of excited pigments is to perform time-resolved fluorescence measurements, in which fluorescence is simply recorded as a function of time after excitation by a short light (laser) pulse. This is the method of choice for the present study. Many other techniques to study the time-resolved kinetics exist, such as transient absorption spectroscopy, photon-echo spectroscopy, etc.

Compared to other techniques, a big advantage of time-resolved fluorescence is that only low-intensity laser pulses are needed, which makes the technique very suitable for studying large biological systems *in vivo*, even intact cells of cyanobacteria.

There are several ways to perform time-resolved fluorescence measurements. The most often used technique is called Time Correlated Single Photon Counting (TCSPC) (see Lakowicz⁶⁴). However, the streak-camera fluorescence detection technique is becoming more and more popular due to several advantages as compared to TCSPC. The main advantage is the ability to measure the temporal

evolution of the entire fluorescence spectrum rather than recording the fluorescence decay at a single wavelength interval in TCSPC. Moreover, the time resolution is better than that of TCSPC. The former one can easily obtain a time resolution of a few ps (even femto-picosecond, see Guide to streak camera, Hamamatsu⁹⁸), which clearly requires much more effort⁹⁹ to be obtained in case of TCSPC. On the other hand, the sensitivity of a TCSPC setup can be far higher because a significantly larger fraction of the emitted photons can be detected. The detailed components of a streak camera and the principle of operation of the synchroscan streak-camera setup are illustrated in Figure 1.2 a) and b), respectively. For more details see van Stokkum et al. 2008¹⁰⁰.

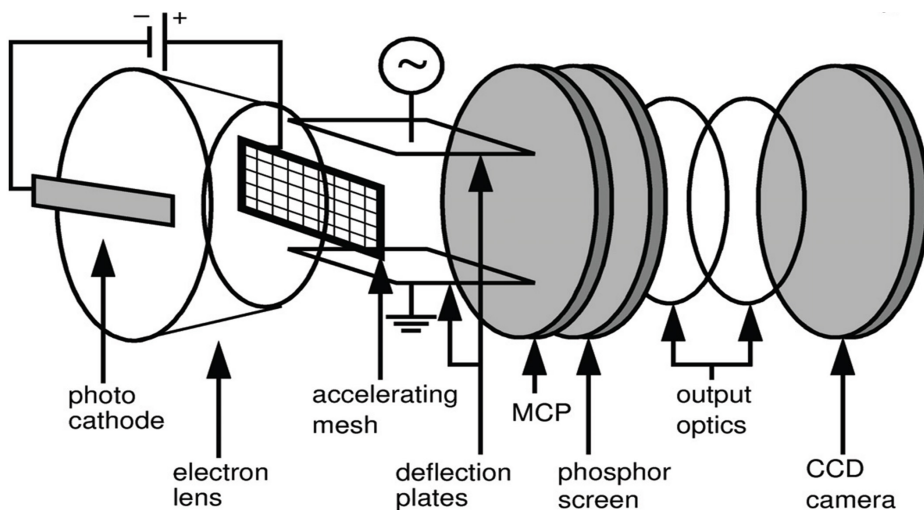


Figure 1.11: Schematic representation of a streak camera, adapted from ref¹⁰⁰.

1.3.2 Data analysis and modeling

Time-resolved fluorescence data is usually analysed by fitting with models that comprise multi-exponential (or stretched exponential) components. Here we will not make use of stretched exponentials. The fitting function at a particular detection wavelength is given by:

$$I(t) = \sum_{i=1}^n A_i \cdot \exp(-k_i \cdot t) \otimes \text{irf}(t) \quad (1.6)$$

where \otimes indicates convolution. A_i are amplitudes, k_i are the decay rate constants, which are the inverse of the fluorescence lifetimes (τ_i) and $\text{irf}(t)$ is the instrument response function. The mathematics used to run the fitting is based on the least squares estimation.

1.3.2.1 Global analysis

As was mentioned above, streak-camera experiments provide two-dimensional data sets, which cover the whole spectrum. In general, for each wavelength, after fitting, we can obtain a group of parameters ($n, A_i, k_i, \text{irf}(t)$). Some of the parameters are not necessarily the same for different traces, whereas others should be identical for obvious reasons. To better determine this group of parameters from multiple decay traces, global analysis is performed, in which decay curves at all wavelengths are fitted simultaneously by forcing some parameters to be identical ("linked" during fitting). The linked parameters can either be A_i or k_i . In case k_i are linked, equation 1.6 becomes 1.7, in which some parameters are shown as functions of wavelength (λ).

$$I(\lambda, t) = \sum_{i=1}^n A_i(\lambda) \cdot \exp(-k_i \cdot t) \otimes \text{irf}(\lambda, t) \quad (1.7)$$

where $A_i(\lambda)$ are called **Decay Associated Spectra (DAS)**, which are very informative as we will become clear in all chapters of this thesis, especially for the assignment of energy transfer steps.

1.3.2.2 Target analysis

Sometimes use is made of a particular target model in the fitting^{101,102}. In one target model, several groups of indistinguishable pigments (so-called compartments) preferably possess their own reasonable physical meaning. This fitting method is termed 'target analysis'. When target analysis is applied, **Species Associated Spectra (SAS)** i.e. the spectrum of each compartment) can be obtained and energy transfer rates connecting them can be determined. The corresponding equation in its general form is given by:

$$I(\lambda, t) = \sum_{l=1}^n c_l(t) \cdot \text{SAS}_l(\lambda) \quad (1.8)$$

where n is the number of compartments and $c_l(t)$ represents the excitation concentration of the compartment. If we put $c_l(t)$ in a matrix, $[c_1(t) \ c_2(t) \ ... \ c_n(t)]^T$ and define it as a vector $c(t)$, then this n -compartments model can be described by the following differential equation:

$$\frac{d}{dt} c(t) = K \cdot c(t) + j(t) \quad (1.9)$$

Where K is the transfer matrix (see ref.¹⁰²), and the vector $j(t) = [j_1(t) \ j_2(t) \ ... \ j_n(t)]^T$ contains elements $j_l(t)$, representing the initial excitation input in the l th compartment.

Note that **SAS** are not generated in the fitting randomly, but with certain spectral shape constraints. In our work, all **SAS** are fitted with skewed Gaussian shapes in the energy domain, (for details see ref.¹⁰⁰).

The software used in Chapter 3&4 (TIM package) is written in FORTRAN and C, as in-house global and target analysis software. It was developed and maintained by Dr. Ivo van Stokkum. In chapter 2&5, the main used software is the R-package TIMP, which is an implementation of TIM in R language, rewritten by Dr. Katharine Mullen et al. Recently, Glotaran as a user friendly interface for the TIMP package was built (and is still under development) by Joris J. Snellenburg et al.¹⁰³. It is also used for the data analysis of this thesis.

1.4 This thesis

Recently, more and more structures of photosynthetic complexes have been determined and also their 3D locations in the thylakoid membrane have become more clear. One major step forward is to study all these complexes as a whole system. In this thesis, I have focused on the initial steps of photosynthesis in cyanobacteria both *in vivo* and *in vitro* by using picosecond time-resolved fluorescence, revealing information about excitation-energy transfer, energy trapping and non-photochemical quenching.

Chapter 2 addresses the PSI and PSII kinetics *in vivo* in the cyanobacterial BE and PAL mutants, both at room temperature and at 77K. The BE mutant is lacking PSII and PBs, while the PAL mutant is lacking only PBs. One goal of this work is to elucidate the PSII kinetics *in vivo*, and the other one is to remove the existing controversies about the kinetics of PSII core complex in literature. To do so, global

analysis and target analysis were combined and several models were tested on the time-resolved fluorescence data obtained with a streak-camera system.

In Chapter 3 the blue-green light induced NPQ mechanism is studied *in vivo* in wild-type *Synechocystis* cells and two mutants with extra and without OCP, respectively (Over_OCP and Δ OCP). The energy transfer kinetics of *Synechocystis* are successfully modelled and by using the resulting model, the site and the rate of quenching of blue-green light induced NPQ could be determined. The possible physical mechanisms underlying this quenching process will be discussed.

Chapter 4 provides a detailed time-resolved fluorescence study of the blue-green light induced NPQ mechanism of isolated PBs from wild-type cells and from two PBs truncated mutants: the CK mutant, lacking the c_PC rods and the CB mutant, lacking both the intermediary and the core-distal c_PC hexamers. The goal of this research is to determine how much the *in vitro* reconstitution system using isolated OCP and isolated PBs can mimic the *in vivo* one regarding the protection mechanism. The results demonstrate that both the mechanism and the site of quenching are the same *in vitro* and *in vivo*.

As an extension of chapters 3 and 4, in Chapter 5, we take one step further, to study the NPQ mechanisms of two PBs-modified mutants of CK and CB *in vivo*. The quenching sites and rates are demonstrated to be very similar as found with the *in vitro* experiments on the corresponding isolated PBs, and the results are also in good agreement with those of wild-type cells, although their overall quenching of fluorescence are very much different from each other.

References

- (1) Blankenship, R. E. *Molecular Mechanisms of Photosynthesis*; John Wiley & Sons, **2002**.
- (2) Govindjee, J. T. B., H. Gest, J.F. Allen *Discoveries in Photosynthesis*; Springer, **2006**.
- (3) van Amerongen, H.; Valkunas, L.; Grondelle, R. v. Exciton Dynamics in Different Antenna Complexes. Coherence and Incoherence. In *Photosynthetic excitons*; World Scientific Publishing Co.Pte.Ltd., **2000**.
- (4) Nozik, A. J.; Miller, J. *Chem Rev* **2010**, *110*, 6443-6445.
- (5) Melis, A. *Energ Environ Sci* **2012**, *5*, 5531-5539.
- (6) Blankenship, R. E.; Tiede, D. M
- (8) Melis, A. *Plant Sci* **2009**, *177*, 272-280.
- (9) Walker, D. A. *J Appl Phycol* **2009**, *21*, 509-517.
- (10) Zhu, X. G.; Long, S. P.; Ort, D. R. *Annu Rev Plant Biol* **2010**, *61*, 235-261.
- (11) Janssen, M.; Tramper, J.; Mur, L. R.; Wijffels, R. H. *Biotechnol Bioeng* **2003**, *81*, 193-210.
- (12) Badin, E. J.; Calvin, M. *J Am Chem Soc* **1950**, *72*, 5266-5270.
- (13) Vermaas, W. F. J. *Photosynthesis and Respiration in Cyanobacteria*. In *eLS*; John Wiley & Sons, Ltd, **2001**.
- (14) Bryant, D. A. *The Molecular Biology of Cyanobacteria*; Springer, **1994**.
- (15) Seckbach, J. *Algae and Cyanobacteria in Extreme Environments*; Springer, **2007**.
- (16) Whitton, B. *The Ecology of Cyanobacteria: their Diversity in time and space*;Kluwer academic publishers, **2002**.
- (17) Herrero, A. and Flores, E.; *The Cyanobacteria: Molecular Biology, Genomics, and Evolution*; Caister Academic Press, **2008**.
- (18) Ruffing, A. M. *Bioengineered bugs* **2011**, *2*, 136-149.
- (19) Heidorn, T.; Camsund, D.; Huang, H. H.; Lindberg, P.; Oliveira, P.; Stensjo, K.; Lindblad, P. *Methods Enzymol* **2011**, *497*, 539-579.
- (20) Kaneko, T.; Sato, S.; Kotani, H.; Tanaka, A.; Asamizu, E.; Nakamura, Y.; Miyajima, N.; Hirose, M.; Sugiura, M.; Sasamoto, S.; Kimura, T.; Hosouchi, T.; Matsuno, A.; Muraki, A.; Nakazaki, N.; Naruo, K.; Okumura, S.; Shimpo, S.; Takeuchi, C.; Wada, T.; Watanabe, A.; Yamada, M.; Yasuda, M.; Tabata, S. *DNA research : an international journal for rapid publication of reports on genes and genomes* **1996**, *3*, 185-209.
- (21) Nelson, N.; Ben-Shem, A. *Nat Rev Mol Cell Bio* **2004**, *5*, 971-982.
- (22) Jordan, P.; Fromme, P.; Witt, H. T.; Klukas, O.; Saenger, W.; Krauss, N. *Nature* **2001**, *411*, 909-917.
- (23) Fromme, P.; Jordan, P.; Krauss, N. *Biochimica et biophysica acta* **2001**, *1507*, 5-31.
- (24) Kargul, J.; Janna Olmos, J. D.; Krupnik, T. *Journal of Plant Physiology* **2012**, *169*, 1639-1653.
- (25) Umena, Y.; Kawakami, K.; Shen, J. R.; Kamiya, N. *Nature* **2011**, *473*, 55-65.
- (26) Ferreira,K.N.; Iverson,M.T.; Maqhlou, K.; Barber,J.;lwata,S. *Science* **2004**, *303*,1831-1838.

- (27) Bricker, T. M.; Frankel, L. K. *Photosynth Res* **2002**, 72, 131-146.
- (28) Nield, J.; Kruse, O.; Ruprecht, J.; da Fonseca, P.; Buchel, C.; Barber, J. *J Biol Chem* **2000**, 275, 27940-27946.
- (29) Büchel, C.; Kuhlbrandt, W. *Photosynth Res* **2005**, 85, 3-13.
- (30) Amunts, A.; Nelson, N. *Bba-Bioenergetics* **2006**, 260-260.
- (31) Ben-Shem, A.; Frolow, F.; Nelson, N. *Nature* **2003**, 426, 630-635.
- (32) Grossman, A. R.; Schaefer, M. R.; Chiang, G. G.; Collier, J. L. *Microbiological reviews* **1993**, 57, 725-749.
- (33) Glazer, A. N.; Lundell, D. J.; Yamanaka, G.; Williams, R. C. *Annales de microbiologie* **1983**, 134B, 159-180.
- (34) Grossman, A. R.; Schaefer, M. R.; Chiang, G. G.; Collier, J. L. *Microbiological reviews* **1993**, 57, 725-749.
- (35) Adir, N. *Photosynth Res* **2005**, 85, 15-32.
- (36) David, L.; Marx, A.; Adir, N. *Journal of molecular biology* **2011**, 405, 201-213.
- (37) Reuter, W.; Wiegand, G.; Huber, R.; Than, M. E. *Proceedings of the National Academy of Sciences of the United States of America* **1999**, 96, 1363-1368.
- (38) Babu, T. S.; Kumar, A.; Varma, A. K. *Plant physiology* **1991**, 95, 492-497.
- (39) de Lorimier, R. M.; Smith, R. L.; Stevens, S. E. *Plant physiology* **1992**, 98, 1003-1010.
- (40) Baniulis, D.; Yamashita, E.; Whitelegge, J. P.; Zatsman, A. I.; Hendrich, M. P.; Hasan, S. S.; Ryan, C. M.; Cramer, W. A. *J Biol Chem* **2009**, 284, 9861-9869.
- (41) Weber, J. *Trends in biochemical sciences* **2007**, 32, 53-56.
- (42) McEvoy, J. P.; Brudvig, G. W. *Chem Rev* **2006**, 106, 4455-4483.
- (43) Dau, H.; Zaharieva, I.; Haumann, M. *Current opinion in chemical biology* **2012**, 16, 3-10.
- (44) Boyer, P. D. *Annu Rev Biochem* **1997**, 66, 717-749.
- (45) Yoshida, M.; Muneyuki, E.; Hisabori, T. *Nat Rev Mol Cell Bio* **2001**, 2, 669-677.
- (46) Weber, J. *Biochim Biophys Acta* **2006**, 1757, 1162-1170.
- (47) Baniulis, D.; Yamashita, E.; Zhang, H.; Hasan, S. S.; Cramer, W. A. *Photochemistry and photobiology* **2008**, 84, 1349-1358.
- (48) Stroebel, D.; Choquet, Y.; Popot, J.-L.; Picot, D. **2003**, 426, 413-418.
- (49) Nogales, J.; Gudmundsson, S.; Knight, E. M.; Palsson, B. O.; Thiele, I. *Proceedings of the National Academy of Sciences of the United States of America* **2012**, 109, 2678-2683.
- (50) Polivka, T.; Sundstrom, V. *Chem Rev* **2004**, 104, 2021-2071.
- (51) Kirilovsky, D. *Photosynth Res* **2007**, 93, 7-16.
- (52) Holt, T. K.; Krogmann, D. W. *Biochim Biophys Acta* **1981**, 637, 408-414.
- (53) Kerfeld, C. A.; Sawaya, M. R.; Brahmamandam, V.; Cascio, D.; Ho, K. K.; Trevithick-Sutton, C. C.; Krogmann, D. W.; Yeates, T. O. *Structure* **2003**, 11, 55-65.
- (54) Wilson, A.; Kinney, J. N.; Zwart, P. H.; Punginelli, C.; D'Haene, S.; Perreau, F.; Klein, M. G.; Kirilovsky, D.; Kerfeld, C. A. *J Biol Chem* **2010**, 285, 18364-18375.
- (55) Liu, T.; Shuai, Y.; Zhou, H. *Acta Cryst. F* **2011**, 67, 1627-1629.
- (56) Kirilovsky, D.; Kerfeld, C. A. *Biochimica et biophysica acta* **2012**, 1817, 158-166.

Introduction

- (57) Mohr, R.; Voss, B.; Schliep, M.; Kurz, T.; Maldener, I.; Adams, D. G.; Larkum, A. D. W.; Chen, M.; Hess, W. R. *Isme J* **2010**, *4*, 1456-1469.
- (58) Chen, M.; Li, Y. Q.; Birch, D.; Willows, R. D. *Febs Lett* **2012**, *586*, 3249-3254.
- (59) Vokacova, Z.; Burda, J. V. *J Phys Chem A* **2007**, *111*, 5864-5878.
- (60) Kirilovsky, D.; Wilson, A. *Photosynth Res* **2007**, *91*, 291-292.
- (61) Polivka, T.; Kerfeld, C. A.; Pascher, T.; Sundstrom, V. *Biochemistry-Us* **2005**, *44*, 3994-4003.
- (62) Polivka, T.; Chabera, P.; Kerfeld, C. A. *Biochimica et biophysica acta* **2012**.
- (63) Berera, R.; van Stokkum, I. H. M.; Gwizdala, M.; Wilson, A.; Kirilovsky, D.; van Grondelle, R. *J Phys Chem B* **2012**, *116*, 2568-2574.
- (64) Lakowicz, J. R. *Principles of Fluorescence Spectroscopy*; Springer, 2006.
- (65) Dexter, D. L. *J Chem Phys* **1953**, *21*, 836-850.
- (66) Scholes, G.D.; Gould, I.R.; Cogdell, R.J. and Fleming, G.R. *J Phys Chem B* **1999**, *103*, 2543-2553.
- (67) König, C and Neugebauer, J; *ChemPhysChem* **2012**, *13*, 386-425.
- (68) Hartmann, L; Goychuk, I; Grifoni, M.; and Hänggi, P. *Physical Review E* **2000**, *61*(5), 4687-4691.
- (69) Makri, N. *Annu. Rev. Phys. Chem.* **1999**, *50*: 167-191
- (70) Yang, M.; Fleming, G. R. *Chem Phys* **2002**, *282*, 161-.
- (71) Olaya-Castro, A.; Scholes, G. D. *International Reviews in Physical Chemistry* **2011**, *30*, 49-77.
- (72) Novoderezhkin, V. I.; Razjivin, A. P. *Photochemistry and photobiology* **1995**, *62*, 1035-1040.
- (73) Womick, J. M.; West, B.; Scherer, N. F.; Moran, A. M. *J Phys B-at Mol Opt* **2012**, *45*.
- (74) Womick, J. M.; Moran, A. M. *J Phys Chem B* **2009**, *113*, 15747-15759.
- (75) Scholes, G. D.; Fleming, G. R.; Olaya-Castro, A.; van Grondelle, R. *Nat Chem* **2011**, *3*, 763-774.
- (76) El Bissati, K.; Delphin, E.; Murata, N.; Etienne, A. L.; Kirilovsky, D. *Bba-Bioenergetics* **2000**, *1457*, 229-242.
- (77) Rakhimberdieva, M. G.; Stadnichuk, I. N.; Elanskaya, T. V.; Karapetyan, N. V. *Febs Lett* **2004**, *574*, 85-88.
- (78) Jallet, D.; Gwizdala, M.; Kirilovsky, D. *Biochimica. et. Biophysica. Acta-Bioenergetics* **2011**, *1817*, 1418-1427.
- (79) Ruban, A. V.; Berera, R.; Illioaia, C.; van Stokkum, I. H. M.; Kennis, J. T. M.; Pascal, A. A.; van Amerongen, H.; Robert, B.; Horton, P.; van Grondelle, R. *Nature* **2007**, *450*, 575-U522.
- (80) van Amerongen, H.; van Grondelle, R. *J Phys Chem B* **2001**, *105*, 604-617.
- (81) Bode, S.; Quentmeier, C. C.; Liao, P. N.; Hafi, N.; Barros, T.; Wilk, L.; Bittner, F.; Walla, P. J. *Proceedings of the National Academy of Sciences of the United States of America* **2009**, *106*, 12311-12316.
- (82) Holt, N. E.; Zigmantas, D.; Valkunas, L.; Li, X. P.; Niyogi, K. K.; Fleming, G. R. *Science* **2005**, *307*, 433-436.

- (83) Dreuw, A.; Fleming, G. R.; Head-Gordon, M. *Phys Chem Chem Phys* **2003**, *5*, 3247-3256.
- (84) Miloslavina, Y.; Wehner, A.; Lambrev, P. H.; Wientjes, E.; Reus, M.; Garab, G.; Croce, R.; Holzwarth, A. R. *Febs Lett* **2008**, *582*, 3625-3631.
- (85) Muller, M. G.; Lambrev, P.; Reus, M.; Wientjes, E.; Croce, R.; Holzwarth, A. R. *Chemphyschem* **2010**, *11*, 1289-1296.
- (86) Kloz, M.; Pillai, S.; Kodis, G.; Gust, D.; Moore, T. A.; Moore, A. L.; van Grondelle, R.; Kennis, J. T. M. *J Am Chem Soc* **2011**, *133*, 7007-7015.
- (87) Wang, Q.; Jantaro, S.; Lu, B. S.; Majeed, W.; Bailey, M.; He, Q. F. *Plant physiology* **2008**, *147*, 1239-1250.
- (88) Singh, S. P.; Kumari, S.; Rastogi, R. P.; Singh, K. L.; Richa; Sinha, R. P. *Afr J Biotechnol* **2010**, *9*, 580-588.
- (89) Mullineaux, C. W.; Emlyn-Jones, D. *J Exp Bot* **2005**, *56*, 389-393.
- (90) Zhang, P. P.; Eisenhut, M.; Brandt, A. M.; Carmel, D.; Silen, H. M.; Vass, I.; Allahverdiyeva, Y.; Salminen, T. A.; Aro, E. M. *Plant Cell* **2012**, *24*, 1952-1971.
- (91) Bibby, T. S.; Nield, J.; Barber, J. *Nature* **2001**, *412*, 743-745.
- (92) Boekema, E. J.; Hifney, A.; Yakushevskaya, A. E.; Piotrowski, M.; Keegstra, W.; Berry, S.; Michel, K. P.; Pistorius, E. K.; Kruip, J. *Nature* **2001**, *412*, 745-748.
- (93) Ihalainen, J. A.; D'Haene, S.; Yermenko, N.; van Roon, H.; Arteni, A. A.; Boekema, E. J.; van Grondelle, R.; Matthijs, H. C. P.; Dekker, J. P. *Biochemistry-Us* **2005**, *44*, 10846-10853.
- (94) Berera, R.; van Stokkum, I. H. M.; d'Haene, S.; Kennis, J. T. M.; van Grondelle, R.; Dekker, J. P. *Biophys J* **2009**, *96*, 2261-2267.
- (95) Hihara, Y.; Sonoike, K.; Ikeuchi, M. *Plant physiology* **1998**, *117*, 1205-1216.
- (96) Sonoike, K.; Hihara, Y.; Ikeuchi, M. *Plant Cell Physiol* **2001**, *42*, 379-384.
- (97) Kopecna, J.; Komenda, J.; Bucinska, L.; Sobotka, R. *Plant physiology* **2012**.
- (98) Hammamsu. **2011**.
- (99) Becker, W. *Advanced Time-Correlated Single Photon Counting Techniques*, 2005.
- (100) van Stokkum, I. H. M.; van Oort, B.; van Mourik, F.; Gobets, B. and van Amerongen, **2008** In *Biophysical Techniques in Photosynthesis, Volume II*, editors: Aartsma, T.J. and Matysik, J., Springer, Dordrecht. P.223-240.
- (101) Beechem, J. M.; Ameloot, M.; Brand, L. *Anal Instrum* **1985**, *14*, 379-402.
- (102) van Stokkum, I. H. M.; Larsen, D. S.; van Grondelle, R. *Bba-Bioenergetics* **2004**, *1657*, 82-104.
- (103) Snellenburg, J. J.; Laptinok, S. P.; Seger, R.; Mullen, K. M.; van Stokkum, I. H. M. *J Stat Softw* **2012**, *49(3)*, 1-22.

Chapter 2

Probing the Picosecond Kinetics of the Photosystem II Core Complex in vivo

This chapter is based on:

Lijin Tian, Shazia Farooq and Herbert van Amerongen
***Physical Chemistry Chemical Physics* 2013, 2013, 15, 3146-3154**

Abstract

Photosystems I (PSI) and II (PSII) are two major pigment-protein complexes of photosynthetic organisms that function in series to convert sunlight energy into chemical energy. We have studied the picosecond fluorescence behaviour of the core of both photosystems *in vivo* by using two *Synechocystis* PCC 6803 mutants: BE cells contain PSI but are lacking both PSII and the light-harvesting complexes called phycobilisomes (PBs) whereas PAL cells contain both PSI and PSII but lack the PBs. Measurements were performed at room temperature and at 77K. The fluorescence kinetics of PSI and PSII can nicely be separated, en passant providing the PSI/PSII ratio. At room temperature, the PSI kinetics are identical to those of isolated PSI whereas the PSII kinetics can equally well be described by the *in vitro* trap-limited model of Miloslavina, Y., Szczepaniak, M., Muller, M.G., Sander, J., Nowaczyk, M., Rogner, M., and Holzwarth, A.R., *Biophys J.* (2009), 96(2), 621–631, and by the transfer-to-the-trap-limited model of van der Weij-de Wit, C. D., Dekker, J. P., van Grondelle, R., van Stokkum, I. H. M., *J Phys Chem A* 2011, 115(16), 3947-3956, albeit that the *in vivo* kinetics turn out to be somewhat slower. At 77K several low-energy pigments are observed in both photosystems which complicate the overall dynamics but the PSII kinetics can still be described by both a trap-limited and a transfer-to-the-trap-limited model.

Introduction

For oxygenic photosynthesis several protein complexes in the thylakoid membrane are required, the major players being photosystem I (PSI), photosystem II (PSII), the cytochrome b_6f complex, and the ATP synthase¹. These complexes work together to ultimately transform sunlight energy into chemical energy. The two photosystems are both large pigment-protein complexes that exist in cyanobacteria as well as in chloroplasts from plants and algae. The PSI core moiety contains about 100 chlorophylls (Chls), and 22 carotenoids (Cars) per P700, the primary electron donor and its structure was determined at 2.5 Å by Jordan et al. and Fromme et al. in 2001^{2,3}. The PSII core complex contains ~35 Chls and ~12 Cars per monomer, and its structure has been determined at 1.9 Å by Umena et al.⁴. The PSII core complex contains the reaction center (RC) that

consists of the D1 and D2 polypeptides, cytochrome b559, and some other proteins encoded by the photosystem b (psb) genes besides six Chls and two pheophytin molecules and several other cofactors. In addition, it is associated with two Chl-binding polypeptides, CP43 and CP47, that function as core antennae, and their structures and functions are well-documented in ref.⁵. Note that both the structure and function of PSI and PSII core complexes are thought to be very similar for virtually all cyanobacteria and plant species with minor differences on the stromal side⁶⁻⁹.

At room temperature, the time-resolved fluorescence kinetics of the PSI core complex are relatively simple and have been well documented (for an overview see ^{10, 11}). In case of *Synechocystis* PCC 6803, most of the time-resolved fluorescence studies on photosystem I, both *in vitro* and *in vivo*, have reported two dominant processes: a fast equilibration component between bulk Chls and red Chls (~5 ps) and a trapping component from the equilibrated system of bulk and red Chls (20-30 ps). Moreover, it was found that there is not much difference between the time-resolved fluorescence PSI in the open state (with P700 being reduced) and in the closed state (with P700 oxidized: P700+)^{12, 13}.

On the other hand, controversial results have been reported for the kinetics of PSII over the past decades. More often than not, different samples show different kinetics. And whereas some groups have claimed that the kinetics of PSII are trap-limited, which assumes exciton equilibration between all Chls to be fast when compared to the primary charge separation time¹⁴⁻¹⁶, others have reported that they are transfer-to-the-trap limited, which means that the energy transfer time from the antenna to the RC in Photosystem II dominates the overall trapping time¹⁷⁻¹⁹ (for reviews about this issue see ²⁰⁻²²).

In contrast to PSI, PSII shows time-resolved fluorescence kinetics that are very much dependent on the fact whether the RCs are in an open (with Q_a oxidized) or closed state (with Q_a reduced).

Although many picosecond fluorescence studies have been performed on isolated core complexes of PSI and PSII^{10,11,15,18,23-25}, a successful, simultaneous study of both photosystem cores *in vivo*, where they work in series and are functionally connected, has not been performed yet. Most studies have been performed in the

presence of additional antenna systems that lead to large heterogeneity of the system^{19, 26-29}. In case of cyanobacteria, the large phycobilisome antennae complicate the fluorescence kinetics considerably³⁰, and moreover, some photosystems are connected to these antennae and others are not.

In this work, we have performed *in vivo* picosecond time-resolved fluorescence measurements on the PAL mutant³¹ of *Synechocystis* PCC 6803 that contains both PSI and PSII cores but no PBs. By using the *in vivo* results on the BE mutant that is lacking both PSII and PBs it turns out to be possible to fully separate the PSI and PSII core kinetics for the PAL mutant *in vivo*. Moreover, we have also performed time-resolved fluorescence measurements on both mutants at 77K. We conclude that both the trap-limited model and the transfer-to-the-trap-limited model can describe the kinetics of the PSII core complex rather well.

Materials and methods

Culture and growth conditions:

For the construction of the BE and PAL mutants we refer to^{11,31,32}. The PAL mutant was grown photoautotrophically in modified BG11 medium³³, with twice the concentration of sodium nitrate and with 10 mM NaHCO₃ added to the medium, while BE cells were grown photoheterotrophically in the presence of 5 mM glucose in BG11 medium. Both types of cells were grown in 250-ml flasks with 60 ml growing volume in a rotary shaker (45 rpm) at 30°C. The PAL mutant was illuminated by white light giving a total intensity of $\sim 30 \mu\text{mol}\cdot\text{m}^{-2}\cdot\text{s}^{-1}$, while the BE cells were grown in $\sim 10 \mu\text{mol}\cdot\text{m}^{-2}\cdot\text{s}^{-1}$. All cells were kept in the logarithmic growth phase by refreshing the medium every few days depending on growing rate. The growing rate of BE was faster than that of the PAL mutant because of the glucose. Cells were concentrated 3-5 times by low-speed centrifugation and dark-adapted at least 10 minutes before the time-resolved fluorescence measurements were started.

Time-resolved fluorescence measurements

Time-resolved fluorescence measurements were performed on a picosecond streak-camera system^{11, 34}. The time window was 800 ps for all measurements.

The excitation spot size was typically $\sim 100\ \mu\text{m}$ in diameter and the laser repetition rate was 250 kHz. Images were corrected for background and detector sensitivity, averaged, and sliced up into traces of 4 nm wide. The instrument response function (IRF) can be described with a double Gaussian, consisting of a dominating narrow Gaussian of $\sim 4.0\ \text{ps}$ full width at half-maximum (FWHM) on top of a minor Gaussian of $\sim 40\text{--}50\ \text{ps}$. A series of laser powers ranging from $5\ \mu\text{W}$ to $200\ \mu\text{W}$ was tested. The samples were rapidly flown during the measurements by using a pump system combined with a cuvette of size $1\ \text{mm} \times 1\ \text{mm} \times 3\ \text{mm}$. To keep the PSII reaction centers open, a speed of 2.5 ml per second was used, in combination with a low laser intensity ($<10\ \mu\text{W}$), while only 0.25 ml per second was used, in combination with a laser power of $100\ \mu\text{W}$ to keep most of the RCs closed in the presence of $80\ \mu\text{M}$ DCMU and under continuous illumination with white light with $\sim 100\ \mu\text{mol} \cdot \text{m}^{-2} \cdot \text{s}^{-1}$ before the cells were flowing into the excitation spot within less than two seconds. All measurements were performed at 21°C and each measurement took ~ 20 minutes. For the 77K measurements, the dark-adapted samples were collected in Pasteur pipettes with $\sim 1\ \text{mm}$ diameter that were then frozen by immersion in liquid nitrogen. The sample concentration was kept low such that the optical density at 670 nm was below 0.2 (light path $\sim 1\ \text{cm}$) in order to avoid significant re-absorption.

Global and target analysis

Data analysis: Data obtained with the streak-camera setup were analysed with the TIMP package for the “R project for Statistical Computing (R Development Core Team 2008)”. For details see ³⁵.

With global analysis the data was fitted globally to a sum of exponential decays convolved with an IRF and the amplitude of each decay component as a function of wavelength was determined, the so-called decay-associated spectrum (DAS); this analysis provides an objective mathematical description of the datasets that can provide insight into the origin of the kinetics of the systems. Note that, the back-sweep effect of streak camera was considered in the fitting software, thus a component with lifetime longer than the time-window can still be estimated precisely³⁶.

Using target analysis the datasets were subsequently fitted with different compartmental schemes (also called target models), and in this way the spectrum of each compartment and the energy transfer rates and decay rates were estimated. The methodology of global analysis and target analysis is described in ref.³⁷.

Results and Discussion

Effect of laser intensity, DCMU, and ferricyanide on the pico- and nanosecond fluorescence kinetics of the PAL mutant.

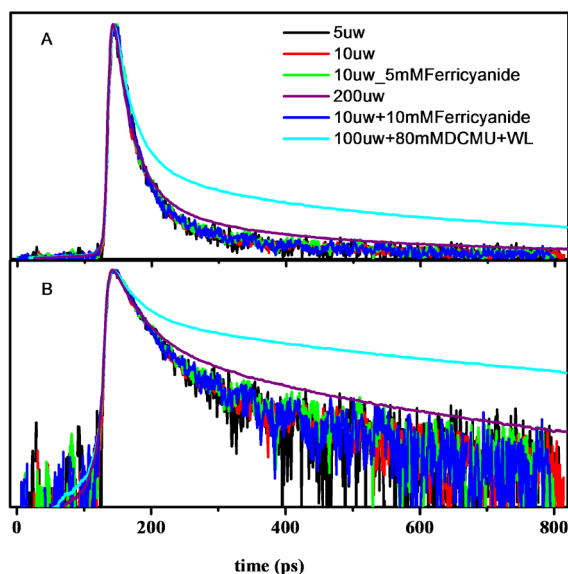


Figure 2.1: Time-resolved fluorescence decay traces of the PAL mutant upon 400 nm excitation using different measurement conditions. All traces were obtained by averaging the decay over the whole wavelength range from 570 nm to 830 nm and they were normalized to their maximum, and shifted to the same starting point for comparison. The intensity is plotted on a linear scale A), and a log scale B); Laser-intensity dependent time-resolved fluorescence measurements were repeated at least three times.

Figure 2.1 shows the fluorescence kinetics of PAL cells under different conditions. At high laser intensities the reaction centers start to become closed, leading to slower kinetics but at relatively low intensities (5-10 μW) they are fully open and the addition of ferricyanide²⁵ that can be used to keep the reaction centres open does not further accelerate the kinetics anymore.

In addition, when the time-resolved fluorescence data as measured with the streak camera are compared with those measured by the single photon counting

setup (with far lower excitation intensities, for details see also Supplementary Information) the kinetics appear to be very similar, further supporting the fact that the reaction centers are indeed open.

To obtain the kinetics of core complexes with the RCs mostly closed, measurements were performed in the presence of 80 μM DCMU at high measuring light intensities (200 μW), in combination with $\sim 100 \mu\text{mol}\cdot\text{m}^{-2}\cdot\text{s}^{-1}$ continuous white light illumination before the cells were flowing into the excitation spot. The steady-state fluorescence of samples with “closed” RCs that can be reconstructed from the time-resolved data by summing the products of DAS and corresponding lifetimes are shown in Fig 2.2 D. It turns out that the fluorescence of “closed” RCs is about 4.6 times as high as in the case of “open” RCs, which is in agreement with previous reports on the effect of reduced Q_A^{15} , confirming that the RCs are indeed fully open or fully closed in the extreme cases.

Kinetics of RCs *in vivo* at RT

Global analysis

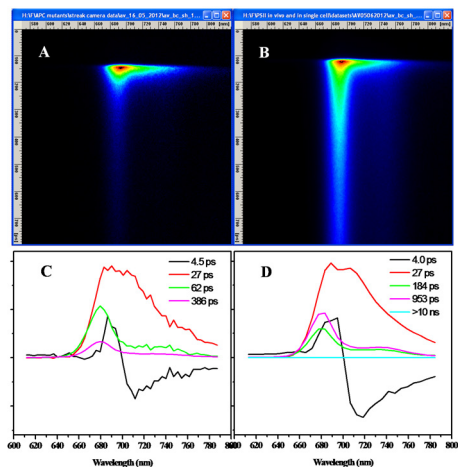


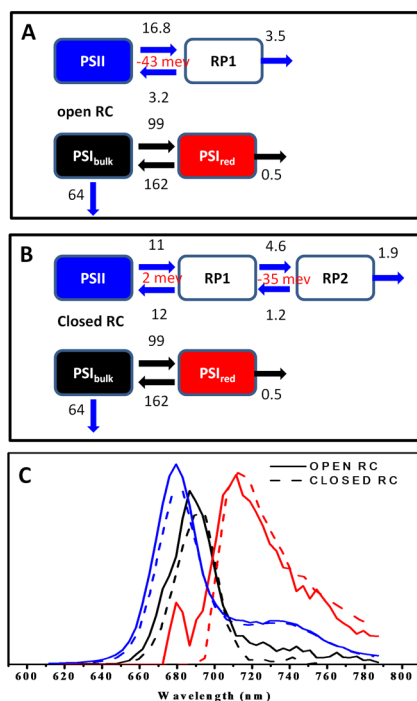
Figure 2.2: Streak images of the PAL mutant with PSII RCs in the “open” (A) and “closed” form (B). These images represent the fluorescence intensity (using a linear color gradient) as a function of time (vertical axis) and wavelength (horizontal axis); every vertical line represents a time trace of fluorescence at the corresponding wavelength, while every horizontal line reflects a fluorescence emission spectrum at a certain delay time. The corresponding decay associated spectra are shown in C) and D) with lifetimes included in the figure.

For cells with closed RCs a much slower decay was observed than in the case of open RCs as is shown in Fig 2.2A and B. To quantify the difference, the corresponding decay-associated spectrum (DAS) and lifetimes are shown in Fig 2.2C and D. A fit with 4 lifetimes for PAL with PSII RC open and 5 lifetimes for PAL

with PSII RC closed leads to a satisfactory description of the data. Note that in a previous study on the BE mutant, containing PSI only, the kinetics were shown to be dominated by a 5.5 ps and a 28 ps component, whereas a slow component of around 500 ps had very little contribution³⁸. The 5.5 ps DAS corresponds to fast energy transfer from pigments fluorescing below 700 nm to pigments fluorescing above 700 nm, reflecting spectral equilibration within PSI. The 28 ps component represents fluorescence decay due to charge separation from the equilibrated excited state of PSI. In case of the PAL mutant, these two lifetime components can be observed again (see also Fig 2.2C and 2.2D) although there is a slight difference in the exact shape and lifetime of especially the fastest component, the lifetime of which is close to the instrument response time of the setup for this time window (IRF is ~5 ps broad). There may also be an additional contribution from a fast equilibration process within PSII, which is more clearly observed in the 77K data (see section 3.3). Nevertheless, it appears that the PSI kinetics can be separated quite well from the kinetics of the rest of the system, both for open and closed RCs. For further discussion of the PSI kinetics we refer to ref³⁸. Two extra components with lifetimes $\tau_3 = 62$ ps and $\tau_4 = 366$ ps are observed for PSII with open RCs and two components with lifetimes of 184 ps and 953 ps when the RCs are closed. One very small component with a lifetime above 10 ns is needed for better fitting in the latter case but it will not be considered further. The DAS that correspond to τ_3 and τ_4 for open and closed RCs show a fluorescence peak at 680 nm as is indeed expected for PSII. It is well known that the PSII charge separation kinetics depends on the reduction state of the secondary electron acceptor Q_A ^{20,39}; for open RCs of PSII, two main lifetimes of 40-80 ps and 200-500 ps have been reported^{14,18,40}. Here the fitted lifetimes of 62 ps and 366 ps lie within those intervals. Similarly, the obtained two lifetimes for closed RC fall within the lifetime intervals of 200-500 ps and 1-10 ns as reported for closed RC's^{18,40}. Note that the lifetime of the 953 ps component is not very accurate.

Target analysis

Target analysis was used to further fit and model the time-resolved results on the PAL cells. Using target analysis for BE cells, we have previously obtained a model to describe the PSI kinetics *in vivo*³⁸. The model comprises one pool of bulk Chls and one of red Chls as shown in Figure 2.3. As the PSI kinetics have been determined before, we keep the corresponding parameters fixed in the modelling of the present work and we focus on the PSII kinetics. Fig. 2.3A shows the compartmental model used for PAL in the “open state”, which represents the well-known exciton/radical pair equilibrium model (“ERPE”) model that contains only two pools for the PSII part^{15,41}. In this model, excitation equilibration over the PSII core is very fast and charge separation to the first radical pair (RP) state occurs from the state where the excitation is thermally equilibrated over all pigments. More pools cannot be resolved from the data without adding further constraints. The two pools are connected by a forward overall primary charge separation rate and a backward charge recombination rate. The overall charge separation rate was determined to be $(66 \pm 11 \text{ ps})^{-1}$, while the fitted charge



recombination rate was $(328 \pm 42 \text{ ps})^{-1}$. The obtained rate for secondary charge separation rate is $(303 \pm 10 \text{ ps})^{-1}$. The estimated errors are further explained in the Supplementary Information. The corresponding species associated spectra (SAS) are shown in solid in Fig 2.3C. The black and red spectra represent the bulk Chls and red Chls of PSI, respectively, while the blue spectrum corresponds to PSII, peaking at 680 nm.

Figure 2.3: Results of target analysis of the fluorescence decay of the PAL mutant with PSII RC in the open and closed form. Kinetic model for PSI with two pools (black and red) (A,B); Kinetic model for PSII with open RCs using two pools (A); PSII with closed RCs using three pools

(B). Note that RP (white) is non-fluorescent, thus, the corresponding target analysis provides only three spectra(C). Rate constants (ns^{-1}) are included in A and B and the estimated errors are around $\sim 20\%$.

The compartmental model shown in Fig 2.3B was used to fit the PAL data obtained with (most of) the RCs closed. In this case, two non-fluorescent radical pair states can be resolved. The obtained SAS are shown in Fig 2.3C in dash. There is rather good agreement between the spectra obtained under different conditions, i.e. with open and closed RCs.

The value of ΔG , reflecting the drop in free energy upon charge separation was calculated using detailed-balance requirements for the rates of overall charge separation and charge recombination and shown in Fig 2.3A and B, respectively. In order to compare the ΔG value in this study to those in previous reports^{19, 24, 25, 29}, we have also fitted the datasets by using the models that were proposed in ref.^{24, 25} in which the RC was separated from the antenna system as explained in the supplementary material. From the fitting quality and SAS, we conclude that those model schemes are also applicable for photosystem II *in vivo*, despite the fact that

the fitted kinetics *in vivo* are somewhat slower.

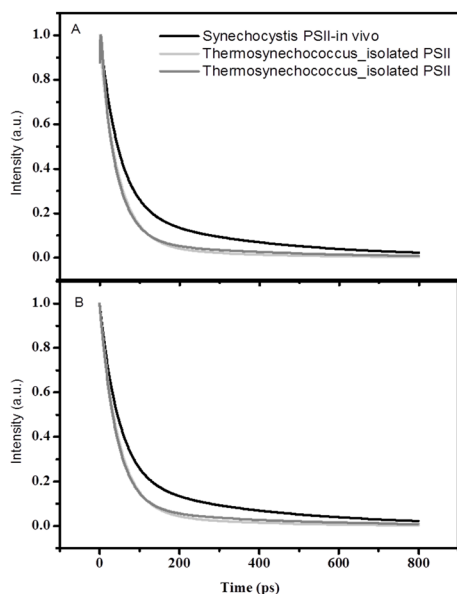


Figure 2.4: Comparison of time-resolved fluorescence of isolated PSII core complexes in the open state from refs^{24, 25} (grey-Miloslavina et al and light grey-van der Weij et al) and of PSII core complexes in the open state in the PAL mutant (black, this work). In A) the following lifetime components were included in the reconstruction: 48 ps & 351 ps—this work; 1.5 ps, 7 ps, 10 ps, 42 ps & 351 ps-Miloslavina et al; and 1.8 ps, 7 ps, 46 ps & 251 ps-van der Weij et al, while in B), only the two longest times components were included in all cases.

To visualize this difference, the PSII fluorescence results obtained in this work and in two previous studies are

compared in Fig 2.4. The curve of PSII with open RC obtained in the present work was reconstructed based on the model shown in Fig 2.3A, while two other curves are based on the models proposed by Miloslavina et al 2006²⁴ and van der Weij et al 2011²⁵, respectively. Note that in ref 19 an excitation wavelength of 663 nm was used to excite mainly the Q_y band of the Chls, while in both ref.20 and this work, an excitation wavelength of 400 nm was used to excite mainly the Soret band of Chls and some carotenoid. Here we assume that the changes of time-resolved fluorescence kinetics caused by employing different excitation wavelengths can be neglected, because the Soret to Q_y band relaxation usually takes place on the sub-ps time scale and so does the energy transfer from carotenoids to Chls⁴². The decay curve obtained by Miloslavina et al. was reconstructed based on the DAS shown in that work, with only τ_1 - τ_5 included in the calculation. The decay curve of van der Weij et al. was reconstructed based on the compartmental scheme shown in reference²⁵ and the initial excitation fractions therein. By comparing these three curves, it is seen that the *in vivo* overall decay (this study) is slower, although the lifetimes are very similar to those of Miloslavina et al., namely 44 ps and 350 ps. On the other hand, the results on the isolated PSII cores are very similar to each other, although they led to very different models to describe the results. The fact that the overall decay is slower *in vivo* is possibly due to a (small and probably unavoidable) charge gradient across the membrane or to small differences between PSII of the different organisms. Concerning the former explanation, we hypothesize that the building up of a charge gradient across the membrane makes it more difficult for electrons to move against the corresponding electric field upon charge separation, thereby slowing down the charge separation kinetics.

Time-resolved fluorescence of BE and PAL mutants at 77K

Global analysis

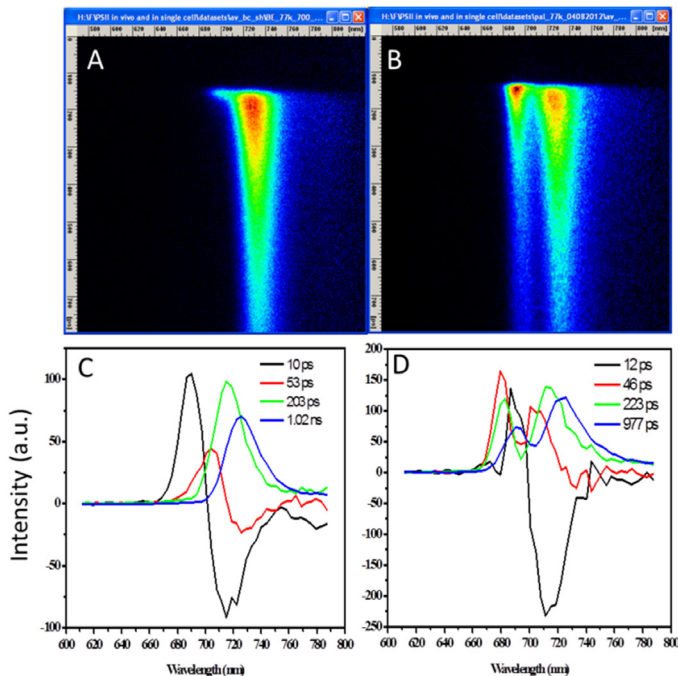


Figure 2.5: Streak images for BE cells (A) and PAL cells (B) at 77K, together with the DAS and corresponding lifetimes (C,D). The excitation wavelength is 400 nm.

The time-resolved fluorescence of the two mutants was also measured at 77K and the streak-camera images together with their corresponding DAS are shown in Figure 2.5. Four

components are necessary to get acceptable fits for both BE and PAL cells. For BE the fastest DAS of 10 ps has a positive peak at 690 nm and a negative one at 715 nm, and it carries the typical signature of an excitation energy transfer (EET) process. Similarly, also the 52 ps DAS reflects energy transfer, showing a positive peak at 700 nm and a negative one at 720 nm. The other two components of 203 ps and 1.02 ns are entirely positive and reflect fluorescence decay, either due to charge separation, or to decay to the ground- or to a triplet state. Similar measurements were reported on the isolated PSI complex in ref.⁴³ that was measured at 5K by using time-correlated single-photon counting (TCSPC) with an IRF of ~40 ps FWHM. In that case 5 lifetimes were used for closed PSI and 6 lifetimes for a ~50%/~50% mixture of P700 reduced/oxidized. Note that, the PSI complexes used by M. Byrdin et al⁴⁴ were isolated from *Synechococcus elongatus*, which contains more red pigments with different spectral characteristics than *Synechocystis*. The fastest lifetime reported is 14 ps for fully closed PSI and 18 ps

for PSI with mixed states. Both these lifetimes are close to the 10 ps that we obtain in the present work, and also the DAS are similar, although for each DAS of 14 ps and 18 ps, the area of the positive part is smaller than the area of the negative part. The second lifetime of 35-40 ps is also close to the 52 ps obtained in this work, while the other lifetime components cannot be compared directly due to the presence of extra red pigments in *Synechococcus* and the fact that the temperature difference between 4K and 77K plays a major role.

In the case of PAL four lifetimes are also needed to describe the data sets and the lifetimes are very similar to those obtained as for the BE mutant but the DAS are clearly different. The fastest DAS is far less conservative for PAL than for BE, and it contains a small dip at 680 nm. It seems that two processes taking place on a similar time scale cannot be separated in the fitting and both contribute to the fastest DAS. A similar situation occurs for the other three DAS: each DAS possesses two peaks, one being very similar to a peak observed for the PSI-containing BE mutant, while the other one apparently originates from PSII. Generally speaking, all PSI DAS found for the BE mutant are also present for the PAL mutant, but they are merged with a contribution from PSII. In previous work of van der Weij et al²⁵, time resolved fluorescence of isolated PSII core complexes from *Synechococcus* were measured at 77K. In their results, six lifetime components were used to fit the data sets. If the fastest component of 3.3 ps and the slowest one of 6 ns are not taken into account, the results are rather similar to ours, considering the lifetime values and the DAS shapes.

Table 2.1: Lifetime components obtained from global analysis of the time-resolved fluorescence data for the BE and PAL mutants under different conditions.

Sample_400 nm_exc.	Lifetimes_PSI (ps)	Lifetimes_PSII (ps)	references
BE_298K	5.4 & 27.8	N.A.	Ref. ³⁶
PAL_298K_open	4.5 & 27	62 & 386	This work
PAL_298K_closed	4.0 & 27	184 & 953	This work
BE_77K	10, 53, 203 & 1020	N.A.	This work
PAL_77K	12, 46, 223 & 977	12, 46, 223 & 977	This work

Target analysis

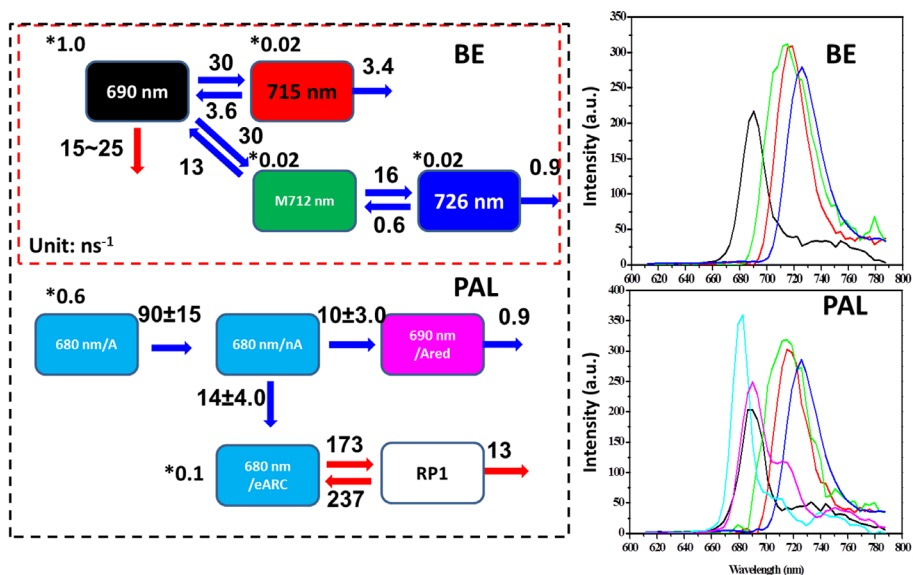


Figure 2.6: Results of target analysis of the 77K time-resolved fluorescence decay kinetics of the BE mutant and the PAL mutant. Kinetic model of BE (PSI in vivo) is shown in the upper left part and includes four pools. The estimated SAS are given in the upper-right panel; The compartment model for the PAL mutant is shown within the black dashed square: The PSI part of the PAL mutant was forced to be identical to that of the BE

mutant; The PSII model includes five pools in total: three pools of 680 nm (cyan), which have the same spectra; one pool of low energy-pigments of 690 nm (magenta); Note that, for these four pools, the name of each pool is labelled after slash (the nomenclature see ref25). And one fifth pool of RP1 (white) is non-fluorescent. The corresponding SAS are shown in the lower-right panel. Rate constants (ns^{-1}) are included in the compartmental scheme with estimated errors. The initial excitation on the 690 nm pool of PS I was set to be 1.0, while the others are given in the figure and are accompanied by an asterisk *.

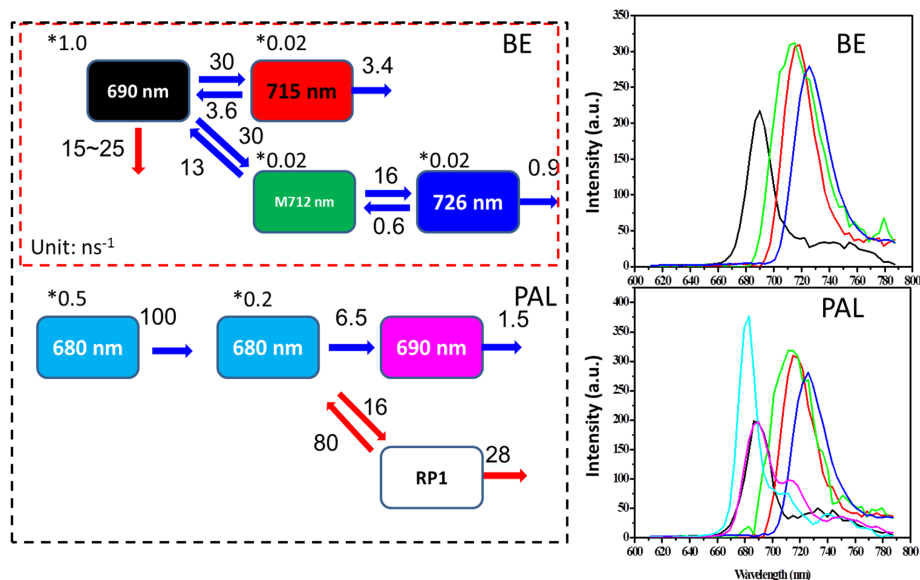


Figure 2.7: An alternative result of target analysis of the 77K time-resolved fluorescence decay of BE mutant and of PAL mutant: same layout was used as in Figure 2.6.

To obtain more information about the kinetics of PSI and PSII and to separate them for the PAL mutant, target analysis was performed. From the BE DAS results, shown in Figure 2.5, it is clear that at least four compartments are required for PSI and the fitted results show one pool of bulk Chls with a maximum at 690 nm and three pools of red pigments with maxima at 712, 715 and 726 nm. Although the first two red spectral species are very close together with their maxima separated only by 3 ± 1 nm, they can be discriminated since they show different kinetics. On the other hand, the fitting errors increase substantially when both species are forced to have the same spectrum in the fitting procedure.

There are at least three EET processes; two of them are directly apparent from

the DAS of the two fastest components, which can be directly translated into energy transfer from the bulk pigments to the 715 nm pool, and energy transfer from the 712 nm to the 726 nm pool, while a third EET process cannot be directly visualized from the DAS, but it must exist due to the large amplitude of the blue DAS that reflects the amount of excitations on 726-nm pigments. Without EET from 690 nm, there would not be such a large contribution from these low-energy pigments, which are only present in low amounts (two or three pigments out of around one hundred). In addition, a direct decay process from the 690 nm pool is required in the model, reflecting charge separation or other quenching processes from the bulk²³. As is shown in Figures 2.6 and 2.7, the SAS of the red spectral forms all have higher amplitudes than the SAS of the bulk pigments. Thus, the low-energy species possess significantly higher transition dipole strengths than the bulk-Chl bands, suggesting that they all originate from strongly coupled Chls, for instance dimers⁴⁵⁻⁴⁸. In the present target analysis we only aim at an accurate mathematical description of the PSI kinetics that can be used to fit the PSII kinetics for the PAL mutant, whilst the origin of these low-energy pigments will not be discussed further. It is for instance not completely certain whether there are indeed three red forms or whether this result is a consequence of dispersive kinetics, which may lead to extra fitting compartments at low temperature.

The obtained parameters for the PSI kinetics were kept fixed in the target analysis for the PAL mutant in order to obtain the PSII kinetics. Two models were used to fit the data: i) the transfer-to-the-trap-limited model as shown in Figure 2.6, which was proposed by van der Weij et al. in 2011²⁵, and ii) a model that is closer to the “trap-limited” model and is shown in Figure 2.7. Model i) describes nicely our dataset, although two modifications are needed with respect to the fitting results of van der Weij et al 2011²⁵: a faster energy transfer step to the low-energy pigments at 690 nm is required to maintain a similar amplitude of the low-energy SAS, (10 ns^{-1} vs. 4 ns^{-1} in ref²⁵). The other modification is that in our model a second radical pair (RP) is not required. With this model, the EET from the compartment of non-equilibrated bulk Chls (nA) to the equilibrated antenna/RC (eARC) is estimated to be around 70 ps. This value is in between the value of ~20 ps that was calculated for EET from CP43 to RC and hundreds of picoseconds that

was calculated for EET from CP47 to RC. Both values are calculated based on the X-ray structure of PSII core complex⁴⁹.

Model ii) is simpler, only four compartments are used to fit the PSII part. The model includes 1) an equilibration step of 10 ps between the majority of the pigments, 2) energy transfer to the pigments responsible for the 690 nm emission, 3) electron transfer to form the first radical pair state after which the electron can either be transferred forward or back. With this model, a number of Chls equilibrate with the RC infinitely fast, while the overall charge separation rate is rather slow (~63 ps). Comparing the two models, model i) gives a slightly lower root mean square error (rms) and the DAS calculated from this model are in good agreement with the global analysis results above, while the rms value of model ii) is slightly worse, 2.64 instead of 2.61. Although the fitting results with model 1 are slightly better, the model also contain one additional compartment which almost inevitably leads to a better fit. Therefore, we conclude that from the current *in vivo* results it is not possible to conclude whether charge separation in PSII is trap-limited or transfer-to-the-trap-limited.

The kinetics of PSI and PSII can be separated both at room temperature and at 77K, and the RC ratio of PSI and PSII is in both cases estimated to be 0.55 ± 0.10 (see Supplementary Information), which is close to the value of 0.72 ± 0.2 as reported by Stadnichuk et al⁵⁰ and ~ 0.76 , a number that we recalculated from the results provided by Krumova et al¹¹.

Conclusions

In summary, our time-resolved fluorescence results on mutant cells of *Synechocystis* pcc 6803 at room temperature show somewhat slower kinetics of the PSII core complex than reported before on isolated ones, whereas the PSI kinetics are similar in both cases. Furthermore, we conclude that the time-resolved fluorescence kinetics of PSII core complex *in vivo* can be described both with a trap-limited model and a transfer-to-the trap-limited model, even at 77K.

Acknowledgements

We thank Dr. Ghada Ajlani (CNRS, Saclay, France) for providing the mutant strains and for valuable discussion. We thank Rob B.M. Koehorst (Wageningen UR) and Arie van Hoek (Wageningen UR) for technical support.

References

- (1) Nelson, N.; Ben-Shem, A. *Nat Rev Mol Cell Bio* **2004**, *5*, 971-982.
- (2) Jordan, P.; Fromme, P.; Witt, H. T.; Klukas, O.; Saenger, W.; Krauss, N. *Nature* **2001**, *411*, 909-917.
- (3) Fromme, P.; Jordan, P.; Krauss, N. *Biochimica et biophysica acta* **2001**, *1507*, 5-31.
- (4) Umena, Y.; Kawakami, K.; Shen, J. R.; Kamiya, N. *Nature* **2011**, *473*, 55-U65.
- (5) Bricker, T. M.; Frankel, L. K. *Photosynth Res* **2002**, *72*, 131-146.
- (6) Nield, J.; Kruse, O.; Ruprecht, J.; da Fonseca, P.; Buchel, C.; Barber, J. *Journal of Biological Chemistry* **2000**, *275*, 27940-27946.
- (7) Buchel, C.; Kuhlbrandt, W. *Photosynth Res* **2005**, *85*, 3-13.
- (8) Amunts, A.; Nelson, N. *Bba-Bioenergetics* **2006**, 260-260.
- (9) Ben-Shem, A.; Frolow, F.; Nelson, N. *Nature* **2003**, *426*, 630-635.
- (10) Gobets, B.; van Grondelle, R. *Bba-Bioenergetics* **2001**, *1507*, 80-99.
- (11) Krumova, S. B.; Laptinok, S. P.; Borst, J. W.; Ughy, B.; Gombos, Z.; Ajlani, G.; van Amerongen, H. *Biophys J* **2010**, *99*, 2006-2015.
- (12) Savikhin, S. In *Photosystem I: the light-driven plastocyanin : ferredoxin oxidoreductase* J, G., Ed.; Springer, Dordrecht,: 2006; Vol. vol 24, p pp 155-175.
- (13) Wientjes, E.; Croce, R. *Photosynth Res* **2012**, *111*, 185-191.
- (14) Schatz, G. H.; Brock, H.; Holzwarth, A. R. *Proceedings of the National Academy of Sciences of the United States of America* **1987**, *84*, 8414-8418.
- (15) Schatz, G. H.; Brock, H.; Holzwarth, A. R. *Biophys J* **1988**, *54*, 397-405.
- (16) Renger, G.; Eckert, H. J.; Bergmann, A.; Bernarding, J.; Liu, B.; Napiwotzki, A.; Reifarth, F.; Eichler, H. J. *Aust J Plant Physiol* **1995**, *22*, 167-181.
- (17) Pawlowicz, N. P.; Groot, M. L.; van Stokkum, I. H. M.; Breton, J.; van Grondelle, R. *Biophysical Journal* **2007**, *93*, 2732-2742.
- (18) Vassiliev, S.; Lee, C. I.; Brudvig, G. W.; Bruce, D. *Biochemistry-Us* **2002**, *41*, 12236-12243.
- (19) Broess, K.; Trinkunas, G.; van der Weij-de Wit, C. D.; Dekker, J. P.; van Hoek, A.; van Amerongen, H. *Biophysical Journal* **2006**, *91*, 3776-3786.
- (20) Vassiliev, S.; Bruce, D. *Photosynth Res* **2008**, *97*, 75-89.
- (21) Renger, T.; Schlodder, E. *J Photoch Photobio B* **2011**, *104*, 126-141.
- (22) Croce, R.; van Amerongen, H. *J Photoch Photobio B* **2011**, *104*, 142-153.
- (23) Melkozernov, A. N.; Lin, S.; Blankenship, R. E.; Valkunas, L. *Biophys J* **2001**, *81*, 1144-1154.

- (24) Miloslavina, Y.; Szczepaniak, M.; Muller, M. G.; Sander, J.; Nowaczyk, M.; Rogner, M.; Holzwarth, A. R. *Biochemistry* **2006**, *45*, 2436-2442.
- (25) van der Weij-de Wit, C. D.; Dekker, J. P.; van Grondelle, R.; van Stokkum, I. H. M. *J Phys Chem A* **2011**, *115*, 3947-3956.
- (26) van Oort, B.; Alberts, M.; de Bianchi, S.; Dall'Osto, L.; Bassi, R.; Trinkunas, G.; Croce, R.; van Amerongen, H. *Biophys J* **2010**, *98*, 922-931.
- (27) van Oort, B.; Amunts, A.; Borst, J. W.; van Hoek, A.; Nelson, N.; van Amerongen, H.; Croce, R. *Biophysical Journal* **2008**, *95*, 5851-5861.
- (28) Tian, L. J.; van Stokkum, I. H. M.; Koehorst, R. B. M.; Jongerius, A.; Kirilovsky, D.; van Amerongen, H. *Journal of the American Chemical Society* **2011**, *133*, 18304-18311.
- (29) Broess, K.; Trinkunas, G.; van Hoek, A.; Croce, R.; van Amerongen, H. *Bba-Bioenergetics* **2008**, *1777*, 404-409.
- (30) Tian, L. J.; Gwizdala, M.; van Stokkum, I. H. M.; Koehorst, R. B. M.; Kirilovsky, D.; van Amerongen, H. *Biophys J* **2012**, *102*, 1692-1700.
- (31) Ajlani, G.; Vernotte, C. *Plant Mol Biol* **1998**, *37*, 577-580.
- (32) Elmorjani, K.; Thomas, J. C.; Sebban, P. *Archives of Microbiology* **1986**, *146*, 186-191.
- (33) Herdman, M.; Delaney, S. F.; Carr, N. G. *Journal of General Microbiology* **1973**, *79*, 233-237.
- (34) van Oort, B.; Murali, S.; Wientjes, E.; Koehorst, R. B. M.; Spruijt, R. B.; van Hoek, A.; Croce, R.; van Amerongen, H. *Chem Phys* **2009**, *357*, 113-119.
- (35) Mullen, K. M.; van Stokkum, I. H. M. *Journal of Statistical Software* **2007**, *18* (3).
- (36) van Stokkum, I. H. M.; van Oort, B.; van Mourik, F.; Gobets, B. and van Amerongen, H. In *Biophysical Techniques in Photosynthesis* ; Springer Dordrecht, 2008 Volume II, P.223-240.
- (37) van Stokkum, I. H. M.; Larsen, D. S.; van Grondelle, R. *Bba-Bioenergetics* **2004**, *1657*, 82-104.
- (38) V Chukhutsina, L. T., G Ajlani, H van Amerongen In *Photosynthesis Research for Food, Fuel and Future*; Kuang, T., Lu, C., Zhang, L., Eds.; Zhejiang University Press, Hangzhou: Beijing, 2010; Vol. Symposium 16, p 465-467.
- (39) Renger, G.; Renger, T. *Photosynthesis research* **2008**, *98*, 53-80.
- (40) van Miegheem, F. J. E.; Searle, G. F. W.; Rutherford, A. W.; Schaafsma, T. J. *Biochimica et biophysica acta* **1992**, *1100*, 198-206.
- (41) van Grondelle, R. *Biochimica et biophysica acta* **1985**, *811*, 147-195.
- (42) Gobets, B.; van Stokkum, I. H. M.; van Mourik, F.; Dekker, J. P.; van Grondelle, R. *Biophys J* **2003**, *85*, 3883-3898.
- (43) Byrdin, M.; Rimke, I.; Schlodder, E.; Stehlik, D.; Roelofs, T. A. *Biophys J* **2000**, *79*, 992-1007.
- (44) Gobets, B.; van Stokkum, I. H. M.; Rogner, M.; Kruij, J.; Schlodder, E.; Karapetyan, N. V.; Dekker, J. P.; van Grondelle, R. *Biophys J* **2001**, *81*, 407-424.
- (45) Wientjes, E.; van Stokkum, I. H. M.; van Amerongen, H.; Croce, R. *Biophys J* **2011**, *101*, 745-754.

- (46) Hayes, J. M.; Matsuzaki, S.; Ratsep, M.; Small, G. J. *J Phys Chem B* **2000**, *104*, 5625-5633.
- (47) Ratsep, M.; Johnson, T. W.; Chitnis, P. R.; Small, G. J. *J Phys Chem B* **2000**, *104*, 836-847.
- (48) Wientjes, E.; van Stokkum, I. H. M.; van Amerongen, H.; Croce, R. *Biophys J* **2011**, *100*, 1372-1380.
- (49) Raszewski, G.; Renger, T. *J Am Chem Soc* **2008**, *130*, 4431-4446.
- (50) Stadnichuk, I. N.; Lukashev, E. P.; Elanskaya, I. V. *Photosynth Res* **2009**, *99*, 227-241.

Supplementary Information

Comparison between the streak-camera data and the TCSPC data of the PAL mutant with fully open RCs of PSII *in vivo*

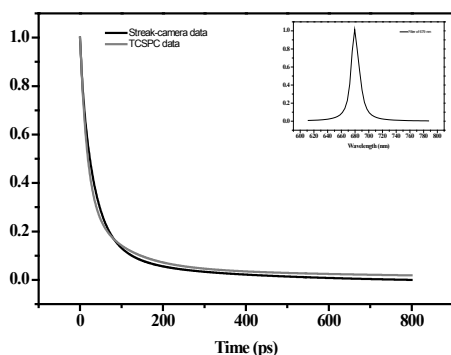


Figure S2.12: The streak camera data and the TCSPC data. To compare the decay curves fairly, both datasets were reconstructed based on the fitting results without including the IRFs. At the same time, the streak-camera data was calibrated by multiplying the DAS with the transmission spectrum (indicated as inset) of the 679 nm interference filter that was used in the TCSPC measurements, thus making

sure that only the emitted photons within that wavelength interval were counted. Measuring conditions: a) TCSPC, laser power-17 μW , $\lambda_{\text{exc}} = 440 \text{ nm}$, with 679 nm interference filter added in front of the detector; b) Streak camera, laser power-10 μW , $\lambda_{\text{exc}} = 400 \text{ nm}$. Note that in the TCSPC measurement, the excitation spot is ~ 100 times bigger than in the streak-camera experiments, which ensures that the intensity is low enough to keep the RCs fully open.

In general, the results obtained with the two setups are very similar to each other, although the TCSPC data is slightly faster in the beginning. They are also slower than the kinetics observed for PSII cores isolated from *Synechococcus elongatus* (see the main manuscript of this work).

Target analysis

To complete a fair comparison between the time-resolved fluorescence decay of PSII with open RCs in our paper and in previously published articles, we have fitted our results to the same model schemes as proposed by van der Weij et al. in 2011¹ and Miloslavina et al. in 2006², respectively. Interestingly, all the models listed below can provide equally good fits of the data.

Model I by van der Weij et al. in 2011

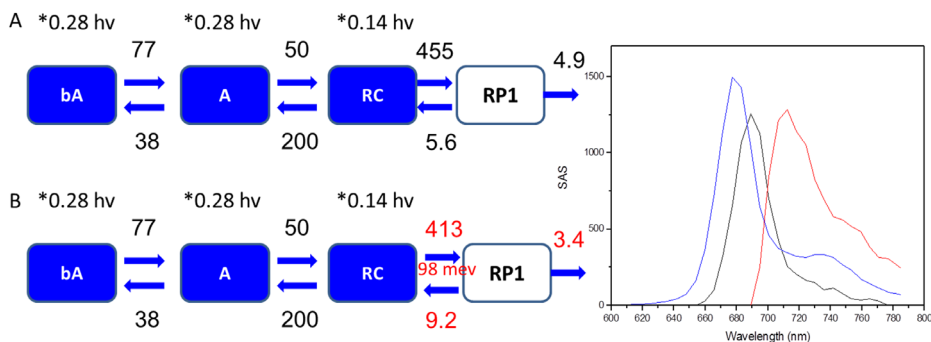


Figure S2.213: Model with slow EET from CP43/47 to RC. The model A represents the compartmental model used by van der Weij et al. in 2011 together with the EET/CS rates. The model B is used on the data set obtained in this work, with several EET transfer rates fixed (in black) while the charge-transfer rates and charge recombination rates were left free (in red). The obtained SAS are shown on the right.

As shown in Figure S2.2, the primary charge separation rate of 413 ns^{-1} is almost identical to the reported value of 455 ns^{-1} by Van der Weij et al., but the charge recombination rate is faster, while the second charge separation rate is slower. The calculated ΔG is -98 meV which is smaller than the on reported by Van der Weij et al. in 2011, namely, -110 meV .

Model II by van der Weij et al. in 2011

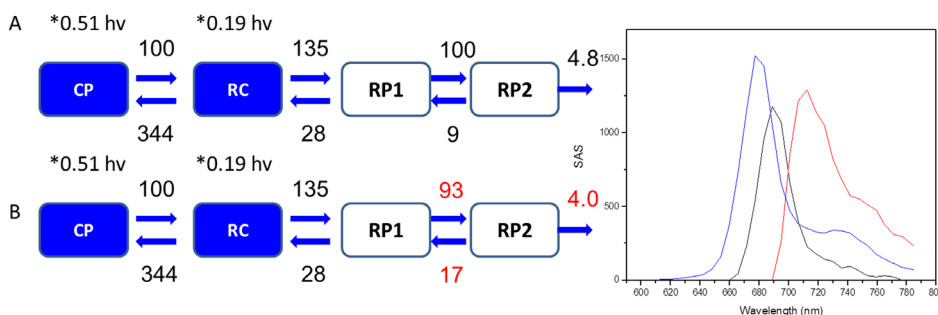


Figure S2.314: Models with fast equilibration between core antenna and RC. Model A) is reported in ref C.D. van der Weij et al. in 2011. Model B) shows the fitting results of the dataset in this work.

As the fitting results in Figure S2.3 show, the free fitting values in model B) are very close to their corresponding ones in model A), the main change concerns the charge recombination rate from RP2 to RP1, which is almost doubled in B).

Model proposed by Miloslavina et al. in 2006

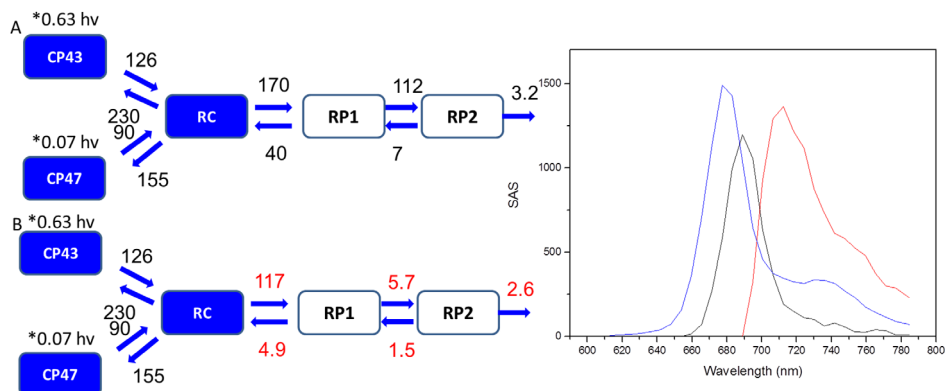


Figure S2.415: Model with fast equilibration between core antenna and RC with CP43 and CP47 separated in the model (their spectra were forced to be same).

With this model (Figure.S2.4), it seems that the second RP is not needed when the RC is open *in vivo*, since the rate of charge recombination is far slower than the primary charge separation rate.

Probing the Picosecond Kinetics of the Photosystem II Core Complex in vivo

Sample_400 nm_exc.	PSI			PSII			PSI/PSII ratio (PSI-96 pigments;PSII-35 pigments)	
	PSI_bulk	PSI_red						
BE_298K	1.0	0.06			N.A.			N.A.
PAL_298K_open	1.0	0.06			Ant*RC*		RP1	0.55
					0.7		0.0	
PAL_298K_closed	1.0	0.06			Ant*RC*	RP1	RP2	0.55
					0.7	0.0	0.0	
BE_77K	1.0	712 nm	715 nm	726 nm	N.A.			N.A.
		0.02	0.02	0.02				
PAL_77K_Model I	1.0	0.02	0.02	0.02	Ant*RC*	RP1	690 nm	0.55
					0.7	0.0	0.0	
PAL_77K_Model II	1.0	0.02	0.02	0.02	Ant*RC*	RP1	690 nm	0.55
					0.7	0.0	0.0	

Table S2.1: Input values for target analysis of BE and PAL mutants, and the calculated PSI/PSII ratios.

Based on these initial energy inputs in PSI and in PSII, we can roughly estimate the PSI/PSII RC ratio in the PAL mutant. In view of the number of Chls ~96 per PSI core vs ~35 per PSII core^{3,4}, a RC ratio of PSI/PSII of $\sim 0.55 \pm 0.10$ was calculated. The error bar of ± 0.10 is estimated based on different repeated measurements and tested models.

All constraints used in the target analysis in the main text

Constraints in general:

- 1) Energy input on each pool is fixed in the fitting, values were listed in Table S2.1;
- 2) Spectra shape constraints---skewed Gaussian shape was used for all the SAS spectra⁵;
- 3) Zero constraint—Amplitudes of SAS were forced to be zero over all wavelength for pools of radical pair (RP) in Figure 2.3, Figure 2.6&2.7. Specific constraints for target analysis 1 (at room temperature)—Figure 2.3:
- 4) Red SAS of open RC as shown in Figure 2.3 was forced to be zero up to 670 nm;
- 5) Rate constants for PSI were fixed to their corresponding values in the PSI model as described before in ref 6&7^{6,7}. Specific constraints for target analysis 2 (model I at 77K)—Figure 2.6:
- 6) In model of BE mutant, energy transfer rates from pigments_690 nm to pigments_715 nm and to pigments_712 nm were forced to be same, which enable us to provide a mathematical description of the PSI kinetics

at 77K;

- 7) Parameters of PSI in PAL mutant were fixed based on the model of BE mutant at 77K ;
- 8) Three pools of 680 nm (cyan) in the PSII branch in PAL mutant were forced to have the same spectra.

Specific constraints for target analysis 3 (model II at 77K)—Figure 2.7:

- 9) Same to 6);
- 10) Same to 7);
- 11) Two pools of 680 nm (cyan) in the PSII branch in PAL mutant were forced to have the same spectra.

Reference:

- (1) van der Weij-de Wit, C. D.; Dekker, J. P.; van Grondelle, R.; van Stokkum, I. H. M. *J Phys Chem A* **2011**, *115*, 3947-3956.
- (2) Miloslavina, Y.; Szczepaniak, M.; Muller, M. G.; Sander, J.; Nowaczyk, M.; Rogner, M.; Holzwarth, A. R. *Biochemistry-Us* **2006**, *45*, 2436-2442.
- (3) Jordan, P.; Fromme, P.; Witt, H. T.; Klukas, O.; Saenger, W.; Krauss, N. *Nature* **2001**, *411*, 909-917.
- (4) Umena, Y.; Kawakami, K.; Shen, J. R.; Kamiya, N. *Nature* **2011**, *473*, 55-60.
- (5) van Stokkum, I.H.M.; Larsen, DS; van Grondelle,R.; *Biochimica et Biophysica Acta (BBA)-Bioenergetics*,2004, 1657 (2), 82-104.
- (6) Chukhutsina, V.; Tian, L.; Ajlani, G.; van Amerongen, H.; in *Photosynthesis Research for Food, Fuel and Future*, eds. T. Kuang, C. Lu and L. Zhang, Zhejiang University Press, Hangzhou, Beijing, 2010, pp. 465-467.
- (7). Tian, L.; van Stokkum, I. H. M.; Koehorst, R. B. M.; Jongerius, A.; Kirilovsky, D. and van Amerongen, H.; *J.Am. Chem. Soc.*, 2011, **133**, 18304-18311.

Chapter 3

Site, rate and mechanism of photoprotective quenching in cyanobacteria

This chapter is based on:

Lijin Tian, Ivo H.M. van Stokkum, Rob B.M. Koehorst, Aniek Jongerius, Diana Kirilovsky and Herbert van Amerongen

***Journal of the American Chemical Society* 133 (45), 18304-18311**

Abstract

In cyanobacteria, activation of the Orange Carotenoid Protein (OCP) by intense blue-green light triggers photoprotective thermal dissipation of excess absorbed energy leading to a decrease (quenching) of fluorescence of the light harvesting phycobilisomes and concomitantly, of the energy arriving to the reaction centers. Using spectrally-resolved picosecond fluorescence we have studied cells of wild-type *Synechocystis sp.* PCC 6803 and of mutants without and with extra OCP (Δ OCP and OverOCP) both in the unquenched and quenched state. With the use of target analysis we managed to spectrally resolve seven different pigment pools in the phycobilisomes and photosystems I and II, and to determine the rates of excitation energy transfer between them. In addition, the fraction of quenched phycobilisomes and the rates of charge separation and quenching were resolved. Under our illumination conditions, $\sim 72\%$ of the phycobilisomes in OverOCP appeared to be substantially quenched. For wild-type cells this number was only $\sim 29\%$. It is revealed that upon OCP activation, a bilin chromophore in the core of the phycobilisome, here called $\text{APC}_{660}^{\text{Q}}$, with fluorescence maximum at 660 nm, becomes an effective quencher that prevents more than 80% of the excitations in the phycobilisome to reach Photosystems I and II. The quenching rate of its excited state is extremely fast, i.e. at least $(\sim 240 \pm 60 \text{ fs})^{-1}$. It is concluded that the quenching is most likely caused by charge transfer between $\text{APC}_{660}^{\text{Q}}$ and the OCP carotenoid hECN in its activated form.

Introduction

Too much light can be lethal for photosynthetic organisms and it can for instance induce photo-oxidative damage of the reaction centers (RCs) ¹⁻³. To protect themselves, plants, algae and cyanobacteria have evolved protective mechanisms such as non-photochemical quenching (qE in plants and qE_{cya} in cyanobacteria) to dissipate excess excited-state energy as heat⁴⁻⁶. The occurrence of qE_{cya} in the cyanobacterium *Synechocystis sp.* PCC 6803 (hereafter called *Synechocystis*) and the involvement of the large extra-membrane cyanobacterial antenna, the phycobilisome (PB) was first suggested by El Bissati et al. using strong blue-green light⁷. Later the action spectrum for qE_{cya} reported by Rakhimberdieva et al.⁸ in a PSII-deficient mutant of *Synechocystis* suggested that blue-green light-activated

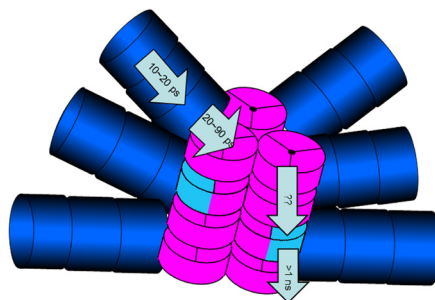
carotenoids were involved in this mechanism. The involvement of the orange carotenoid protein (OCP) in qE_{cya} was next identified by Wilson et al.⁹, and it was found that a reversible conformational change of OCP from its inactive orange form (OCP^0) to its active red form (OCP^r), triggered by blue-green light is responsible for qE_{cya} ¹⁰. The conformational change is accompanied by a red shift of the absorption maximum of the OCP pigment, 3'-hydroxyechinenone (hECN)¹⁰. The activation of the OCP is a very low quantum yield reaction and it is light intensity dependent¹⁰. Only the OCP^r can bind to the PB and trigger the quenching of the PB¹¹. Another protein called the Fluorescence Recovery Protein (FRP) is essential to recover the full antenna capacity under low-light conditions after exposure to high irradiance. This protein by interacting with OCP^r , induces its conversion to OCP^0 and helps the detachment of the OCP from the PB^{11,12}. The process of qE_{cya} was investigated in numerous studies during the past few years⁸⁻²⁰.

Genes encoding for homologues of the *Synechocystis* OCP are present in most PB-containing cyanobacteria and all these strains are able to perform qE_{cya} ¹⁷. The quenching efficiency depends on the concentration of OCP. This was demonstrated by studying a mutant over-expressing OCP (OverOCP), that shows more quenching than the wild-type (WT) under the same high-light condition and a mutant not capable of synthesizing OCP (ΔOCP), which shows no quenching at all^{9,10}. Note that in WT cells grown at low- or medium-light conditions the number of OCP's is lower than the number of PBs and presumably not all PBs can be quenched²¹. Nevertheless, even under these conditions, the qE_{cya} mechanism is photoprotective. The ΔOCP *Synechocystis* mutant is more sensitive to high-light conditions than the WT⁹. Moreover, cyanobacteria strains containing the OCP are more resistant to photoinhibition than strains lacking the OCP and the qE_{cya} mechanism¹⁷. Under stress conditions, like iron starvation, the ratio OCP to phycobilisomes increases inducing a much larger energy and fluorescence quenching rendering the cells more resistant to environmental changes¹⁶. The fluorescence recovery depends on the FRP to OCP ratio¹¹. Thus in WT cells total fluorescence recovery is reached in only 10 min while in the overOCP strain more than 30 min are needed to recover the full antenna capacity at 32°C. In

addition, this reaction is largely temperature dependent: Below 10 °C almost no recovery is observed^{10,14}.

In *Synechocystis*, the light-harvesting PB contains six C-phycocyanin (C-PC) rods and three allophycocyanin (APC) core cylinders. Each C-PC rod is composed of three hexamer disks with a maximum absorbance at 620 nm and maximum fluorescence at 640-650 nm. Each APC cylinder contains four trimer disks with maximum absorbance at 650 nm. The two APC cylinders which are closest to the membrane contain two trimer discs formed by 3 $\alpha\beta$ APC emitting at 660 nm (APC₆₆₀) and two trimers in which one of the α or the β APC subunits is replaced by a special subunit, ApcD, ApcF or ApcE, emitting at 680 nm (APC₆₈₀). These terminal emitters function as spectral bridges between PB and photosystems. The third APC cylinder contains only $\alpha\beta$ APC trimers emitting at 660 nm. All of these pigment-proteins (phycobiliproteins) are bound together by several types of linker peptides²²⁻²⁶. PBs form a rather efficient antenna system, funneling more than 90% of the captured energy via APC₆₈₀ to the lower energy Chls within PSI and PSII, where the photochemical reactions are performed^{22,23,27,28}. A schematic overview of the PB organization is given in Fig. 3.1 together with a global description of previously resolved excitation energy transfer times in *Synechocystis*^{13,26,29,30}.

Figure 3.1: Schematic representation of a *Synechocystis* sp. PCC 6803 PB and previously determined excitation energy transfer times. Dark blue corresponds to C_PC (emitting at 640~650 nm), magenta to APC₆₆₀ (emitting at 660 nm) and cyan to APC₆₈₀ (emitting at ~680 nm). The longest lifetime corresponds to decay to the ground state.



It is already known that qE_{cy} does not occur in the outer rods that contain the C-PC pigments thanks to various mutant studies^{8,13,15,18}. This has just been confirmed by *in vitro* reconstitution experiments showing that OCP^r can bind to PB containing only the core, thereby completely quenching its fluorescence. In contrast, OCP^r is unable to quench the fluorescence of PB containing only PC rods¹¹. Therefore, the quenched species should be either an APC₆₆₀ or an APC₆₈₀ pigment in the APC core^{18,20}. It is one of the goals of the present study to find out

where exactly in the PB qE_{cya} takes place. The differences in the fluorescence maxima of the various pigments should facilitate the analysis of the ultrafast fluorescence data sets and enable the identification of the quenching site.

qE_{cya} is accompanied by a spectral and conformational change of the carotenoid hECN bound to OCP but it is unknown what the molecular quenching mechanism is. By comparing the spectrally resolved picosecond fluorescence kinetics in the presence and absence of qE_{cya} we intend to determine the rate of quenching which should then hopefully shed light on the underlying physical mechanism, which is also still unknown.

We have performed picosecond fluorescence measurements on *Synechocystis* WT cells and cells of the OverOCP and Δ OCP mutants in a) the unquenched state, b) the quenched state and c) the state after recovering from quenching. A compartmental model was constructed to describe excitation-energy transfer and trapping in *Synechocystis* using target analysis. From the target analysis it was concluded where qE_{cya} takes place and what the (molecular) rate of quenching is. This also allowed us to draw conclusions about the mechanism of quenching and to calculate which percentage of the PB excitations reach PSI and PSII in the presence of qE_{cya} .

Materials and Methods

Strains and growth conditions

The construction of the mutants without OCP protein (Δ OCP) and with over-expressed OCP protein (OverOCP) was described before (for details see ^{9,10}).

WT and mutant cells were grown photoautotrophically in a modified BG11 medium³¹ containing also 10 mM NaHCO_3 and twice the concentration of sodium nitrate. Cells were shaken in a rotary shaker (45 rpm) at 30°C and illuminated by white lamps at $40 \mu\text{mol}\cdot\text{m}^{-2}\cdot\text{s}^{-1}$. Mutants were grown in the presence of antibiotics (spectinomycin $25 \mu\text{g}\cdot\text{ml}^{-1}$, streptomycin $10 \mu\text{g}\cdot\text{ml}^{-1}$). All cells were grown in 250-ml flasks with a growing volume of 60 ml, and maintained in the logarithmic growth phase with optical densities at 800 nm (OD_{800}) between 0.6 and 0.8 (scattering) by refreshing the medium every two-three days.

To improve the signal-to-noise ratio of the time-resolved fluorescence measurements cell suspensions were concentrated 3-5 times. The final suspensions were dark-adapted for 5 minutes before performing the fluorescence measurements.

Fluorescence measurements

Steady-state fluorescence

Steady-state fluorescence spectra were recorded with a Jobin Yvon Fluorolog FL3-22 spectrofluorimeter and corrected for wavelength-dependent sensitivity of the detection and fluctuations in lamp output. The excitation wavelength was 590 nm; a band width of 5 nm was used for excitation and emission. Fluorescence emission spectra were recorded using a step size of 0.5 nm. Cell suspensions were diluted to a final Chl concentration of 1.0 $\mu\text{g/ml}$ and measured in a cuvette with a 3-mm light path to avoid significant self-absorption. Cells were quenched by illuminating with 500 nm light at $\sim 220 \mu\text{E}\cdot\text{m}^{-2}\cdot\text{s}^{-1}$ for 10 minutes at 20°C and emission spectra were recorded immediately after quenching.

Time-resolved fluorescence

Time-resolved fluorescence spectra were recorded with a sub-picosecond streak-camera system combined with a grating (50 grooves/mm, blaze wavelength 600 nm) with the central wavelength set at 700 nm, having a spectral width of 260 nm (for details see³²). Excitation light was vertically polarized, the spot size diameter was typically $\sim 100 \mu\text{m}$ and the laser repetition rate was 250 kHz. The detector polarizer was set at magic angle orientation. Great care was taken to minimize the path length (typical $\sim 100 \mu\text{m}$) to allow measurements on high-concentration samples ($\text{OD}_{680} > 3$) without significant self-absorption. Two excitation wavelengths were used: 590 nm and 400 nm. To avoid photodamage and to induce $q\text{E}_{\text{cyt}}$ in the entire cuvette (see below), the sample was stirred with a magnetic stirring bar (rate $\sim 10 \text{ Hz}$) and the laser power at 590 nm was adjusted to $15 \pm 3 \mu\text{W}$. At 400 nm, the power was adjusted to $\sim 30 \pm 3 \mu\text{W}$. Images of 800 ps and 2 ns time windows were obtained for each sample and corrected for background and photocathode shading, and then sliced up into traces of 4 nm width.

For both excitation wavelengths, the instrument response function (IRF) was described with a double Gaussian, consisting of a Gaussian of ~ 9 ps FWHM (90% of IRF area) on top of a Gaussian of 100 ps FWHM (10% of IRF area).

For measuring time-resolved fluorescence of cells during quenching, an actinic white light source was used in combination with a 500 nm broad band filter (K50) giving an intensity of $\sim 350 \mu\text{E}\cdot\text{m}^{-2}\cdot\text{s}^{-1}$. The volume used for fluorescence excitation/detection was spatially well separated from the actinic light beam (a cylinder of ~ 5 mm diameter*1 cm length); the entire volume of the sample was 4 ml. One measurement was performed as follows: First, after 5 minutes of dark adaptation of the cells, fluorescence streak images were recorded for unquenched cells. Then cells were quenched by actinic illumination at 20°C for one hour (to obtain the maximal quenching possible at the light intensity used) while stirring; during subsequent measurements on quenched cells, the actinic illumination was kept on to maintain the quenched state. Finally, streak images were recorded after allowing the cells to fully recover from qE_{cya} for one hour in the dark. At 20°C, fluorescence recovery is slower than at 32°C and for the overOCP strain it can take almost one hour. ΔOCP , being the perfect control sample because it does not show qE_{cya} , was measured in exactly the same way as WT and Over OCP cells. A high signal-to-noise ratio was achieved by averaging 100 single images, each obtained after analog integration of 10 exposures of 1.112 s. Measurements were performed at room temperature (about 20°C) and lasted 3 hours for each sample.

Data analysis

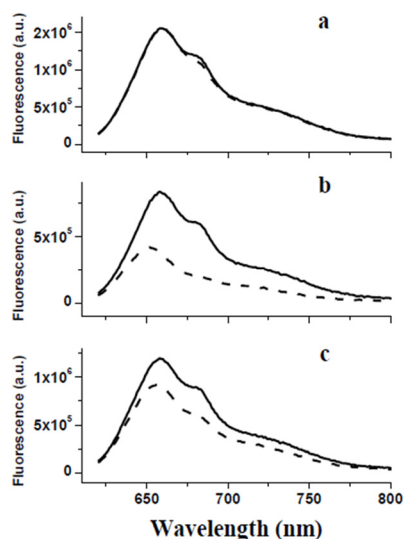
Data obtained with the streak-camera setup were first globally analyzed with the R package TIMP (for details see ^{33,34}). The methodology of global analysis is described in ³⁵: with global analysis the data were fitted as a sum of exponential decays convolved with an IRF and the amplitudes of each decay component as a function of wavelength are called decay-associated spectra (DAS). Subsequently ‘target analysis’ was performed as described in the supporting information.

Results

Steady-state fluorescence

Steady-state fluorescence spectra of unquenched cells of WT, OverOCP, and Δ OCP were recorded upon 590 nm excitation (Fig. 3.2). The spectra are very similar for all unquenched cells, showing two main peaks at 660 nm and 680 nm. The 660 nm maximum originates from APC₆₆₀ and the one at 680 nm from APC₆₈₀ and/or Chl. Fig. 3.2 also shows the spectra after 10 minutes of illumination with 220 $\mu\text{E}\cdot\text{m}^{-2}\cdot\text{s}^{-1}$ blue-green light. For WT cells, this causes $\sim 20\%$ fluorescence quenching, while for OverOCP more than 50% quenching occurs. As expected, no quenching is observed for Δ OCP cells.

Figure 3.2: Room-temperature fluorescence spectra upon 590 nm excitation of cells. (1 μg Chl/mL) before (solid lines) and after (dashed lines) blue-green light illumination (220 $\mu\text{E}\cdot\text{m}^{-2}\cdot\text{s}^{-1}$), (a) Δ OCP, (b) OverOCP, (c) WT.



Time-resolved fluorescence

To determine the quenching kinetics, time-resolved fluorescence of mutant and WT cells were measured with a picosecond streak-camera system. The cells were studied in three different states: before illumination (unquenched), after illumination with strong quenching-inducing light (quenched) (illumination is continued during the measurement) and 1 hour after switching off the quenching light (recovered). Either 590 nm laser pulses were used, exciting mainly C-PC (Figs 3.3a b), or 400 nm pulses, exciting mainly Chls in PSI and PSII (Figs 3.3c d). Fig.3.3a shows that the spectrum is shifting to longer wavelengths in time (red-shifting) after 590 nm excitation, which is due to down-hill excitation energy transfer (EET). In contrast, Fig.3.3c shows that after 400 nm excitation the spectrum is slightly blue-shifting (indicated by the black arrow). The blue-shift is due to the fact that long-wavelength PSI fluorescence is shorter-lived than PSII fluorescence that

contributes more at shorter wavelengths. A comparison of Figs.3.3a and 3.3b clearly shows that the fluorescence of unquenched OverOCP (Fig.3.3a) is longer-lived than that of quenched OverOCP (Fig.3.3b). The WT cells also show faster decay of the excited state after induction of qE_{cya} , albeit less pronounced. The quenching appears to be completely reversible, meaning that the fluorescence streak images of cells that are recovered from qE_{cya} are virtually identical to the ones before qE_{cya} . As expected, no significant changes are observed for the ΔOCP cells. Upon 400 nm excitation, the effects of qE_{cya} are far less noticeable for all cell types and only a minor decrease in intensity can be observed on the short-wavelength side for WT and OverOCP cells, where PBs dominate the fluorescence.

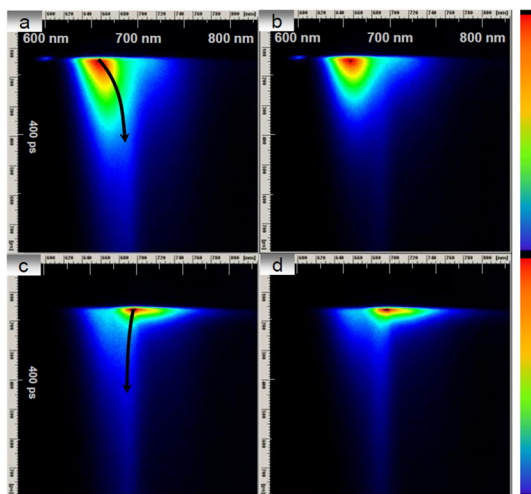


Figure 3.3: Streak-camera images of unquenched (a,c) and quenched (b,d) OverOCP cells. These images represent the fluorescence intensity (using a linear color gradient) as a function of time (vertical axis) and wavelength (horizontal axis); every vertical line represents a time trace of fluorescence at the corresponding wavelength, while every horizontal line reflects a fluorescence emission spectrum after a certain delay time. In a and b, C-Phycocyanin was selectively excited at 590 nm and in c and d, Chls were selectively excited at 400

nm; all time-resolved fluorescence measurements represented in this work were repeated at least three times with cells grown on different days.

Modeling results

To get quantitative information from these images, both global analysis and target analysis were performed. Global analysis provides a minimal mathematical description of the data revealing the wavelength dependence of EET and excitation trapping. Based on this kinetic information, combined with *a priori* knowledge of the photosynthetic system, target analysis was used to construct a

specific compartmental model with corresponding rate constants to obtain a realistic description of the system. By exploring the model that fits best to the data, kinetic constants for the various processes (energy transfer, trapping and quenching) could be determined.

Global analysis

OverOCP

Typical unquenched (black) and quenched (red) traces for excitation at 590 nm are depicted in Fig.3.4 and quenching appears to be particularly well visible at 662 and 683 nm.

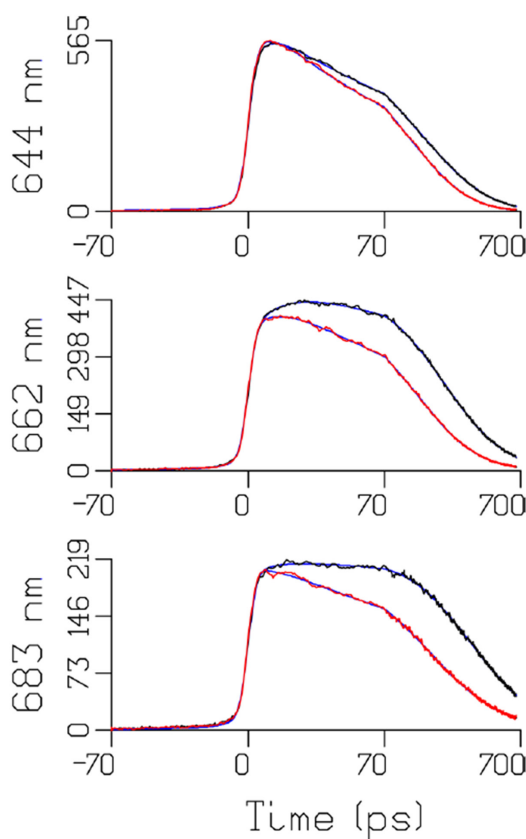


Figure 3.4: Emission traces at 644, 662, and 683 nm of unquenched (black) and quenched (red) OverOCP upon 590 nm excitation. Note that the time axis is linear until 70 ps, and logarithmic thereafter. Blue lines indicate the global analysis fit with five lifetimes.

Global analysis of 50 emission traces of OverOCP cells reproducibly required five lifetimes. The results are shown in Fig.3.5a and corresponding lifetimes are given in Table 3.1. Induction of qE_{cya} by strong blue-green light leads to marked changes of several DAS. After switching off the blue-green light, quenching effects disappeared

completely in approximately 1 hour at 20°C, demonstrating the reversibility of

qE_{cya} . After cells had “recovered” from qE_{cya} , the DAS were identical to those before qE_{cya} .

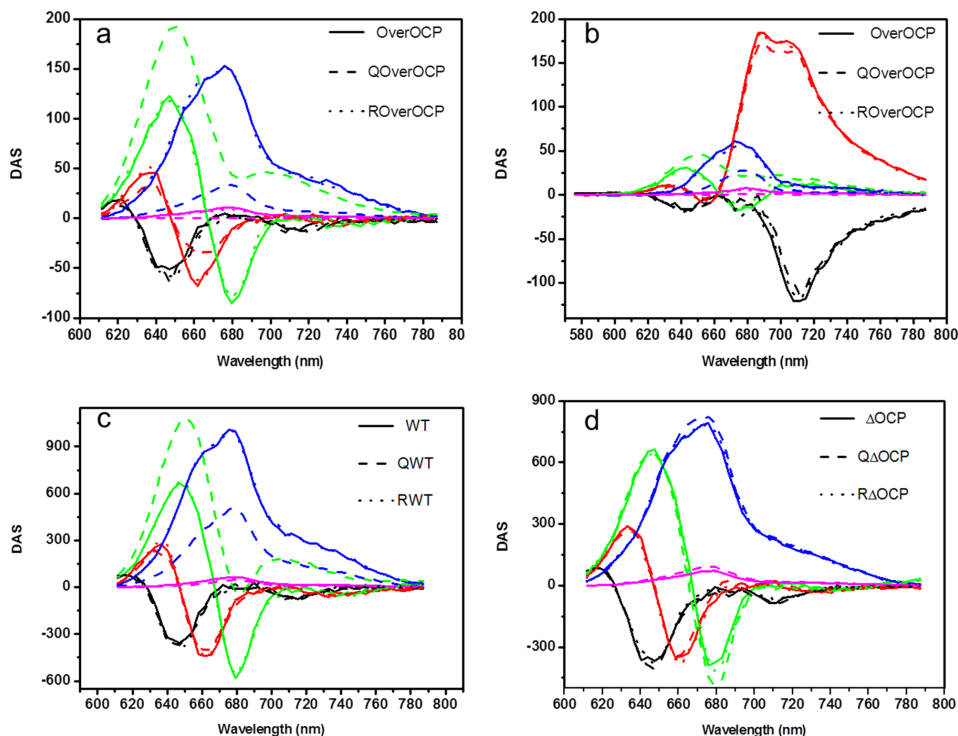


Figure 3.5: DAS of intact cells. OverOCP (a,b), WT (c), and Δ OCP (d), after 590 nm (a,c,d) or 400 nm excitation (b). Spectra correspond to ‘unquenched’ (solid), ‘quenched’ (dashed), labeled with Q or ‘recovered’ cells (dotted), labeled with R.

The black DAS in Fig 3.5 reflect excitation equilibration (predominantly downhill EET) in C-PC with a time constant of 8 ps, displaying a positive/negative signature, characteristic for energy transfer. The acceptor states have a higher dipolar strength than the donor states (see e.g.³⁶) leading to a predominantly negative DAS. These DAS and their corresponding lifetimes remain unaltered upon qE_{cya} induction, showing that the corresponding transfer process is not influenced by quenching.

Lifetimes (ps)	λ_{ex}	tau 1	tau 2	Tau 3	tau 4	tau 5
OverOCP/ROverOCP	590 nm	8	36	128	204	>500 ps
QOverOCP	590 nm	8	26	105	301	>500 ps
OverOCP/ROverOCP	400 nm	6	22	134	232	>500 ps
QOverOCP	400 nm	6	23	120	367	>500 ps
WT/RWT	590 nm	9	39	122	195	>500 ps
QWT	590 nm	8	36	116	239	>500 ps
Δ OCP/Q Δ OCP/R Δ OCP	590 nm	8	38	121	205	>500 ps

Table 3.1: lifetimes estimated from global analysis of the fluorescence data obtained for the various cells in different states. The colors of the lifetimes correspond to the colors of the DAS in Fig. 3.5. And the samples were named the same as in Fig. 3.5.

The red DAS with ~30 ps lifetime to a large extent reflect downhill EET from C-PC to APC₆₆₀. They are only slightly influenced by quenching because the changes in lifetime and DAS are rather small, especially when compared to the changes observed for the slower components.

The green DAS for unquenched and recovered cells with a lifetime of 130 ps reflect to a large extent EET from APC₆₆₀ to APC₆₈₀ + Chls. Like the ~30 ps component, they have the characteristic conservative shape with positive amplitude at short wavelengths and negative amplitude at longer wavelengths, meaning that excited-state population disappears from pigments fluorescing somewhat above 650 nm to pigments with a fluorescence maximum somewhat below 680 nm. This component is strongly influenced by the quenching; the lifetime decreases and the shape changes drastically. It loses its characteristic conservative transfer character, indicating that excitations on APC₆₆₀ are quenched, and this leads to a shortening of the APC₆₆₀ excited-state lifetime and a decrease in energy transfer. From these DAS it is not directly clear which percentage of the APC pigments is quenched and what the quenching rate is. These issues will be addressed below using the target analysis approach.

The dark blue DAS with 200~300 ps lifetime reflect excitation trapping by the RCs (charge separation). The DAS represents an equilibrated excitation distribution over C-PC, APC₆₆₀, APC₆₈₀ and Chls. Upon induction of qE_{cyt} the intensity of this

component decreases drastically, due to the fact that many excitations are already quenched on APC₆₆₀ before they can reach APC₆₈₀ and Chls.

The cyan DAS with lifetimes above 500 ps have very small amplitudes. The lifetime is not well determined using the 800 ps time window; it can be varied from 600 ps to a few ns in the fit without influencing shape and position of the DAS. In datasets obtained with a 2 ns time window the corresponding lifetime was determined to be ~700 ps. These DAS probably reflect competition between secondary charge separation and charge recombination (see e.g. ³⁷), which explains why its amplitude decreases upon quenching.

Global analysis of the results that are obtained upon 400 nm excitation, leads to the DAS that are shown in Fig.3.5b. Using 400 nm pulses, excitations are mainly created in PSI and PSII and only 10% is created in PB ³⁰, leading to the fluorescence on the short-wavelength side of the image. The latter excitations give rise to the same DAS and quenching kinetics as the excitations created by 590 nm laser pulses (see Fig.3.5b). The dominating component of 22 ps (red DAS in Fig.3.5b) represents emission from Chls in PSI ^{30,38,39}, which appears to be hardly quenched.

WT and ΔOCP

The DAS that are obtained for unquenched WT and ΔOCP cells (see Fig.3.5c and 3.5d, respectively) are virtually identical to those obtained for unquenched OverOCP cells. This shows that the organization of the photosynthetic system is identical in all cases, but also it testifies to the high reproducibility of both measurement and analysis. The fluorescence kinetics of ΔOCP cells are hardly affected by illumination with strong blue-green light but for WT cells similar changes are induced as for OverOCP cells, although the effects of qE_{cya} are less pronounced. EET within the C-PC rods and from C-PC to APC are nearly unaffected in WT cells since the 2 DAS with the shortest lifetimes remain nearly the same. The 3rd DAS, which is conservative in the absence of quenching, becomes strongly non-conservative, again reflecting quenching of APC₆₆₀. However, the strong dip around 680 nm indicates that still a substantial amount of EET towards APC₆₈₀ and Chls takes place, also explaining why the 4th and 5th DAS decrease less in intensity for WT than for OverOCP. It is not immediately clear whether a larger fraction of

PB remains unquenched as compared to OverOCP or whether the quenching rate is smaller. This issue will be addressed below.

In summary, global analysis of the presented time-resolved fluorescence data indicates that APC₆₆₀ is quenched directly *in vivo*. However, it is not clear which fraction of the PB is quenched and what the rate of quenching is. In order to resolve these issues, target analysis was performed.

Target analysis

It is known that PBs can transfer energy to both PSI and PSII^{27,28}. Thus a good model requires the presence of PB coupled to PSII (PB-PSII) and to PSI (PB-PSI). In order to obtain acceptable fitting results, it turned out that the amount of excitations being transferred from PB to PSII and PSI had to be rather similar (for more details see SI). PB was allowed to be quenched or unquenched and the fraction of quenched PB was included as a free fitting parameter. Quenched PB-PSII and PB-PSI are shown in Fig. 6 whereas the unquenched versions are omitted from the figure for clarity. It has been reported that also uncoupled PB should be present²⁹ but since the corresponding lifetime of 1.2-1.5 ns was not observed in our study, their amount was considered to be insignificant.

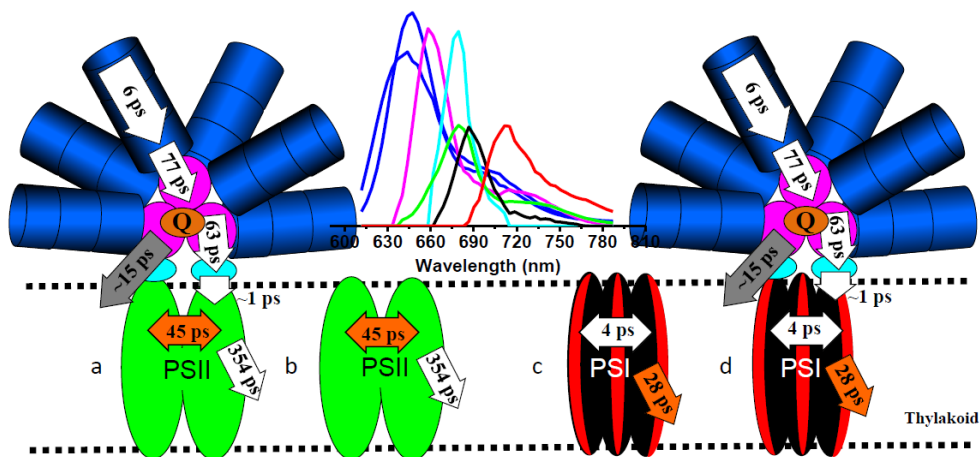


Figure 3.6: Schematic model showing the downhill energy transfer and trapping processes in *Synechocystis* with characteristic transfer times (a transfer time is defined

as 1/transfer rate). SAS (fitting results) are shown in colors that refer to the protein complexes holding the corresponding pigments. Inverse rates of uphill energy transfer are omitted for clarity but can be found in the supporting information (Figure S3.2)

A correct description of the 400 nm data requires the presence of two additional pigment-protein structures: PSII and PSI without any coupled PBs (schematic structures of PSII and PSI are also included in Fig.3.6). Details about the fitting and input parameters are shown in the Supporting Information (Figure S3.2 and Table S3.1). The SAS resulting from the analysis are assigned based on the positions of their maxima: the two blue SAS correspond to short- and long wavelength forms of C-PC (here named PC-S and PC-L, respectively); the magenta SAS with maximum around 660 nm corresponds to APC₆₆₀; the cyan SAS and the green SAS with maximum around 680 nm to APC₆₈₀ and Chls in PSII respectively. The black and red SAS originate from bulk Chls (688 nm) and red Chls (712 nm) in PSI, respectively, which is in perfect agreement with previous reports on isolated PSI^{38,40}. As pointed out in the supplementary information, also energy transfer rates are in agreement with reports on PSI, PSII and PBs and sub-complexes thereof and the same is true for the fluorescence spectra (SAS) of the various pigments.

In order to determine in which of the different pigment pools the blue-green light-induced quenching takes place, one additional decay rate constant k_Q (reflecting the quenching) was added in turn to the various compartments and the data for the quenched cells was fitted keeping all other rate constants the same as for the unquenched cells. The results were unequivocal: only quenching of the APC₆₆₀ compartment leads to a satisfactory fit of the data and the corresponding quenching rate is $66 \pm 15 \text{ ns}^{-1}$ for OverOCP. Putting the quencher in another compartment resulted in fits of lesser quality or led to unrealistic SAS. Another important finding was that not all PBs are quenched. For OverOCP the percentage of quenched PBs was found to be ~72%.

With the same model, the data on WT cells could be fitted equally well, the main difference being that only ~29% of all PBs appeared to be quenched whereas the quenching rate was 54 ns^{-1} rather similar to that of OverOCP. This explains why in steady-state spectra, the quenching ratio in WT cells is only about one third of that in OverOCP cells.

For the Δ OCP mutant the same target model was successfully applied (results not shown) for all three measuring states (before, during and after applying high intensity blue-green light) and the results are similar to those for unquenched WT and OverOCP cells.

Discussion

The location, rate and efficiency of qE_{cya}

It was demonstrated before with steady-state fluorescence measurements on various *Synechocystis* mutants and *in vitro* reconstitution experiments that quenching takes place in the APC core of the PB^{9,11,13,15} and our current data confirm this. However, due to fast EET from APC₆₆₀ to APC₆₈₀/Chls it could not be determined before whether APC₆₆₀ was quenched or APC₆₈₀²⁰ and also the quenching rate remained unknown. It is now revealed that quenching takes place at the level of APC₆₆₀ and not APC₆₈₀. The rate of quenching of the APC₆₆₀ pool turns out to be $66 \pm 15 \text{ ns}^{-1}$ (which is equivalent to $(16 \pm 4 \text{ ps})^{-1}$). This is extremely fast and leads to efficient quenching. From the parameters obtained with the target analysis it can be concluded that in the presence of qE_{cya} , 80% of the excitations that are harvested by a quenched PB is dissipated as heat before reaching PSII and PSI (see SI). Our results indicate that both PSI and PSII are protected. However, not all PBs are in the quenched state. The number of quenched PBs depends on the ratio OCP^r to PB¹¹. In WT cells, there is only 1 OCP per 2-3 PB. Moreover, not all OCP is expected to be in the OCP^r state in the used light conditions, although the exact amount of activated OCP is unknown. Indeed we found that only 29% of the PBs were quenched for WT cells. For OverOCP cells, the concentration of OCP is about 7-8 fold higher than in WT, meaning more than 2-3 OCP per PB²¹. Consistently, the number of quenched PBs is substantially higher, namely 72%.

The mechanism of qE_{cya} at the molecular level

Our present study has disclosed that one of the APC₆₆₀ pigments is directly quenched (from now on we call this quenched pigment APC₆₆₀^Q). The overall quenching rate of the APC₆₆₀ pool appears to be $66 \pm 15 \text{ ns}^{-1}$ or $(16 \pm 4 \text{ ps})^{-1}$. Since there are approximately 66 APC₆₆₀ pigments present in one PB core, the molecular

quenching rate of APC_{660}^Q is at most $(0.24 \pm 0.06 \text{ ps})^{-1}$, corresponding to 16/66 ps in case EET within the APC_{660} pool is infinitely fast. In the case of infinitely fast EET the probability that the excitation is on the quenched pigment is 1/66 which slows down the molecular quenching rate by a factor of 66. Slower EET requires an even faster quenching rate (see e.g. ³⁷).

It has been hypothesized that the C-terminal OCP domain, by interacting with the center of an APC trimer, may bring the carotenoid into proximity of the APC chromophores, whereas light-induced carotenoid changes could then regulate the interaction between the carotenoid and the APC chromophores (either $\alpha 84$ or $\beta 84$) ¹⁰. Support for this hypothesis comes from the fact that the C-terminal domain of OCP is structurally similar to the 7.8 kDa core linker protein that is bound within the central aperture of the APC trimer and directly interacts with the $\beta 84$ chromophores of two APC subunits. The present findings indeed confirm the direct quenching of one of the APC chromophores and the ultrafast quenching rate suggests extremely strong coupling between one of the APC chromophores and the OCP carotenoid hECN.

One could envision several carotenoid-induced quenching mechanisms occurring based on the analogy of chlorophyll quenching by carotenoids: 1) excitonic coupling ⁴¹⁻⁴³ between APC_{660}^Q and hECN, 2) EET from APC_{660}^Q to the S_1 state of hECN ^{44,45}, 3) electron transfer from hECN to APC_{660}^Q ⁴⁶. The same three mechanisms were also recently identified for tetrapyrrole singlet excited state quenching by carotenoids in artificial systems ⁴⁷.

The fact that the quenching rate is faster than $(1 \text{ ps})^{-1}$ rules out the first mechanism because the excited-state decay rate would be a weighted average of the excited-state decay rate of APC_{660} and of hECN in the absence of interaction ⁴³. Because the excited-state lifetime of hECN is above 1 ps and that of APC_{660} even above 1 ns, it is impossible to obtain an average lifetime which is 0.24 ps or even shorter.

It is more difficult to estimate whether EET from APC_{660}^Q to the S_1 state of hECN might happen with a rate of $(0.24 \pm 0.06 \text{ ps})^{-1}$. Up to now, rates of EET from the lowest excited state of (B)Chls/bilins to the carotenoid S_1 state have not been measured for pigment-protein complexes. However, various studies have reported

rates for EET from the carotenoid S_1 state to the lowest Q_y states of (bacterio)chlorophylls. Both types of rates are expected to be similar because the electronic coupling mechanism is the same, while mainly the relative ordering of the energy levels of both molecules differs in both cases. Carotenoid-to-BChl a energy transfer times involving the S_1 state were reported to be of the order of several ps for light-harvesting complexes from purple bacteria⁴⁸⁻⁵². This is an order of magnitude slower than the obtained quenching rate in the present study. A larger spread in transfer times was reported for Chl a containing light-harvesting complexes LHCI and CP29⁵³⁻⁵⁶. Whereas Croce et al. hardly observed any transfer from the S_1 state in LHCI from plants⁵³, a time constant of ~ 1 ps was reported by Gradinaru et al.⁵⁴, whereas Walla et al. found several transfer times, ranging from ~ 200 fs to over 7 ps⁵⁵. For CP29, Croce et al. reported different transfer times for the different carotenoids in CP29⁵⁶, the fastest being 700 fs, whereas Gradinaru et al. found a time of around 1 ps⁵⁴.

It is important to note that a transient absorption study was performed on a model system made up of a zinc phthalocyanine (Pc) molecule (similar to Chl) covalently linked to carotenoids with 9, 10, or 11 conjugated carbon-carbon double bonds⁵⁷. By increasing the number of double bonds the S_1 energy level becomes lower than the lowest excited singlet energy level of the Pc molecule. EET could be observed from Pc to the Car in the case of 10 and 11 conjugated double bonds and the transfer rates varied from $(56 \text{ ps})^{-1}$ to $(17 \text{ ps})^{-1}$, depending on solvent polarity and conjugation length, i.e. far slower than the observed quenching rate in the present study. We conclude that most of the experimentally obtained transfer rates are slower or even far slower than the lower limit for the quenching rate of $(0.24 \pm 0.06 \text{ ps})^{-1}$ but we cannot entirely exclude that EET from APC^Q_{660} to the S_1 state of hECN might be responsible for qE_{cyt} .

Finally, it has been reported that in plants nonphotochemical quenching can occur via charge transfer within a closely coupled excited pair of a Chl a molecule and a zeaxanthin carotenoid molecule with a time constant between 0.1 and 1.0 ps, leading to fluorescence quenching of Chl^{46,58}. The rate of $(\sim 0.24 \pm 0.06 \text{ ps})^{-1}$ for APC quenching in cyanobacteria falls nicely within this interval. Therefore, based on the available data, it appears most likely that charge transfer from the red form of

hECN in OCP to APC_{660}^Q in the PB core is responsible for the blue-green light-induced non-photochemical quenching in cyanobacteria.

ACKNOWLEDGMENT

We thank Dr. S. Liptonok (Ecole Polytechnique, 91128 Palaiseau, France) and J. Snellenburg (VU Amsterdam University) for help with the use of the TIMP package, C. Wolfs (Wageningen UR) for help in growing the cells and Arie van Hoek (Wageningen UR) for technical support. This work was supported by a fellowship to L.T. from the Graduate School Experimental Plant Sciences (EPS), Wageningen, The Netherlands, by the Dutch Ministry of ELI through the BioSolar Cells Project and by the European community via the HARVEST project.

References

- (1) Aro, E.-M.; Virgin, I.; Andersson, B. *Biochimica et Biophysica Acta (BBA) - Bioenergetics* **1993**, *1143*, 113-134.
- (2) Tyystjarvi, E. *Coordination Chem Rev* **2008**, *252*, 361-376.
- (3) Vass, I. *Physiologia Plantarum* **2011**, *142*, 6-16.
- (4) Horton, P.; Ruban, A. V.; Walters, R. G. *Annu Rev Plant Phys* **1996**, *47*, 655-684.
- (5) Niyogi, K. K. *Annu Rev Plant Phys* **1999**, *50*, 333-359.
- (6) Kirilovsky, D. *Photosynthesis Research* **2007**, *93*, 7-16.
- (7) El Bissati, K.; Delphin, E.; Murata, N.; Etienne, A. L.; Kirilovsky, D. *Biochimica Et Biophysica Acta-Bioenergetics* **2000**, *1457*, 229-242.
- (8) Rakhimberdieva, M. G.; Stadnichuk, I. N.; Elanskaya, T. V.; Karapetyan, N. V. *FEBS Letters* **2004**, *574*, 85-88.
- (9) Wilson, A.; Ajlani, G.; Verbavatz, J. M.; Vass, I.; Kerfeld, C. A.; Kirilovsky, D. *Plant Cell* **2006**, *18*, 992-1007.
- (10) Wilson, A.; Punginelli, C.; Gall, A.; Bonetti, C.; Alexandre, M.; Routaboul, J. M.; Kerfeld, C. A.; van Grondelle, R.; Robert, B.; Kennis, J. T. M.; Kirilovsky, D. *P Natl Acad Sci USA* **2008**, *105*, 12075-12080.
- (11) Gwizdala, M.; Wilson, A.; Kirilovsky, D. *Plant Cell* **2011**, *23*, 2631-2643.
- (12) Boulay, C.; Wilson, A.; D'Haene, S.; Kirilovsky, D. *Proceedings of the National Academy of Sciences of the United States of America* **2010**, *107*, 11620-11625.
- (13) Scott, M.; McCollum, C.; Vasil'ev, S.; Crozier, C.; Espie, G. S.; Krol, M.; Huner, N. P. A.; Bruce, D. *Biochemistry* **2006**, *45*, 8952-8958.
- (14) Rakhimberdieva, M. G.; Bolychevtseva, Y. V.; Elanskaya, I. V.; Karapetyan, N. V. *Febs Letters* **2007**, *581*, 2429-2433.
- (15) Rakhimberdieva, M. G.; Vavilin, D. V.; Vermaas, W. F. J.; Elanskaya, I. V.; Karapetyan, N. V. *Biochimica Et Biophysica Acta-Bioenergetics* **2007**, *1767*, 757-765.
- (16) Wilson, A.; Boulay, C.; Wilde, A.; Kerfeld, C. A.; Kirilovsky, D. *Plant Cell* **2007**, *19*, 656-672.
- (17) Boulay, C.; Abasova, L.; Six, C.; Vass, I.; Kirilovsky, D. *Biochimica Et Biophysica Acta-Bioenergetics* **2008**, *1777*, 1344-1354.
- (18) Rakhimberdieva, M. G.; Elanskaya, I. V.; Vermaas, W. F. J.; Karapetyan, N. V. *Biochimica Et Biophysica Acta-Bioenergetics* **2010**, *1797*, 241-249.
- (19) Wilson, A.; Kinney, J. N.; Zwart, P. H.; Punginelli, C.; D'Haene, S.; Perreau, F.; Klein, M. G.; Kirilovsky, D.; Kerfeld, C. A. *Journal of Biological Chemistry* **2010**, *285*, 18364-18375.
- (20) Rakhimberdieva, M. G.; Kuzminov, F. I.; Elanskaya, I. V.; Karapetyan, N. V. *Febs Letters* **2011**, *585*, 585-589.
- (21) Kirilovsky, D.; Kerfeld, C. A. *Biochimica Et Biophysica Acta* **2011**, DOI:10.1016/j.bbabo.2011.04.013.
- (22) Glazer, A. N. *Biochim Biophys Acta* **1984**, *768*, 29-51.

- (23) Grossman, A. R.; Schaefer, M. R.; Chiang, G. G.; Collier, J. L. *Microbiol Rev* **1993**, 57, 725-749.
- (24) MacColl, R. *Journal of Structural Biology* **1998**, 124, 311-334.
- (25) Adir, N. *Photosynthesis Research* **2005**, 85, 15-32.
- (26) Arteni, A. A.; Ajlani, G.; Boekema, E. J. *Biochimica Et Biophysica Acta-Bioenergetics* **2009**, 1787, 272-279.
- (27) Ashby, M. K.; Mullineaux, C. W. *Photosynthesis Research* **1999**, 61, 169-179.
- (28) Dong, C.; Tang, A.; Zhao, J.; Mullineaux, C. W.; Shen, G.; Bryant, D. A. *Biochimica et Biophysica Acta (BBA) - Bioenergetics* **2009**, 1787, 1122-1128.
- (29) Bittersmann, E.; Vermaas, W. *Biochim Biophys Acta* **1991**, 1098, 105-116.
- (30) Krumova, S. B.; Laptinok, S. P.; Borst, J. W.; Ughy, B.; Gombos, Z.; Ajlani, G.; van Amerongen, H. *Biophys J* **2010**, 99, 2006-2015.
- (31) Rippka, R.; Deruelles, J.; Waterbury, J. B.; Herdman, M.; Stanier, R. Y. *J Gen Microbiol* **1979**, 111, 1-61.
- (32) Stokkum, I. H. M.; Oort, B.; Mourik, F.; Gobets, B.; Amerongen, H. In *Biophysical Techniques in Photosynthesis*; Aartsma, T. J., Matysik, J., Eds.; Springer Netherlands: 2008; Vol. 26, p 223-240.
- (33) Laptinok, S. P.; Borst, J. W.; Mullen, K. M.; van Stokkum, I. H. M.; Visser, A. J. W. G.; van Amerongen, H. *Phys Chem Chem Phys* **2010**, 12, 7593-7602.
- (34) Mullen, K. M.; van Stokkum, I. H. M. *J Stat Softw* **2007**, 18, 1-46.
- (35) van Stokkum, I. H. M.; Larsen, D. S.; van Grondelle, R. *Biochimica Et Biophysica Acta-Bioenergetics* **2004**, 1657, 82-104.
- (36) van Amerongen, H.; Valkunas, L.; van Grondelle, R. *Photosynthetic excitons*; World Scientific Publishing Co.Pte.Ltd.; 2000.
- (37) Broess, K.; Trinkunas, G.; van Hoek, A.; Croce, R.; van Amerongen, H. *Biochimica Et Biophysica Acta-Bioenergetics* **2008**, 1777, 404-409.
- (38) Gobets, B.; van Grondelle, R. *Biochimica Et Biophysica Acta-Bioenergetics* **2001**, 1507, 80-99.
- (39) van Oort, B.; Amunts, A.; Borst, J. W.; van Hoek, A.; Nelson, N.; van Amerongen, H.; Croce, R. *Biophysical Journal* **2008**, 95, 5851-5861.
- (40) Gobets, B.; van Stokkum, I. H. M.; van Mourik, F.; Dekker, J. P.; van Grondelle, R. *Biophysical Journal* **2003**, 85, 3883-3898.
- (41) Lampoura, S. S.; Barzda, V.; Owen, G. M.; Hoff, A. J.; van Amerongen, H. *Biochemistry* **2002**, 41, 9139-9144.
- (42) Bode, S.; Quentmeier, C. C.; Liao, P. N.; Hafi, N.; Barros, T.; Wilk, L.; Bittner, F.; Walla, P. J. *Proceedings of the National Academy of Sciences of the United States of America* **2009**, 106, 12311-12316.
- (43) van Amerongen, H.; van Grondelle, R. *J Phys Chem B* **2001**, 105, 604-617.
- (44) Ruban, A. V.; Berera, R.; Illoaia, C.; van Stokkum, I. H. M.; Kennis, J. T. M.; Pascal, A. A.; van Amerongen, H.; Robert, B.; Horton, P.; van Grondelle, R. *Nature* **2007**, 450, 575-U22.
- (45) Young, A. J.; Phillip, D.; Ruban, A. V.; Horton, P.; Frank, H. A. *Pure Appl Chem* **1997**, 69, 2125-2130.

- (46) Holt, N. E.; Zigmantas, D.; Valkunas, L.; Li, X. P.; Niyogi, K. K.; Fleming, G. R. *Science* **2005**, *307*, 433-436.
- (47) Kloz, M.; Pillai, S.; Kodis, G.; Gust, D.; Moore, T. A.; Moore, A. L.; van Grondelle, R.; Kennis, J. T. *J Am Chem Soc* **2011**, *133*, 7007-15.
- (48) Walla, P. J.; Linden, P. A.; Hsu, C. P.; Scholes, G. D.; Fleming, G. R. *Proc Natl Acad Sci U S A* **2000**, *97*, 10808-13.
- (49) Zhang, J.-P.; Fujii, R.; Qian, P.; Inaba, T.; Mizoguchi, T.; Koyama, Y.; Onaka, K.; Watanabe, Y.; Nagae, H. *The Journal of Physical Chemistry B* **2000**, *104*, 3683-3691.
- (50) Polívka, T.; Pullerits, T.; Frank, H. A.; Cogdell, R. J.; Sundström, V. *The Journal of Physical Chemistry B* **2004**, *108*, 15398-15407.
- (51) Cong, H.; Niedzwiedzki, D. M.; Gibson, G. N.; LaFountain, A. M.; Kelsh, R. M.; Gardiner, A. T.; Cogdell, R. J.; Frank, H. A. *J Phys Chem B* **2008**, *112*, 10689-703.
- (52) Polivka, T.; Frank, H. A. *Accounts Chem Res* **2010**, *43*, 1125-1134.
- (53) Croce, R.; Müller, M. G.; Bassi, R.; Holzwarth, A. R. *Biophysical Journal* **2001**, *80*, 901-915.
- (54) Gradinaru, C. C.; van Stokkum, I. H. M.; Pascal, A. A.; van Grondelle, R.; van Amerongen, H. *The Journal of Physical Chemistry B* **2000**, *104*, 9330-9342.
- (55) Walla, P. J.; Linden, P. A.; Ohta, K.; Fleming, G. R. *The Journal of Physical Chemistry A* **2001**, *106*, 1909-1916.
- (56) Croce, R.; Müller, M. G.; Caffarri, S.; Bassi, R.; Holzwarth, A. R. *Biophysical Journal* **2003**, *84*, 2517-2532.
- (57) Berera, R.; Herrero, C.; van Stokkum, I. H. M.; Vengris, M.; Kodis, G.; Palacios, R. E.; van Amerongen, H.; van Grondelle, R.; Gust, D.; Moore, T. A.; Moore, A. L.; Kennis, J. T. M. *Proceedings of the National Academy of Sciences of the United States of America* **2006**, *103*, 5343-5348.
- (58) Ahn, T. K.; Avenson, T. J.; Ballottari, M.; Cheng, Y. C.; Niyogi, K. K.; Bassi, R.; Fleming, G. R. *Science* **2008**, *320*, 794-797.

Supporting materials

Target analysis of NPQ in cyanobacteria *in vivo*

The target analysis takes into account the following *a priori* knowledge:

- PBs can transfer energy to both PSII and PSI^{1,2}.
- Part of PSII and PSI is not coupled to PBs³.
- Approximately 10% of the 590 nm excitations is absorbed by PSII and PSI, the remainder is absorbed by PC-S⁴.
- Approximately 10% of the 400 nm excitations is absorbed by PBs, mainly by PC-S and PC-L. The remainder is absorbed by PSII and PSI⁴.
- A fraction of the PBs is thought to be unquenched. For WT it is known that OCP is present in a substoichiometric amount as compared to PBs⁵.
- PSII can be in an open or a closed state.
- All energy transfer is in principle reversible.

The *a priori* knowledge is partly visualized in the cartoon model depicted in Fig.S3.1.

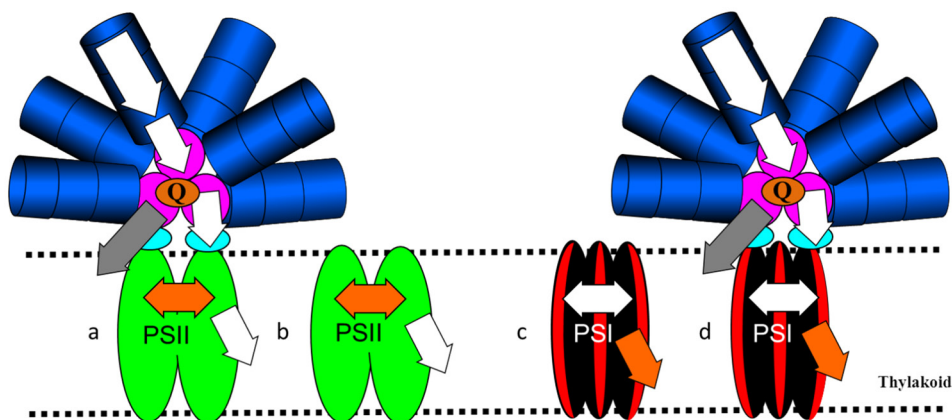


Fig.S3.1: Cartoon model of excitation energy, electron transfer and excited-state quenching in the thylakoid membrane of cyanobacteria. Arrows indicate the flow of excitation energy, charge separation (orange arrow) and excited-state quenching (grey). Q indicates that a PBS can be quenched. Two additional assemblies have been omitted for clarity: One is like the 'a' assembly but it is not quenched (NQ instead of Q) and the other is like assembly 'd' and is also not quenched.

Fig.S3.1 contains six different assemblies of pigment-protein complexes: PSI and PSII without any coupled PB, PSII and PSI coupled to PBs that can be quenched (Q), PSI and PSII coupled to PBs that cannot be quenched (NQ, not depicted in the cartoon). The 590 nm excitation light preferentially excites PB (90%), thus not providing much information on PSI and PSII kinetics. The 400 nm excitation light preferentially excites PSI and PSII (90%), thus providing the missing information. In order to describe the complete dynamics four PBs compartments are distinguished: PC-S, PC-L, APC₆₆₀, and APC₆₈₀. It is well known that PSI can be adequately described with two compartments: bulk Chl (about 100 Chl, including RC), from which charge separation occurs and which is in equilibrium with red Chl (6 Chl) ^{6,7}, the PSII core 35 Chls are present. When the PSII RC is open, charge separation is not entirely irreversible, and an equilibrium^{8,9} between the excited state of the system and the first radical pair state is needed to describe PSII core emission. When the PSII RC is closed, the equilibrium with the first radical pair state shifts towards the excited state. Since the exact amount of open PSII RCs is not known, PSII core emission is described with two compartments: antenna plus RC (35 Chl) in equilibrium with a non radiative (NR) compartment, where the rate constants of this equilibrium are free fitting parameters, and thus can effectively describe a mixture of open and closed RCs.

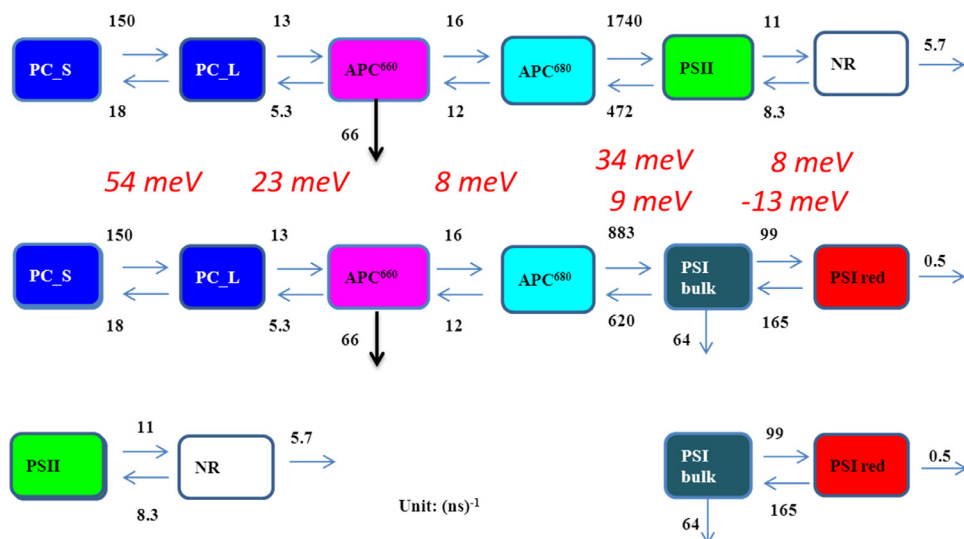


Fig.S3.2: Kinetic scheme used for target analysis of time-resolved fluorescence data of quenched and unquenched cyanobacteria in vivo. Rates estimated from the OverOCP data in Fig.S3.3 (further explanation, see below) are given in (ns)⁻¹. Differences in free energy between compartments were calculated from these estimated rates and are indicated in red italic.

In the target analysis 28 compartments are used as partly depicted in Fig.S3.2: PSII and PSI without any coupled PBs each require two compartments; the PBs “energy funnel” PC-S, PC-L, APC₆₆₀, APC₆₈₀ can be either quenched or unquenched, and it can be in equilibrium with PSII or PSI. This leads to $2 \times 2 + 4 \times (4 + 2) = 28$ compartments. Fortunately, the Species Associated Spectra (SAS) of PC-S, PC-L, APC₆₆₀, APC₆₈₀, PS II, PS I bulk (PSIb), PS I red (PSIr) can be linked, and only 7 SAS need to be estimated. The nonradiative (NR) compartment has a zero SAS. Note that the rate constants of the energy funnel PC-S, PC-L, APC₆₆₀, APC₆₈₀ are assumed to be identical for the four different cases (PB-PS II Q, PB-PS II NQ, PB-PS I Q, PB-PS I NQ), and also the rate constants of PSII or PSI are assumed to be identical for the three different cases (without any coupled PBs, Q and NQ). Several possibilities for the quenching of PBs were tested, and in Fig.S3.2 only the most important quenching rate, from APC₆₆₀ is shown. Thus in total 18 different rate constants are needed to describe one experiment. This is much more than

the five lifetimes estimated from the global analysis. Therefore, four different experiments (see also Fig.S3.3) are analysed simultaneously: unquenched 590 (black), quenched 590 (red), unquenched 400 (blue), quenched 400 (green) nm excitation. This simultaneous target analysis allows to resolve all SAS (see below). Also alternative kinetic schemes were tried. Most important was a scheme where the quenching starts from APC_{680} instead of APC_{660} because it is not immediately obvious from the global analysis where in the core the quenching takes place. However, this fit resulted in a huge increase in the root mean square error (rmse), and it proved to be impossible to describe the data with this scheme. This made us conclude that the quenching is not located on APC_{680} . Therefore we report here only on the scheme of Fig.S3.2.

Input parameters

Next to the rate constants, also the inputs (fractions of excitation) to the different PC-S, PC-L (only with 400 nm excitation), PSII, PSI bulk, PSI red compartments must be estimated. But the values of these inputs are mutually dependent. The following *a priori* knowledge/assumptions /definitions are employed:

- The relative absorption of PSII at 590 nm is given by the parameter ε_{590}^2 (2 for PSII) which is fixed at 1, and the absorption of PSII at 400 nm is a parameter ε_{400}^2 to be estimated. Likewise, parameters ε_{590}^c and ε_{400}^c (c for phycoCyanin) reflect the relative absorption of PBSs at 590 and 400 nm.
- PSI absorbs α times more than PSII. Thus ε_{590}^1 (1 for PSI) is α times ε_{590}^2 , and $\varepsilon_{400}^1 = \alpha \cdot \varepsilon_{400}^2$. In view of the ~106 vs. 35 Chls, α is fixed at 3.
- The red Chl compartment of PSI is represented by a fraction r , and the PS I bulk compartment by $1-r$. In view of the 6 red Chls r is fixed at 0.06.
- PC-S and PC-L have equal absorption at 400 nm, and only PC-S absorbs at 590 nm.
- A fraction $c2$ of the PBs is linked to PSII and a fraction $c1 = 1 - c2$ to PSI. It is assumed that $c1 = c2 = 0.5$. This ratio was necessary to get a reasonable PSI/II ratio and SAS with comparable amplitudes for all pigments.
- PBs can be in a quenched state (fraction q) or in an unquenched state (fraction $1-q$) and the parameter q has to be estimated.

- The input to PSII and PSI without any coupled PB at 590 nm is represented by the parameters $I2_{590}$ and $I1_{590}$ (I for loose). Since $\varepsilon2_{590} \equiv 1$, $I2_{400} = I2_{590} \cdot \varepsilon2_{400}$ and $I1_{400} = I1_{590} \cdot \varepsilon2_{400}$.

There are 17 compartments that receive input:

- PC-S, PC-L quenched or unquenched, in equilibrium with PSII or PSI: 2x4
- PSII, PSIIb, PSIIr coupled to PBs quenched or unquenched, and not coupled to PBs (loose): 3x3.

Using the above assumptions and definitions the input to these 17 compartments with 400 and 590 nm excitation (totalling 34 input values) are described by only six free parameters: Quenching fraction q , absorption parameters $\varepsilon2_{400}$, εc_{400} , εc_{590} , $I2$ and $I1$.

For example: the input to the nonquenched PSIIr coupled to PBs at 400 nm is given by

$$(1-q) \cdot r \cdot \varepsilon1_{400} \cdot c1 = (1-q) \cdot r \cdot \alpha \cdot \varepsilon2_{400} \cdot c1 = (1-q) \cdot 0.06 \cdot 3 \cdot \varepsilon2_{400} \cdot 0.5$$

Spectral assumptions

As explained above, only 7 SAS need to be estimated. The following spectral assumptions have been used:

- to estimate the equilibrium between PS I bulk and PS I red: $SAS_{PSIr} = 0$ below 686 nm,
- to facilitate resolution of SAS, and to ensure nonnegativity:
 $SAS_{APC660} = 0$ below 634 nm,
- $SAS_{APC680} = 0$ below 661 nm and above 715 nm,
- $SAS_{PSIIb} = 0$ below 665 nm and above 770 nm,
- $SAS_{PSII} = 0$ below 640 nm.

Thus the number of free spectral parameters (50 different wavelengths) was reduced from $7 \cdot 50 = 350$ to 259.

Other parameters

In Materials and Methods the instrument response function (IRF) was already introduced; it is described with a double Gaussian, consisting of a narrow Gaussian of 9 ps FWHM (90% of the IRF area) on top of a broader Gaussian of 100 ps FWHM (10% of the IRF area). The location of this IRF is wavelength-dependent

due to the streak-camera properties, and it is well described by a parabola¹⁰. The simultaneous analysis of four experiments requires three relative scaling parameters.

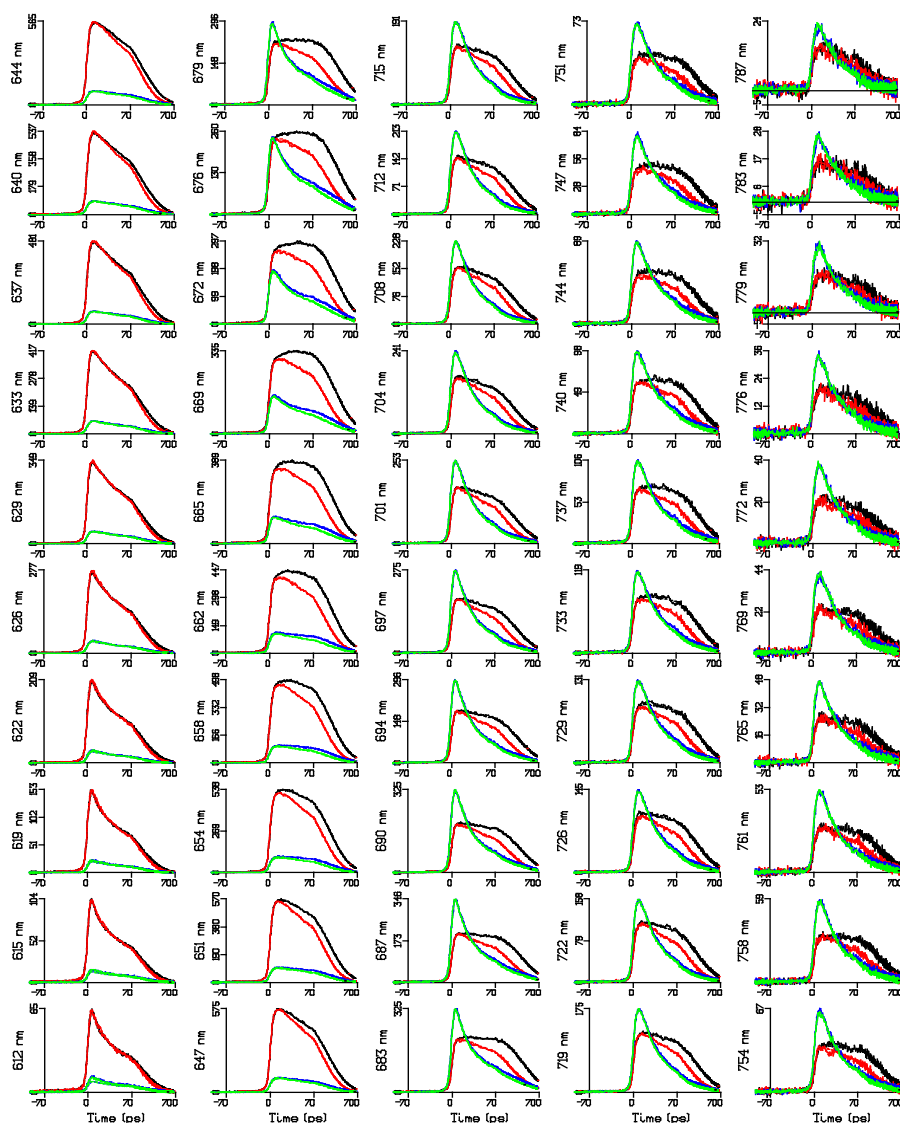


Fig.S3.3 Emission of OverOCP at 50 wavelengths, as obtained from the four streak images in Fig.3.2. Key: unquenched 590 (black), quenched 590 (red), unquenched 400 (blue),

quenched 400 (green) nm excitation. Note that the time axis is linear until 70 ps and logarithmic thereafter. Dashed lines indicate the simultaneous target analysis fit.

Simultaneous target analysis

In the above we have explained how we can compute the concentrations of all compartments. For each of the seven emitting species (PC-S, PC-L, APC₆₆₀, APC₆₈₀, PS II, PS I bulk, and PS I red), we can add the concentrations of all compartments belonging to that species. Thus we arrive at a concentration matrix C for each excitation wavelength (400 and 590 nm) and each state (quenched or unquenched). The model for the simultaneous target analysis now reads

$$\begin{bmatrix} \Psi_{U,590} \\ \Psi_{Q,590} \\ \Psi_{U,400} \\ \Psi_{Q,400} \end{bmatrix} = \begin{bmatrix} C_{U,590} \\ \alpha_1 C_{Q,590} \\ \alpha_2 C_{U,400} \\ \alpha_3 C_{Q,400} \end{bmatrix} SAS^T$$

where Ψ indicates the data measured in each of the four experiments (U or Q, with 400 or 590 nm excitation) and the α_i are the three relative scaling parameters. All unknown parameters (kinetic, input or SAS) are now estimated with the help of the partitioned variable projection algorithm (van Stokkum, Larsen et al. 2004; Mullen and van Stokkum 2009). Furthermore, after convergence, the linear approximation covariance matrix allows us to estimate the precision of the estimated parameters. With the good quality of fit (see below) the relative precision of the estimated parameters was better than 10%, with the exception of the rates that describe the fast energy transfer between APC₆₈₀ and PS II or PS I bulk.

Quality of the fit

The parameter estimation resulted in parameters that describe the model fit to the data, and the corresponding residuals. The rmse of the fit was 1.69, which is less than 1% of the maximum of most of the traces in Fig.S3.3 (the absolute maximum of these data was 575 at 647 nm). In addition, for each of the four experiments the matrix of residuals was analysed by Singular Value Decomposition¹⁰. This enabled us to spot trends in the residuals and locate the

lack of fit in the time or wavelength domain. The left singular vectors in Fig.S3.4a,c indicate that the maximum lack of fit is around the IRF maximum. This indicates that the fit can be further improved by a more flexible IRF description.

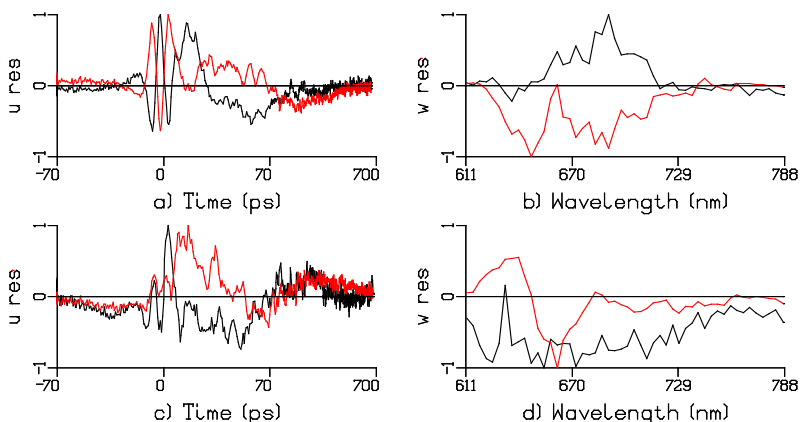


Fig.S3.4 First left (a,c) and right (b,d) singular vectors resulting from Singular Value Decomposition of the matrix of residuals of the four OverOCP experiments fitted in Fig.S3.3. Key: unquenched 400 (black in a,b), quenched 400 (red in a,b) unquenched 590 (black in c,d), quenched 590 (red in c,d) nm excitation. Note that the time axis in (a,c) is linear until 70 ps and logarithmic thereafter.

identity	loose PS I	loose PS II	PSII_PBS	PSI_PBS	total PS II	total PS I	PS I/II ratio	PBS_Q	PBS_NQ	PBS_tot	total	PS II	PS I	PBS
U over 590 exc	16.7 ^a	2.3 ^b	0.5	1.5	2.8	18.2	6.5	107.5	42.5	150.0 ^c	171.0	1.6%	10.6%	87.7%
Q over 590 exc	16.7	2.3	0.5	1.5	2.8	18.2	6.5	107.5	42.5	150.0	171.0	1.6%	10.6%	87.7%
U over 400 exc	199.8	27.6	6.0	18.0	33.6	217.8	6.5	13.2	5.2	18.4 ^d	269.8	12.4%	80.7%	6.8%
Q over 400 exc	199.8	27.6	6.0	18.0	33.6	217.8	6.5	13.2	5.2	18.4	269.8	12.4%	80.7%	6.8%
U WT 590 exc	16.7	2.3	0.5	1.5	2.8	18.2	6.5	41.6	108.4	150.0	171.0	1.6%	10.6%	87.7%
Q WT 590 exc	16.7	2.3	0.5	1.5	2.8	18.2	6.5	41.6	108.4	150.0	171.0	1.6%	10.6%	87.7%
U WT 400 exc	199.8	27.6	6.0	18.0	33.6	217.8	6.5	6.4	16.8	23.2	274.6	12.2%	79.3%	8.5%
Q WT 400 exc	199.8	27.6	6.0	18.0	33.6	217.8	6.5	6.4	16.8	23.2	274.6	12.2%	79.3%	8.5%

a.Parameter $l1_{590}$; b. Parameter $l2_{590}$ c.Parameter $\mathcal{E}C_{590}$ d.Parameter $\mathcal{E}C_{400}$

Table S3.1 Input values for target analysis of OverOCP and WT, and derived numbers: fraction excited PBS, PS I, PS II and PS I/II ratio. Footnotes refer to parameters of Table S3.2

With 590 nm excitation we excite about 88% PBs, and 12% photosystems. Conversely, with 400 nm excitation we excite 6.8% and 8.5% PBs for OverOCP and

WT respectively, and 93.2 (91.5) % photosystems. Both are in accordance with the literature (Krumova, Laptinok et al. 2010). The PS I/II ratio is about 6.5 on a Chl basis.

The estimated parameters are shown in Fig.S3.2 (rate constants), Fig.S3.5 (SAS), Table S3.1 (input parameters) and Table S3.2 (absorption and quenching parameters). Most of the rate constants can be estimated with a relative precision of about 10%, except for the fastest rates that describe the coupling of APC₆₈₀ and PSII or PSIIb. These rates are most probably too fast to be resolved precisely with the present experiments. As a consequence, also the APC₆₈₀ SAS is estimated less precisely than the other six SAS.

Table S3.2 Quenching and absorption parameters (note that by definition $\varepsilon_{590}^2 \equiv 1$).
For definitions see text.

	k_Q (1/ns)	q	ε_{400}^2	ε_{590}^2	ε_{400}
Over_OCP	66	72%	12	150	18.4
WT	54	29%	12	150	23.2

According to the fitting results, about 72% of the PBs appeared to be quenched for Over_OCP, whereas for WT the fraction q was only about 29%. In the quenched PBs, the quenching rate of the APC₆₆₀ compartment was about 66/ns. The value of 12 for parameter ε_{400}^2 corresponds in Fig.S3.6G to a ratio of 12 for the amplitudes of the dashed and solid concentration profiles.

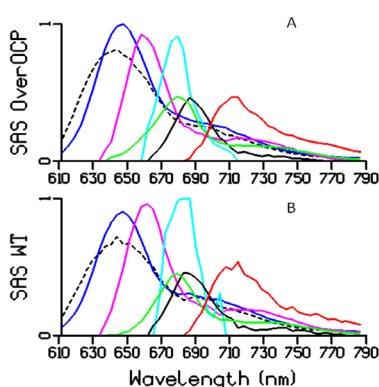


Fig.S3.5 SAS estimated from the target analysis using the kinetic scheme in Fig.S3.2. Key: PC-S (black dash), PC-L (blue), APC₆₆₀ (magenta), APC₆₈₀ (cyan), PS II (green), PS I bulk (black), PS I red (red). (A) OverOCP, (B) WT.

The plausibility of the estimated parameters was judged by the following criteria: realistic shapes of the estimated SAS, and realistic areas of the SAS in accordance with literature^{11,12,13}. We aimed for approximately equal areas of the four PB SAS, and equal areas of the PSII, PSIIb, PSIIr SAS. The

area of a PS SAS relative to that of a PB SAS was taken to be about 0.6. The lifetimes calculated from the estimated rate constants of the energy funnel PC-S, PC-L, APC₆₆₀, APC₆₈₀ and of PSI are globally in accordance with previous experimental results presented in literature^{6,14}.

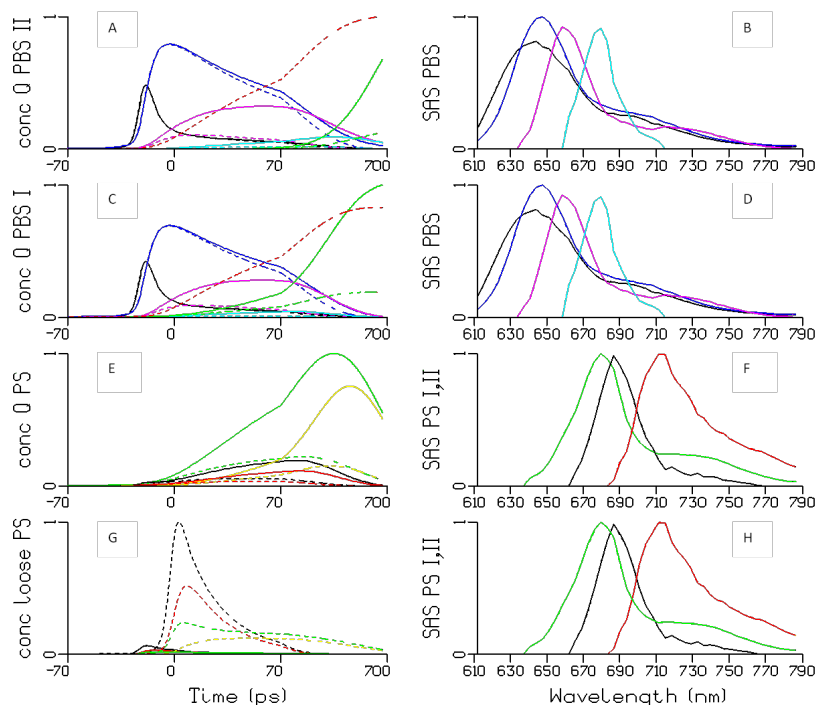


Fig.S3.6 Concentration profiles (left hand column) and SAS (right hand column) estimated from the target analysis of OverOCP using the kinetic scheme of Fig.S3.2. The PBs in panels A and C are connected to PSII and PSI, respectively. In (A,C,E) solid and dashed indicate concentrations for the unquenched and quenched case, respectively. Key to A-D: PC-S (black), PC-L (blue), APC₆₆₀ (magenta), APC₆₈₀ (cyan), integrated nonphotochemical quenching (red), integrated photochemical quenching (green). Key to E-H: PS II (green), PS I bulk (black), PS I red (red in E-G) and NonRadiative (yellow). In (G) solid and dashed indicate 590 and 400 nm excitation, respectively. Note that the time axis is linear until 70 ps, and logarithmic thereafter.

The quenching mechanism is further illustrated in Fig.S3.6. The solid lines in panels A,C,E reflect the unquenched situation, where the equilibria cause

multiexponential decay kinetics for all concentration profiles. Panels A,B depict the energy funnel PC-S, PC-L, APC₆₆₀, APC₆₈₀; for clarity the information of the attached PSII has been omitted here. Panels C,D visualize the quenching of PB coupled to PSI. Note that the difference between panels A and C is visible as a small, long lasting emission which can be attributed to the equilibrium of PBs and the partially closed PSII RCs. Most important is the concentration of the quenched excitations. The integrated *nonphotochemical* quenching is indicated in dashed red, whereas the integrated *photochemical* quenching is depicted in green in A,C. In the computation of *photochemical* quenching in the partially closed PSII RC we have integrated all excitations that decay via the NR compartment. The solid green is the *photochemical* quenching in unquenched conditions, note that this rises quickly for PSI, whereas for PSII it rises slowly because of the equilibrium and long lifetimes. The dashed green represents the photosystems with quenched PB. Clearly, the yield of photosynthesis is reduced by more than 80%. In the quenched PB, the dashed lines show the largest differences for APC₆₆₀, and of course also for APC₆₈₀ which receives its input from APC₆₆₀. In the photosystems that are in turn coupled to APC₆₈₀ the same non-photochemical quenching is visible in panels E,F as a large difference between the solid and dashed lines. The dynamics of the photosystems without PB is visible in panels G,H. The PSIIb, PSIIr equilibrium is established in about 4 ps, and after this the equilibrated PSI decays in about 28 ps by charge separation (photochemical quenching). These *in vivo* results are in agreement with the properties of cyanobacterial PSI *in vitro*^{6,7} and *in vivo*⁴. Finally, PSII equilibrates with the NR compartment in about 45 ps, which is in accordance with the observed lifetime (dominantly 49 ps) for primary charge separation in PSII core^{8,9}. Thereafter, the equilibrated PSII decays slowly with 354 ps. The large amplitude of this slow decay component indicates that the PSII RC is partially closed.

Reconstruction of the steady-state spectra

The results from the target analysis can be used to predict the contributions of each of the SAS to the steady-state spectrum. We used the estimated input and kinetic parameters of OverOCP with 590 nm excitation to compute the steady-

state concentration of each of the species. The kinetic scheme of Figure S3.2 results in concentrations of each compartment described by six (PSII, PSI coupled to PBs quenched or unquenched) or two (loose PSII, PSI) exponential decays. Then the concentration of each compartment was integrated over time, and the contributions of all compartments belonging to a species were summed. Thus we arrived at the amplitudes of the SAS contributions depicted in Figure S3.7A and B. The sum of all these contributions is the reconstructed steady-state spectrum in the unquenched (A) or quenched (B) state. The agreement with the measured steady-state spectra of Figure 3.2B is considered good. Thus we have explained both the change in shape and in amplitude of Figure 3.2B.

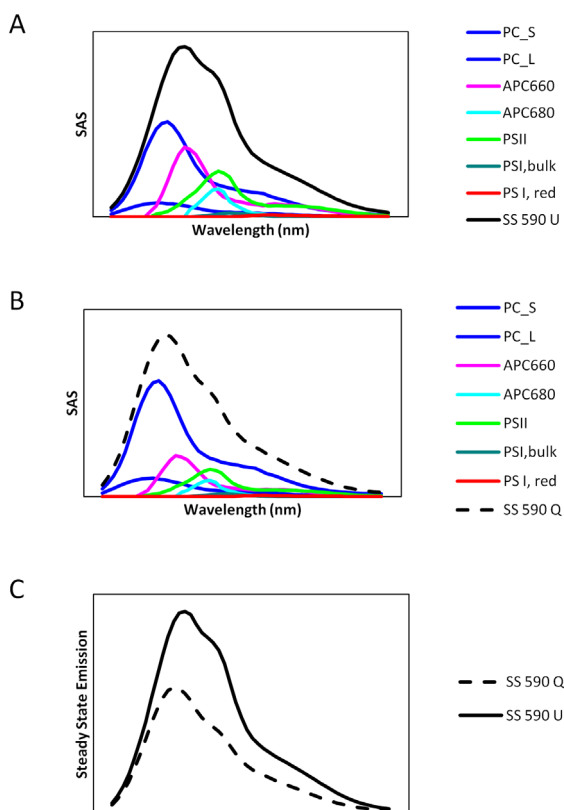


Fig.S3.7 Reconstructed steady-state spectra of OverOCP with 590 nm excitation in the unquenched and quenched state using the kinetic scheme of Fig.S3.2 and the inputs of Table S3.1. In panels A and B, spectral contributions of each species are shown. The black curves represent the sum of these for the unquenched (solid) and quenched (dash) state, and are shown again in panel C.

WT target analysis

The four WT experiments have been subjected to target analysis analogously to the four OverOCP experiments. For comparison, the estimated quenching and input parameters have been

added to Table S3.1 and S3.2. The estimated quenching fraction was 29%, and the quenching rate was 54/ns. This value agrees with the more precise value of

$kQ = (66 \pm 15) / ns$ that was determined from the OverOCP experiments. The estimated SAS are depicted in Fig.S3.5B. These WT SAS agree well with the OverOCP SAS of Fig.S3.5A. The largest differences are present for the APC₆₈₀ SAS (cyan), which is the most difficult one to resolve. The estimated rate constants differ from those in Figure S3.2 mainly for the description of the equilibrium within PSII, which indicates variation in the fraction of closed PSII RCs.

References

- (1) Ashby, M. K.; Mullineaux, C. W. *Photosynth Res* **1999**, *61*, 169.
- (2) Dong, C.; Tang, A.; Zhao, J.; Mullineaux, C. W.; Shen, G.; Bryant, D. A. *Biochimica et Biophysica Acta (BBA) - Bioenergetics* **2009**, *1787*, 1122.
- (3) Ohki, K.; Okabe, Y.; Murakami, A.; Fujita, Y. *Plant Cell Physiol* **1987**, *28*, 1219.
- (4) Krumova, S. B.; Laptinok, S. P.; Borst, J. W.; Ughy, B.; Gombos, Z.; Ajlani, G.; van Amerongen, H. *Biophys J* **2010**, *99*, 2006.
- (5) Kirilovsky, D.; Kerfeld, C. A. *Bba-Bioenergetics* **2012**, *1817*, 158.
- (6) Gobets, B.; van Grondelle, R. *Biochimica Et Biophysica Acta-Bioenergetics* **2001**, *1507*, 80.
- (7) Gobets, B.; van Stokkum, I. H. M.; Rogner, M.; Kruip, J.; Schlodder, E.; Karapetyan, N. V.; Dekker, J. P.; van Grondelle, R. *Biophysical Journal* **2001**, *81*, 407.
- (8) van der Weij-de Wit, C. D.; Dekker, J. P.; van Grondelle, R.; van Stokkum, I. H. M. *The Journal of Physical Chemistry A* **2011**, null.
- (9) Miloslavina, Y.; Szczepaniak, M.; Muller, M. G.; Sander, J.; Nowaczyk, M.; Rogner, M.; Holzwarth, A. R. *Biochemistry* **2006**, *45*, 2436.
- (10) van Stokkum, I. H. M.; van Oort, B.; van Mourik, F.; Gobets, B.; van Amerongen, H. In *Biophysical Techniques in Photosynthesis Vol. II*; Aartsma, T. J., Matysik, J., Eds.; Springer: Dordrecht, The Netherlands, 2008, p 223.
- (11) Cohen-Bazire, G.; Beguin, S.; Rimon, S.; Glazer, A. N.; Brown, D. M. *Arch Microbiol* **1977**, *111*, 225.
- (12) Porra, R. J.; Thompson, W. A.; Kriedemann, P. E. *Biochim Biophys Acta* **1989**, *975*, 384.
- (13) Debreczeny, M. P.; Sauer, K.; Zhou, J. H.; Bryant, D. A. *J Phys Chem-Us* **1995**, *99*, 8420.
- (14) Bittersmann, E.; Vermaas, W. *Biochim Biophys Acta* **1991**, *1098*, 105.

Chapter 4

Picosecond Kinetics of Light Harvesting and Photoprotective Quenching in WT and Mutant Phycobilisomes Isolated from the Cyanobacterium *Synechocystis* PCC 6803

This chapter is based on:

Lijin Tian, Michal Gwizdala, Ivo H.M. van Stokkum, Rob B.M. Koehorst, Diana Kirilovsky and Herbert van Amerongen *Biophysical Journal* 102 (7), 1692-1700

Abstract

In high-light conditions cyanobacteria dissipate excess absorbed energy as heat in the light-harvesting phycobilisomes in order to protect the photosynthetic system against photodamage. This process requires the binding of the red active form of the Orange Carotenoid Protein, that can effectively quench the excited state of one of the allophycocyanin bilins. Recently, an *in vitro* reconstitution system was developed using isolated OCP and isolated PBs from *Synechocystis* PCC 6803. Here we have used spectrally-resolved picosecond fluorescence to study wild-type and two mutated PBs. The results demonstrate that the quenching for all types of PBs takes place on an allophycocyanin bilin emitting at 660 nm (APC_Q^{660}) with a molecular quenching rate that is faster than $(1 \text{ ps})^{-1}$. Moreover, it is concluded that both the mechanism and the site of quenching are the same *in vitro* and *in vivo*. Thus, utilization of the *in vitro* system should make it possible in the future to elucidate whether the quenching is caused by charge transfer between APC_Q^{660} and OCP or by excitation energy transfer from APC_Q^{660} to the S_1 state of the carotenoid a distinction that is very hard if not impossible to make *in vivo*.

Introduction

The remarkable process of photosynthesis that captures light energy and transforms it into chemical energy is vital for nearly all life on Earth. It is carried out by a wide variety of organisms, such as plants, algae, diatoms and many species of bacteria. Cyanobacteria, probably being the oldest oxygen-evolving organisms, are believed to have played an essential role in the formation of our planet and our atmosphere ~2.5 billion years ago¹. Even now, they are still active all around the world, living in a large variety of environmental conditions and contributing substantially to the global carbon cycling². Like higher plants they contain photosystems I and II that work in series and are responsible for the splitting of water and the release of oxygen. The central parts of these photosystems, i.e. the reaction centers and the core light-harvesting complexes are nearly identical for plants and cyanobacteria but the outer light-harvesting complexes are entirely different^{3,4}: Whereas plants possess intrinsic membrane

proteins that all belong to the Lhc family (see e.g. Croce and van Amerongen, 2011)⁵, cyanobacteria, like red algae, possess water-soluble phycobilisomes (PBs) that are attached to the PSI- and PSII-containing thylakoid membrane⁶. PBs of *Synechocystis* PCC 6803 (hereafter called *Synechocystis*) are well organized light-harvesting complexes composed of phycobiliproteins (the phycobilin pigments are open-ring tetrapyrroles) and polypeptides, which are anchored to the stromal side of the thylakoid membrane⁶⁻⁸. They form a funnel for excitations directed towards PSI and PSII. They comprise approximately six C-phycocyanin (C-PC) rods and three allophycocyanin (APC) core cylinders (Fig 4.1). Each C-PC rod is composed of three hexameric disks (18 pigments per hexamer) with a maximum absorbance at 620 nm and maximum fluorescence at 640-650 nm. Each APC cylinder contains four trimer disks (6 pigments per trimer), and each trimer has three monomers in which a monomer is a dimer of α^{APC} and β^{APC} polypeptides. Most of the pigments in the APC core have maximum absorbance at 650 nm and maximum emission at 660 nm (APC₆₆₀) with only a few exceptions: Each of the two APC cylinders closest to the membrane contains two trimers in which one of the α or β APC subunits is replaced by other subunits with bilins of lower excited-state energy^{7,9-11}. In one trimer, one polypeptide subunit of α^{APC} in one monomer is replaced by α^{APC-B} (ApcD)¹² (Fig 4.1). And in another trimer, in one monomer both subunits α^{APC} - β^{APC} are replaced; the β^{APC} polypeptide subunit is replaced by $\beta^{APC-\beta^{18}}$ (ApcF)¹², while the α^{APC} polypeptide subunit is replaced by α^{Lcm} (ApcE)¹³. ApcE or Lcm is also the core-membrane linker. These modified subunits, show maximum fluorescence emission between 676-683 nm and together they are named APC₆₈₀. These low-energy bilins are responsible for direct excitation energy transfer (EET) to the photosystems. Time-resolved fluorescence kinetics of PBs was extensively studied in the past¹⁴⁻¹⁷ and very recently we obtained a comprehensive picture of the entire EET process in WT *Synechocystis* PCC 6803. Various downhill energy-transfer steps within the PBs could be observed, including EET within C_PC with a time constant of 6 ps, EET from C_PC to APC with a time constant of 77 ps, and EET from APC₆₆₀ to APC₆₈₀ with a time constant of 63 ps whereas the uphill back-transfer rates can be calculated using detailed-balance considerations. From APC₆₈₀ excitation energy is rapidly (exact transfer rates are not known) transferred

to the chlorophylls (Chls) in photosystem I and photosystem II, where charge separation takes place¹⁸.

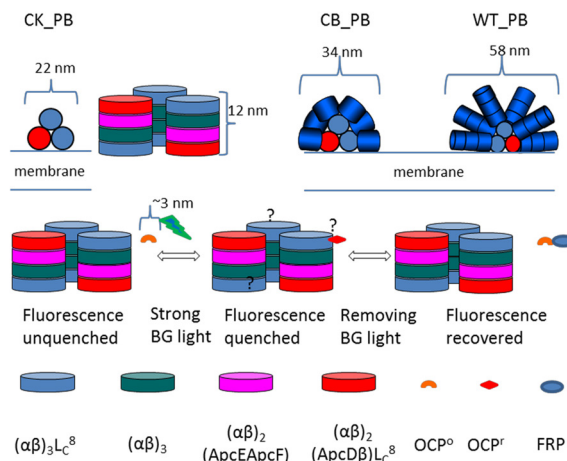


Figure 4.1 The structure of each type of PB is shown schematically: Phycocyanin rods in blue (108 pigments for CB_PB and 324 pigments for WT_PB), allophycocyanin that fluoresces at 660 nm in light blue and bluish green (66 pigments in total) and the low-energy part of allophycocyanin in magenta and red (6 pigments in total). The approximate length for each subunit is based on previous studies³¹. And “?” indicates the potential pigments that OCPⁱ interacts with.

Cyanobacteria have developed mechanisms that serve to protect the organisms against over-excitation in high-light conditions¹⁹⁻²³. Too high light intensities cause saturation of the photosynthetic machinery, leading to increased triplet formation on the Chls that in turn causes the production of singlet-oxygen, a highly reactive oxygen species that can lead to severe damage and even the death of the organism^{24,25}. By increased dissipation of excited-state energy as heat in high-light conditions, a phenomenon called nonphotochemical quenching (NPQ), many organisms get rid of excess excitation energy. The underlying molecular mechanisms can strongly vary from species to species and even within the same organism^{18,26-29}. One of the NPQ mechanisms in cyanobacteria, called the OCP-related NPQ mechanism, is triggered by strong blue-green light. The OCP-related

NPQ mechanism requires the presence of PB and Orange Carotenoid Protein (OCP) in the intact cell³⁰.

OCP is a water soluble 35-kDa protein which binds the keto-carotenoid, 3'-hydroxyechinenone. The structure of the *Synechocystis* OCP was determined at 1.6 Å^{31,32}, showing two domains: an α -helical N-terminal domain and an α/β C-terminal domain. OCP is a blue-light-photoactive protein, identified as the trigger of the OCP-dependent NPQ in cyanobacteria. During this OCP-related NPQ mechanism, OCP changes from a stable orange form (OCP^o) into a metastable red form (OCP^r) as a response to strong blue-green light. Unlike OCP^o, the OCP^r form can bind tightly to the APC core, thereby inducing thermal dissipation of the excited PB and concomitantly it quenches the PB fluorescence^{33,34}. It was reported that in the quenched state, the decrease in excitation energy transfer from the PBs to the photosystems leads to a drop of about 30-40% in the activity of PSI and PSII in *Synechocystis* PCC 6803 cells³⁵.

In a previous paper, we reported on the kinetics of this OCP-dependent non-photochemical quenching mechanism in vivo and demonstrated that quenching occurs at the level of APC₆₆₀ and the quenching site was termed APC^Q₆₆₀. Recently the induction of OCP-related NPQ was successfully reconstructed in vitro using isolated PBs and OCP³³. It was demonstrated that during this process OCP^r is binding to PBs while OCP^o is not. Moreover it was shown that the addition of fluorescence recovery protein (FRP) can destabilize the binding of OCP^r to PBs and accelerate the fluorescence recovery³³. In that study three different PBs were used: PBs (CK_PBs) from a CK mutant which is completely lacking the C_PC rods³⁶, PBs (CB_PBs) from a CB mutant which is lacking both the intermediary and the core-distal C_PC hexamers³⁷, and PBs (WT_PBs) from wild-type cells. The structures of these PBs are shown in Fig 4.1. The binding site of OCP^r appeared to be on the allophycocyanin core. It was noticed that the binding of OCP to CK-PBs is weaker than to the other PBs, suggesting an important role of PC rods in the stabilization of the binding.

The fact that this OCP-related NPQ mechanism can now be reconstructed and studied in vitro for PBs with different sizes is important because it provides the possibility to study the physical mechanism underlying the quenching process in

vitro making use of ultrafast transient absorption techniques, something that is not easily feasible in vivo. However, this of course requires that the quenching mechanism is the same in vivo and in vitro, also for the different types of PBs. In this work we have measured the time- and spectrally-resolved fluorescence of three different types of PBs, both in their unquenched and quenched state. The later state was obtained by complexing the PBs with OCP^r. This should allow us to establish whether the quenching site, rate and mechanism are the same in vitro and in vivo and to determine what the influence of the PB composition is on the light-harvesting and NPQ properties.

Materials and methods

Isolation of phycobilisomes and formation of OCP-PB complexes

Details about the isolation protocols can be found in the work of Gwizdala et al³³. and references therein. OCP-PB complexes were prepared in the same way as before at room temperature with an OCP:PB ratio of 40:1 for CK_PB and CB_PB, and with a ratio of 20:1 for WT_PB.

Steady-state fluorescence

Steady-state fluorescence spectra were recorded with a Jobin Yvon Fluorolog FL3-22 spectrofluorimeter and corrected for wavelength-dependent sensitivity of the detection and fluctuations in lamp output. The excitation wavelength was 590 nm; a band pass of either 1 or 2 nm was used for both the excitation and emission monochromator. Fluorescence emission spectra were recorded using a step size of 0.5 nm and an integration time of 0.1 second. OCP-PB complexes were quenched by illuminating WT_PB (for ~5 minutes) and CB_PB and CK_PB (for ~20 minutes) at 20°C in 0.8 M phosphate with an actinic white light source in combination with a 500 nm broad band filter (K50) giving an intensity of ~800 $\mu\text{E}\cdot\text{m}^{-2}\cdot\text{s}^{-1}$. Before performing the steady-state fluorescence measurements and inducing nonphotochemical quenching, the optical density of all samples was adjusted to ~0.2 at the absorption maximum for a pathlength of 1 cm. The emission spectra were recorded immediately after quenching. One single measurement was finished in ~30 seconds, and during this short period, recovery

is practically absent for CB_PB and WT_PB, while only a few percent of CK_PB recovers according to ref.33.

Time-resolved fluorescence

Time-resolved fluorescence spectra were recorded with a (sub-) picosecond streak-camera system combined with a grating (50 grooves/mm, blaze wavelength 600 nm) with the central wavelength set at 700 nm, having a spectral width of 260 nm (for details see (38-40)). Excitation light was vertically polarized, the spot size diameter was typically $\sim 100\ \mu\text{m}$ and the laser repetition rate was 250 kHz. The detector polarizer was set at magic angle orientation. An excitation wavelength of 590 nm was used. The sample was stirred with a magnetic stirring bar (rate $\sim 10\ \text{Hz}$) and the laser power at 590 nm was adjusted to $30 \pm 3\ \mu\text{W}$. Images of 800 ps and 2 ns time window were obtained for WT_PB and for the other samples only the 2-ns time window was used. A high signal-to-noise ratio was achieved by averaging 100 single images, each obtained after analog integration of 10 exposures of 1.112 s. Images were corrected for background and photocathode shading, and were sliced up into traces of 4 nm width.

The instrument response function (IRF) was described with a double Gaussian shape; in the 2 ns time window, it consists of a Gaussian of $\sim 20\ \text{ps}$ FWHM (90% of IRF area) on top of a Gaussian of 100 ps FWHM (10% of IRF area), while in the 800 ps time window, it becomes a Gaussian of $\sim 9\ \text{ps}$ FWHM (90% of IRF area) on top of a Gaussian of 60 ps FWHM (10% of IRF area).

For measuring time-resolved fluorescence of PBs in the quenched state, samples of OCP-PBs were first quenched in the same way as was done for the steady-state fluorescence measurements, and then streak images were collected immediately after the induction of the quenching. During one sequence of 100 images, no differences were observed in the lifetimes and spectral shapes for any of the three quenched samples meaning that the recovery process is sufficiently slow to perform the measurements on quenched samples. Because of the relatively faster recovery from NPQ, OCP-CK_PB data was collected not after but during actinic illumination with blue-green light. The sample volume used for fluorescence excitation/detection was spatially well separated from the actinic light beam (a

cylinder of ~5 mm diameter×1 cm length)¹⁸; the entire volume of the sample was 4 ml and the sample was stirred continuously. All measurements were performed at room temperature (about 20°C) and lasted approximately 20 minutes for each sample.

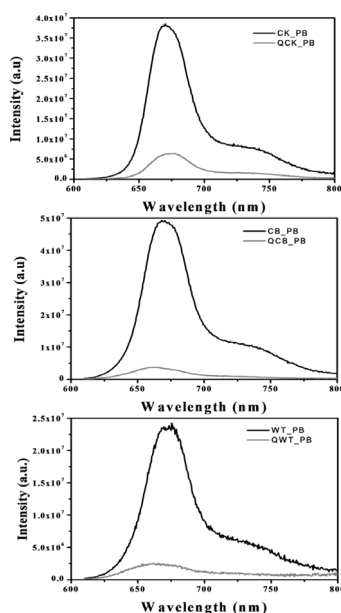
Data analysis

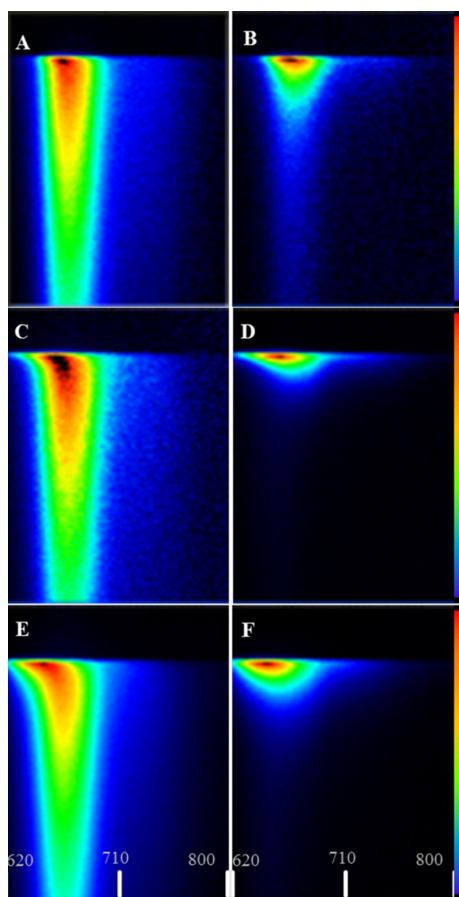
Data obtained with the streak-camera setup were first globally analyzed either with the R package TIMP or its graphical user interface of Glotaran. For details see⁴¹⁻⁴³. The methodologies of global analysis and target analysis are described in⁴⁴: with global analysis the data were fitted as a sum of exponential decays convolved with an IRF and the amplitudes of each decay component as a function of wavelength are called decay-associated spectra (DAS). Subsequently target analysis was performed in order to obtain the species-associated spectra (SAS), to identify the site of the quenching, and to describe the energy transfer rates between pigment species and to determine the rate of quenching. The kinetic model used here is entirely consistent with the model used for the target analysis of the in vivo data¹⁸.

Results

Figure 4.2 Steady-state fluorescence spectra. Isolated CK_PBs (top), CB_PBs (middle) and WT_PBs (bottom) before (unquenched, black lines) and after (quenched, grey lines) illumination with high-intensity blue-green light. The fluorescence excitation wavelength is 590 nm. Spectra have been normalized to equal absorption at 590 nm for the unquenched and the quenched PBs.

Figure 4.2 shows the fluorescence quenching of PBs in the presence of OCP after strong blue-green light illumination (see Materials and Methods for details). The amount of fluorescence quenching is 84% for CK_PB, 92%





for CB_PB and 89% for WT_PB (percentage of the maximal peak intensity). The results are similar as before^{33,45}.

Figure 4.3 Time-resolved fluorescence data obtained with the streak-camera setup using a time window of 2 ns with 590 nm excitation A,B) CK_PB, C,D) CB_PB, E,F) WT_PB; A,C,E) correspond to unquenched PBs and B,D,F) to quenched PBs. All images represent the fluorescence intensity (using a linear color gradient) as a function of time (vertical axis, 2 ns) and wavelength (horizontal axis, nm).

To study the energy-transfer processes and the quenching kinetics in different PBs, time-resolved fluorescence measurements were performed with a picosecond streak-camera system(46). An excitation wavelength of 590 nm was used that selectively excites (> 90 %) APC₆₆₀ in CK_PB or C_PC pigments (> 90 %) in

CB_PB and WT_PB. Streak images of unquenched PBs are shown in Fig.4.3 (A,C,E) and of OCP-quenched PBs in Fig.4.3 (B,D,F). Note that in CK_PB, the spectrum is hardly shifting in time while the spectra of the other two types of PBs are clearly shifting to the red, i.e. to longer wavelengths. The shifting is due to excitation-energy transfer (EET) to pigments that fluoresce at longer wavelengths. A comparison of the left and right panels shows the dramatic shortening of the fluorescence lifetimes for the quenched PBs.

To describe the streak images quantitatively, global analysis was employed, which led to the DAS that are shown in Fig 4.4.

Picosecond Kinetics of Light Harvesting and Photoprotective Quenching in WT and Mutant Phycobilisomes Isolated from the Cyanobacterium *Synechocystis* PCC 6803

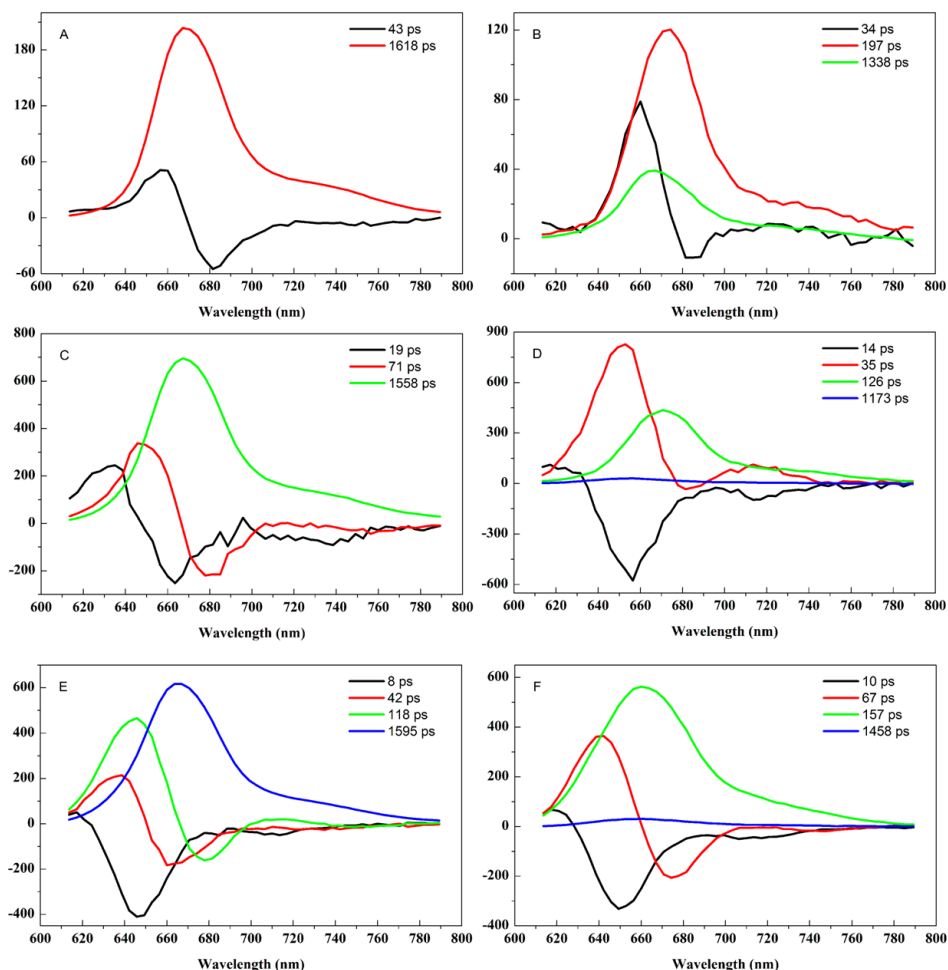


Figure 4.4 Global-fitting results (DAS) of the time-resolved fluorescence data obtained with the streak-camera setup using either a time window of 2 ns or 800 ps. A,B) CK_PB and OCP-CK_PB after strong blue-green light illumination; C,D) CB_PB and OCP-CB_PB after strong blue-green light illumination; E,F) WT_PB and OCP-WT_PB after strong blue-green light illumination.

The corresponding lifetimes are presented in each figure. Spectra have been normalized to an equal number of absorbed photons at 590 nm, both for the unquenched and the quenched PBs.

The data of unquenched CK_PB can be fitted by two main components as shown in Fig.4.4A. The fastest component of 43 ps has a spectrum that has a positive part peaking at 660 nm, and a negative part with similar area peaking around 680 nm, mainly reflecting excitation energy transfer (EET) from APC₆₆₀ to APC₆₈₀. The 1.6 ns DAS is positive over the entire wavelength region with maximum emission around 670 nm, mainly reflecting decay of excitations that are thermally equilibrated over APC₆₆₀ and APC₆₈₀. Global analysis of the data of quenched CK_PB requires at least three lifetime components (see Fig.4.4B). The 34-ps DAS exhibits a positive amplitude at 660 nm and a negative amplitude at 680 nm. However, in this case the area of the positive part is clearly larger than that of the negative part, and also larger than the positive part of the 43 ps-DAS for unquenched CK_PB. This suggests that substantial excited-state decay already occurs on a time scale of tens of ps, leading to accelerated depopulation of excited APC₆₆₀ molecules and concomitantly a decreased amount of EET to APC₆₈₀. It should be noted that the negative part of the DAS is not completely disappearing which is partly due to the fact that not all PBs are quenched (see below). The 197-ps component corresponds to quenched PBs, whereas the 1338-ps component corresponds to some unquenched species, that has a somewhat blue-shifted DAS as compared to the 1.6-ns DAS in unquenched CK_PB. This is probably due to the presence of a small amount of not-well-connected PBs or disconnected APC₆₆₀ trimers.

Figs 4.4C and 4.4D show the global-analysis results of unquenched and quenched CB_PB, with 3 and 4 components, respectively. For CB_PB, the obtained 19 ps-DAS has more or less a conservative spectral shape with a positive peak at 635 nm and a negative one at 660 nm which represents to a large extent EET from C_PC to APC₆₆₀. The 71 ps component is positive at 650 nm and negative at 677 nm, reflecting EET to APC₆₈₀. An all-positive spectrum of 1.6 ns is peaking at 670 nm. Blue-green-light quenching causes dramatic changes in the DAS as is shown in Fig.4.4D: the fastest component (14 ps) of the quenched state has a dominating negative peak around 660 nm, with a higher amplitude than the 19 ps component of the unquenched state. In contrast, the second component (35 ps) has a larger positive amplitude than the second component (71 ps) for the unquenched complex, also peaking around 650 nm. The lifetime is much shorter and the

negative part peaking around 680 nm is strongly reduced. The all-positive DAS with a lifetime of 126 ps has a spectral shape that is similar to that of the 1.6 ns component of the unquenched PBs which corresponds to the disappearance of equilibrated excited-state energy, mainly due to quenching. In addition, the spectral shape and lifetime are also similar to those of the 197-ps component of the CK_PB. The longest lifetime component of 1.2 ns peaking around 650 nm has a small amplitude (~3 %) and probably relates to a small amount of free PC species.

Both for the unquenched and quenched WT_PBs, four components are needed to get satisfactory fits of the data. Three clear EET steps can be observed (Fig. 4.4E). The DAS of the fastest component of 8 ps is almost entirely negative with a peak around 645 nm. This reflects EET within C-PC from blue pigments with relatively low dipole strength to somewhat more red-shifted pigments with higher dipole strength¹⁸. The 42-ps component shows a positive peak at 640 nm and a negative one at 663 nm and mainly reflects EET from C-PC to APC₆₆₀ (see also Tian et al.¹⁸). The 118-ps component has a positive peak around 645 nm and a negative one at 680 nm, reflecting EET to APC₆₈₀. The 1.6-ns DAS has its main peak at 667 nm which is due to decay of excited-state-equilibrated PBs.

Under quenching conditions, the fastest component is hardly influenced, indicating that the quenching is not happening on the pigments in C_PC. The 67-ps DAS has a typical EET shape and it is more or less the average of the 42-ps and 118-ps components that are observed for the unquenched PBs. The long-lived DAS (1595 ps) that was observed for the unquenched PBs is now absent and instead a similar DAS is observed with a far shorter lifetime of 157 ps. Finally, a small contribution is observed characterized by a lifetime of 1.5-ns and a blue-shifted (as compared to the 157-ps component) emission spectrum, possibly originating from a small fraction of unconnected C_PC.

Discussion

As was shown above, the binding of the activated form of OCP to the different types of PBs in vitro leads to strong changes in the steady-state and time-resolved fluorescence properties of the PBs. It was demonstrated before that for WT

Synechocystis cells *in vivo*, OCP-induced NPQ leads to the direct quenching of APC₆₆₀ with a quenching rate of approximately (~ 15 ps)⁻¹¹⁸. The fact that OCP is able to induce fluorescence quenching in PBs lacking one or two of the APC₆₈₀ indeed confirmed that the site of quenching must be APC₆₆₀¹¹. It is important to note that in WT *Synechocystis* cells only 30% of the PBs was quenched due the presence of substoichiometric amounts of OCP with respect to the amount of PBs, which was probably caused by the fact that the cells were grown in relatively low-light conditions. In OCP overexpressing strains, in a PSI/PSII less *Synechocystis* mutant and in strains growing in high-light conditions, high quantities of OCP are present in the cell and concomitantly a high percentage of fluorescence quenching is observed^{34,45,47}. In order to sort out whether also *in vitro* APC₆₆₀ is the quencher in complexes of PBs with activated OCP, and to determine the fraction of quenched PBs and the rate of quenching we have performed target analysis.

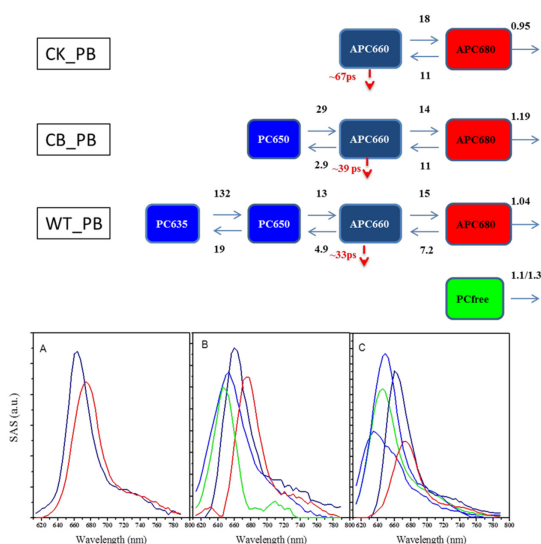


Figure 4.5 Kinetic schemes for target analysis of the time-resolved fluorescence data of unquenched and quenched isolated PBs. Each compartment represents a pool of pigments. Energy-transfer rates between these pools (shown in ns⁻¹) and their spectra were estimated from the fitting: (A) CK_PB, (B) CB_PB and (C) WT_PB. The inverse quenching rate is shown in red (in ps). Note that according to the fitting results not all CK_PBs contain a quencher; details are given in the text.

Different compartmental models were constructed (see Fig. 4.5) in analogy with our recent study on entire cells in order to fit/describe the data¹⁸. Each compartment is composed of a pool of pigments with similar fluorescence spectra. The fitting results for the isolated PBs are also shown in Fig. 4.5. For all compartments Species Associated Spectra (SAS) and also the rates of excitation-energy transfer between different compartments were estimated. All spectra and most of the transfer rates are nearly identical to those obtained for intact cells. The quenching site and rate for each PB were estimated by fitting both unquenched and quenched datasets simultaneously; more details about the fittings are described in the Supporting Material.

The target analysis for CK_PB is relatively simple since only two compartments are needed as shown in Fig 4.5; one corresponds to APC₆₆₀ and the other to APC₆₈₀, and the corresponding spectra are given in blue and red, respectively. One more C_PC spectrum (in blue) could be resolved for CB_PB, corresponding to C_PC. For WT_PB two C_PC pools could be resolved (shown as blue) and the model established here for WT_PBs is identical to the one obtained for whole cells in vivo¹⁸. Note that there are always some free species with green SAS as shown in Fig 4.5 present in CB or WT with a contribution of 5~6 %, decaying with a lifetime around 1 ns.

It is found that quenching only happens on 85% of the CK_PB's under our experimental conditions, while 100% of the CB_PB's and WT_PB's appear to be quenched. The compartment in which the quenching takes place is unequivocally the one of APC₆₆₀ in all cases. The quality of the fitting decreases substantially and/or unrealistic SAS are obtained when it is assumed that quenching occurs in one of the other compartments (for further details see Supporting Material). If we fit the data to the kinetic scheme of WT_PB in figure 4.5 and we require the quencher to be in compartment 3 then the estimated species-associated spectrum (SAS) peaks around 660 nm. If the quencher is forced to be in compartment 4, the fitting at early times becomes worse (compare fig. S4.2) but the peak of the SAS of the quenched compartment is again around 660 nm. It is inherent to the (early) kinetic data that the quenching takes place in the APC₆₆₀ compartment, no matter what the exact details of the kinetic scheme are.

Therefore, the location of the quenching appears to be the same as in vivo¹⁸. The quenching rate for CK_PB is $(67 \pm 7 \text{ ps})^{-1}$ while it is $(39 \pm 4 \text{ ps})^{-1}$ for CB_PB and $(33 \pm 3 \text{ ps})^{-1}$ for WT_PB.

It was observed before that the relative amount of quenching for isolated PBs increases in the following order: CK_PB, WT_PB, CB_PB³³. These results were reproduced in the present study (Fig.4.2) The target analysis results enable us to estimate the contribution of each compartment to the total steady-state spectrum both for the quenched and unquenched PBs and to determine the origin of the changing quenching ratios. The reconstructed spectra and the corresponding quenching ratios are shown in Fig.S4.6, Fig.S4.7 and Fig. S4.8 in the Supporting Material and are fully in agreement with the previously observed results³³.

Concerning the quenching mechanism, the quenching rates of $(39 \pm 4 \text{ ps})^{-1}$ in CB_PB and $(33 \pm 3 \text{ ps})^{-1}$ in WT_PB are (only) somewhat slower than the one of $(16 \pm 4 \text{ ps})^{-1}$ obtained for intact cells. It was concluded before that the rate of $(16 \pm 4 \text{ ps})^{-1}$ corresponds to a quenching rate of the excited state of the pigment that is directly quenched ($\text{APC}_{660}^{\text{Q}}$) is extremely fast¹⁸, namely $(240 \pm 60 \text{ fs})^{-1}$ ($= (16 \pm 4 \text{ ps})^{-1} / 66$ where 66 is the number of APC_{660} pigments) or even faster and in the present case the molecular quenching rate must also be extremely fast, namely $(500 \pm 50 \text{ fs})^{-1}$ or faster. Both the similar fast quenching rate and the same identity of the quenched species leave little doubt that the quenching in vitro proceeds via the same mechanism as in vivo. It was suggested in our previous work that quenching is most likely caused by charge transfer between $\text{APC}_{660}^{\text{Q}}$ and the OCP carotenoid hECN in its activated form but it could not be entirely excluded that EET from $\text{APC}_{660}^{\text{Q}}$ to the S1 state of hECN might be responsible for this OCP-related NPQ mechanism¹⁸. Both processes depend critically on the mutual interactions (overlap of molecular wavefunctions) and slight structural differences in the complex between OCP and $\text{APC}_{660}^{\text{Q}}$ are probably responsible for the differences in quenching rate. Ultrafast transient absorption measurements will be needed to discriminate between these two possibilities. Whereas these measurements are extremely demanding if not impossible for intact cells they can now be performed on quenched PBs in vitro, since apparently the quenching mechanism is the same.

It is of relevance to mention that although the in vitro quenching rate is still extremely fast it would only lead to quenching of ~66% of the excitations in the PBs in vivo whereas the previously determined percentage is 80% in vivo. This percentage of 66% can be calculated using the fact that the rate of transfer from APC to the photosystems is $(63 \text{ ps})^{-1}$ and the rate of quenching is directly competing with this transfer rate (18). Therefore, the extremely fast quenching rate that is obtained in vivo is crucial for the efficiency of quenching. It is of interest to note that the quenching in CK_PB is even slower $(67 \text{ ps})^{-1}$, which suggests that the presence of C_PC is required for the tight binding between OCP^r and PBs. It was already reported before that the binding of OCP to CK_PB is weaker than to WT_and CB_PB³³, and now it is found that this leads to a lower percentage of quenched PBs but also to a slower quenching rate. With this rate of quenching the efficiency of quenching would be round 50% in vivo. The slower quenching rate and the lower binding strength both contribute to explain the low amplitude of fluorescence quenching observed in CK cells compared to that observed in WT cells³⁰.

Conclusions

All types of isolated PBs that were studied here show a large amount of nonphotochemical quenching upon binding of the red active form OCP. In all cases the quenching occurs in the core of the PBs on APC₆₆₀ and not on APC₆₈₀. However, also the presence of C_PC has some influence on the quenching, since the rate of quenching increases from $(67 \pm 7 \text{ ps})^{-1}$ for CK_PB to $(39 \pm 4 \text{ ps})^{-1}$ for CB_PB and $(33 \pm 3 \text{ ps})^{-1}$ for WT_PB. Although the latter rate is still a factor of 2 slower than the one in vivo, it is concluded that both the site and mechanism of quenching are the same in all PBs, both in vitro and in vivo. Full assembly in vivo leads to the fastest quenching rate and this rate is required to compete with excitation-energy transfer to the photosystems, allowing efficient photoprotection.

ACKNOWLEDGMENT

We thank Arie van Hoek (Wageningen UR) for excellent technical support. This work was supported by a fellowship to L.T. by the Graduate School Experimental Plant Sciences (EPS), Wageningen, The Netherlands, and by the European community via the HARVEST project and by the Dutch Ministry of ELI through the BioSolar Cells Project. M.G. is supported by the European community via a fellowship of the HARVEST project. Research in D.K. group is supported by the CEA, CNRS and ANR (CYANOPROTECT), France.

References

- (1) Rasmussen, B.; Fletcher, I. R.; Brocks, J. J.; Kilburn, M. R. *Nature* **2008**, *455*, 1101-1104.
- (2) Potts, B. A. W. M. *The ecology of cyanobacteria: their diversity in time and space*; Kluwer Academic Publishers, 2002.
- (3) Golbeck, J. H. *Annu Rev Plant Phys* **1992**, *43*, 293-324.
- (4) Barber, J.; Nield, J. *Philosophical Transactions of the Royal Society of London Series B-Biological Sciences* **2002**, *357*, 1329-1335.
- (5) Croce, R.; van Amerongen, H. *J Photoch Photobio B* **2011**, *104*, 142-153.
- (6) Adir, N. *Photosynthesis Research* **2005**, *85*, 15-32.
- (7) Glazer, A. N. *Biochimica Et Biophysica Acta* **1984**, *768*, 29-51.
- (8) Arteni, A. A.; Ajlani, G.; Boekema, E. J. *Biochimica Et Biophysica Acta-Bioenergetics* **2009**, *1787*, 272-279.
- (9) Lundell, D. J.; Glazer, A. N. *The Journal of biological chemistry* **1983**, *258*, 902-908.
- (10) Sidler, W. In *The Molecular Biology of Cyanobacteria*; Bryant, D. A., Ed.; Kluwer Academic Publishers, Dordrecht, The Netherlands: 1994, p 139-261.
- (11) Jallet, D.; Gwizdala, M.; Kirilovsky, D. *Biochimica et Biophysica Acta (BBA) - Bioenergetics*.
- (12) Lundell, D. J.; Glazer, A. N. *J Biol Chem* **1983**, *258*, 894-901.
- (13) Redlinger, T.; Gantt, E. *P Natl Acad Sci USA* **1982**, *79*, 5542-5546.
- (14) Suter, G. W.; Mazzola, P.; Wendler, J.; Holzwarth, A. R. *Biochimica et Biophysica Acta (BBA) - Bioenergetics* **1984**, *766*, 269-276.
- (15) Mullineaux, C. W.; Holzwarth, A. R. *Biochimica Et Biophysica Acta* **1991**, *1098*, 68-78.
- (16) Bittersmann, E.; Vermaas, W. *Biochim Biophys Acta* **1991**, *1098*, 105-116.
- (17) Krumova, S. B.; Laptinok, S. P.; Borst, J. W.; Ughy, B.; Gombos, Z.; Ajlani, G.; van Amerongen, H. *Biophysical Journal* **2010**, *99*, 2006-2015.
- (18) Tian, L.; Stokkum, I. H. M. v.; Koehorst, R. B. M.; Jongerius, A.; Kirilovsky, D.; Amerongen, H. v. *Journal of the American Chemical Society* **2011**, *133*, 18304-18311.
- (19) Kirilovsky, D. *Photosynth Res* **2007**, *93*, 7-16.

- (20) Karapetyan, N. V. *Biochemistry-Moscow* **2007**, *72*, 1127-1135.
- (21) Ihalainen, J. A.; D'Haene, S.; Yeremenko, N.; van Roon, H.; Arteni, A. A.; Boekema, E. J.; van Grondelle, R.; Matthijs, H. C. P.; Dekker, J. P. *Biochemistry-Us* **2005**, *44*, 10846-10853.
- (22) Yeremenko, N.; Kouril, R.; Ihalainen, J. A.; D'Haene, S.; van Oosterwijk, N.; Andrizhiyevskaya, E. G.; Keegstra, W.; Dekker, H. L.; Hagemann, M.; Boekema, E. J.; Matthijs, H. C. P.; Dekker, J. P. *Biochemistry-Us* **2004**, *43*, 10308-10313.
- (23) Zhu, Y.; Graham, J. E.; Ludwig, M.; Xiong, W.; Alvey, R. M.; Shen, G.; Bryant, D. A. *Arch Biochem Biophys* **2010**, *504*, 86-99.
- (24) Aro, E. M.; Virgin, I.; Andersson, B. *Biochim Biophys Acta* **1993**, *1143*, 113-134.
- (25) Vass, I. *Physiol Plant* **2011**, *142*, 6-16.
- (26) Finazzi, G.; Johnson, G. N.; Dall'Osto, L.; Zito, F.; Bonente, G.; Bassi, R.; Wollman, F. A. *Biochemistry-Us* **2006**, *45*, 1490-1498.
- (27) Ruban, A. V.; Lavaud, J.; Rousseau, B.; Guglielmi, G.; Horton, P.; Etienne, A. L. *Photosynth Res* **2004**, *82*, 165-175.
- (28) Ruban, A. V.; Berera, R.; Iliaia, C.; van Stokkum, I. H.; Kennis, J. T.; Pascal, A. A.; van Amerongen, H.; Robert, B.; Horton, P.; van Grondelle, R. *Nature* **2007**, *450*, 575-578.
- (29) Holt, N. E.; Zigmantas, D.; Valkunas, L.; Li, X. P.; Niyogi, K. K.; Fleming, G. R. *Science* **2005**, *307*, 433-436.
- (30) Wilson, A.; Ajlani, G.; Verbavatz, J. M.; Vass, I.; Kerfeld, C. A.; Kirilovsky, D. *Plant Cell* **2006**, *18*, 992-1007.
- (31) Kerfeld, C. A.; Sawaya, M. R.; Brahmandam, V.; Cascio, D.; Ho, K. K.; Trevithick-Sutton, C. C.; Krogmann, D. W.; Yeates, T. O. *Structure* **2003**, *11*, 55-65.
- (32) Wilson, A.; Kinney, J. N.; Zwart, P. H.; Punginelli, C.; D'Haene, S.; Perreau, F.; Klein, M. G.; Kirilovsky, D.; Kerfeld, C. A. *J Biol Chem* **2010**, *285*, 18364-18375.
- (33) Gwizdala, M.; Wilson, A.; Kirilovsky, D. *Plant Cell* **2011**, *23*, 2631-2643.
- (34) Gorbunov, M. Y.; Kuzminov, F. I.; Fadeev, V. V.; Kim, J. D.; Falkowski, P. G. *Biochimica et Biophysica Acta (BBA) - Bioenergetics* **2011**, *1807*, 1591-1599.
- (35) Rakhimberdieva, M. G.; Elanskaya, I. V.; Vermaas, W. F. J.; Karapetyan, N. V. *Biochimica Et Biophysica Acta-Bioenergetics* **2010**, *1797*, 241-249.
- (36) Ajlani, G.; Vernet, C. *Plant Molecular Biology* **1998**, *37*, 577-580.
- (37) Ughy, B.; Ajlani, G. *Microbiology-Sgm* **2004**, *150*, 4147-4156.
- (38) Stokkum, I. H. M.; Oort, B.; Mourik, F.; Gobets, B.; Amerongen, H. In *Biophysical Techniques in Photosynthesis*; Aartsma, T. J., Matysik, J., Eds.; Springer Netherlands: 2008; Vol. 26, p 223-240.
- (39) van Oort, B.; Amunts, A.; Borst, J. W.; van Hoek, A.; Nelson, N.; van Amerongen, H.; Croce, R. *Biophysical Journal* **2008**, *95*, 5851-5861.
- (40) Van Oort, B.; Murali, S.; Wientjes, E.; Koehorst, R. B. M.; Spruijt, R. B.; van Hoek, A.; Croce, R.; van Amerongen, H. *Chemical Physics* **2009**, *357*, 113-119.
- (41) Laptenok, S. P.; Borst, J. W.; Mullen, K. M.; van Stokkum, I. H. M.; Visser, A. J. W. G.; van Amerongen, H. *Phys Chem Chem Phys* **2010**, *12*, 7593-7602.
- (42) Mullen, K. M.; van Stokkum, I. H. M. *J Stat Softw* **2007**, *18*, 1-46.

Chapter 4

- (43) Snellenburg, J. J.; Laptanok, S. P.; Seger, R.; Mullen, K. M.; Van Stokkum, I. H. M. *journal of statistical software* **2012**, 49(3) 1-22.
- (44) van Stokkum, I. H. M.; Larsen, D. S.; van Grondelle, R. *Biochimica Et Biophysica Acta-Bioenergetics* **2004**, 1657, 82-104.
- (45) Rakhimberdieva, M. G.; Kuzminov, F. I.; Elanskaya, I. V.; Karapetyan, N. V. *Febs Letters* **2011**, 585, 585-589.
- (46) van Stokkum, I. H. M.; Gobets, B.; Gensch, T.; van Mourik, F.; Hellingwerf, K. J.; van Grondelle, R.; Kennis, J. T. M. *Photochem Photobiol* **2006**, 82, 380-388.
- (47) Wilson, A.; Punginelli, C.; Gall, A.; Bonetti, C.; Alexandre, M.; Routaboul, J. M.; Kerfeld, C. A.; van Grondelle, R.; Robert, B.; Kennis, J. T. M.; Kirilovsky, D. *Proceedings of the National Academy of Sciences of the United States of America* **2008**, 105, 12075-12080.

Supporting Materials

Target analysis and the quality of the fit

Target analysis was performed by using the scheme as shown in Fig.4.4 of the main manuscript. For each type of PB, the data sets of unquenched and quenched PBs were fitted simultaneously. For the quenched case, an extra quenching parameter was added either on the pool of APC660 or APC680. No constraint was imposed on any fitting parameters. It was found that in all cases, quenching on APC660 provided the best fitting results. The high fitting quality is clearly visualized by the nice overlap between the fitted curves (dash) and the measured traces (solid) covering the whole wavelength range as shown in Fig.S4.1 for CK_PB, in Fig.S4.3 for CB_PB and in Fig. S4.4 for WT_PB. In each fitting procedure, the best root mean square (RMS) error was aimed for.

Determination of the quenching site

As mentioned above, the quenching site was searched for by adding an extra decay parameter on either APC660 or APC680. Here, the CK_PB is taken as an example, because it provides the easiest illustration. Putting the quencher on APC660 provides good fitting results and produces the nice SAS as shown in Fig 4.4B, corresponding to the fluorescence spectra of APC660 or APC680. The rms is 2.055. Putting the quencher on APC680 provides a significantly less good fit, especially around 660 nm. The lack of fit is clear by comparing Figs.S4.2A and B. and also the rms is higher: 2.130. In addition, the spectrum of APC680 (as shown in Fig.S4.2.C dash) is strongly blue-shifted to 667 nm..

In the case of CB_PB and WT_PB, putting the quencher on APC680 lead to clearly wrong SAS (not shown). For instance, if in the case of CB_PB the quenching is forced to be on the third component, its maximum shifts to around 660 nm and the peak of the second component shifts to around 672 nm. Moreover, the rms becomes 2.82, whereas it is 2.52 when the quencher is forced to be on 2nd component and also the spectra are far better. Similar results are obtained for WT cells.

Comparison of SAS estimated from individual target analysis on different PBs

The normalized SAS of all PBs are shown in Fig.S4.5. Although the spectra of different PBs are not 100% identical for supposedly identical compartments, they show a high level of consistency and the differences between different compartments are far higher than between “identical” compartments. Of course, the corresponding energy transfer rates as shown in the scheme of Fig.4.4 are also not absolutely identical but they are rather close.

Reconstruction of the steady-state spectra

From target analysis, the steady-state spectra of both the quenched and unquenched PBs can be reconstructed as is shown in Figs. S4.6, S4.7, and S4.8 and the contribution of each compartment to the total steady-state spectrum is given. As expected, the PC pigments contribute to a large fraction of the total fluorescence in quenched CB_PB and WT_PB as can be seen in Fig.S4.7B and Fig.S4.8B. The more PC is present, the smaller the quenching ratio is. CK_PB shows the smallest quenching ratio under the same conditions, which is caused by a large fraction of unquenched PBs (~15% in our case) in combination with a slower quenching rate.

Picosecond Kinetics of Light Harvesting and Photoprotective Quenching in WT and Mutant Phycobilisomes Isolated from the Cyanobacterium *Synechocystis* PCC 6803

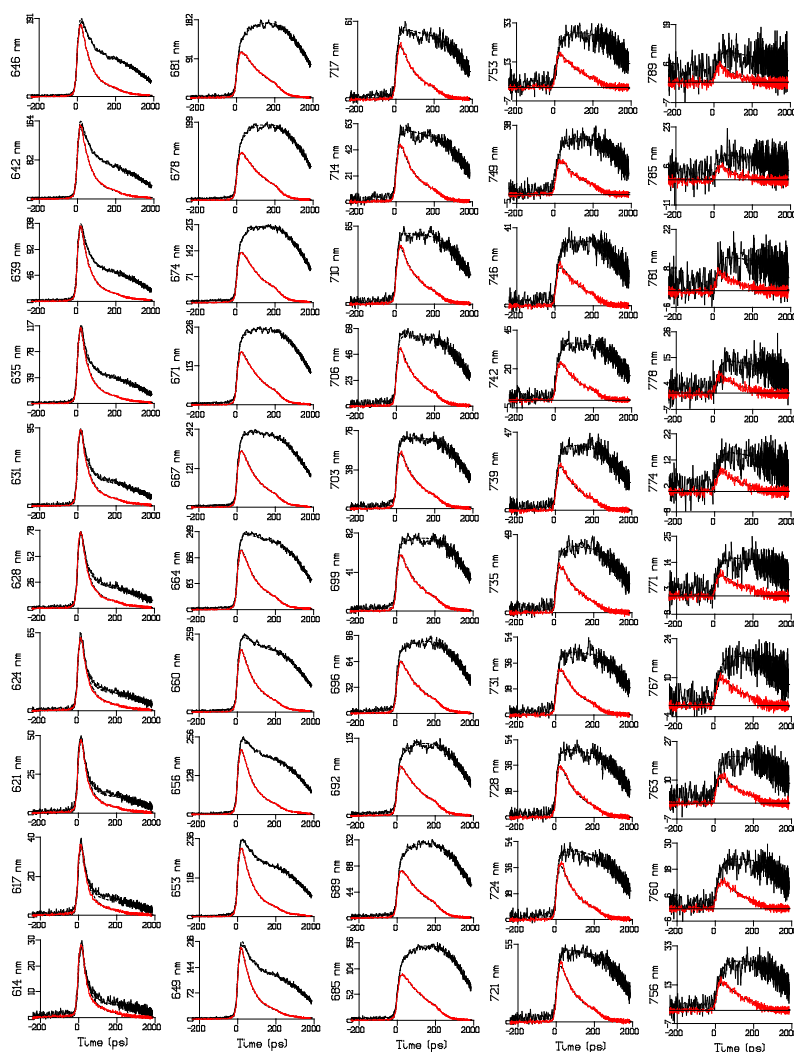


Figure.S4.1 Emission of CK_PB at 50 wavelengths (indicated in the abscissa label) after 590 nm excitation, as obtained from the streak images in Fig.4.2.a,d Key: unquenched (black), quenched (red). Dashed lines indicate the simultaneous target analysis fit. Note that the time axis is linear until 200 ps and logarithmic thereafter. Note also that each panel is scaled to its maximum. Overall rms error of the fit was 2.055.

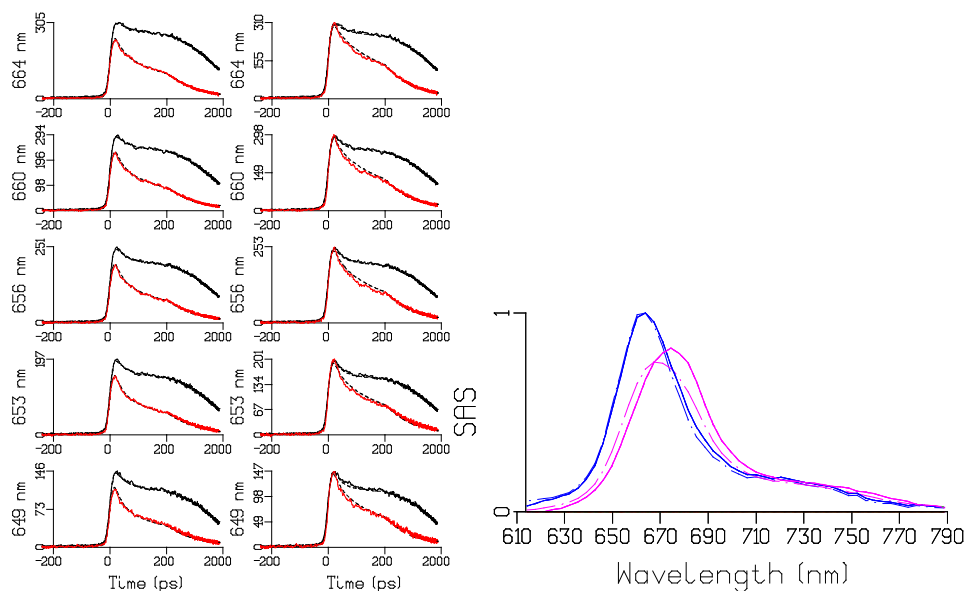


Figure.S4.2 comparison of fits of emission of CK_PB after 590 nm excitation at five selected wavelengths. (A) using a target model with quenching from APC₆₆₀ (overall rms error of the fit 2.055). **(B)** using a target model with quenching from APC₆₈₀ (overall rms error of the fit 2.130). Key to A,B: unquenched (black), quenched (red). Dashed lines indicate the simultaneous target analysis fit. Note that the time axis is linear until 200 ps and logarithmic thereafter. Note also that each panel is scaled to its maximum. **(C)** Comparison of estimated SAS using a target model with quenching from APC₆₆₀ (solid) and from APC₆₈₀ (dotted). Key: APC₆₆₀ (blue) and APC₆₈₀ (magenta).

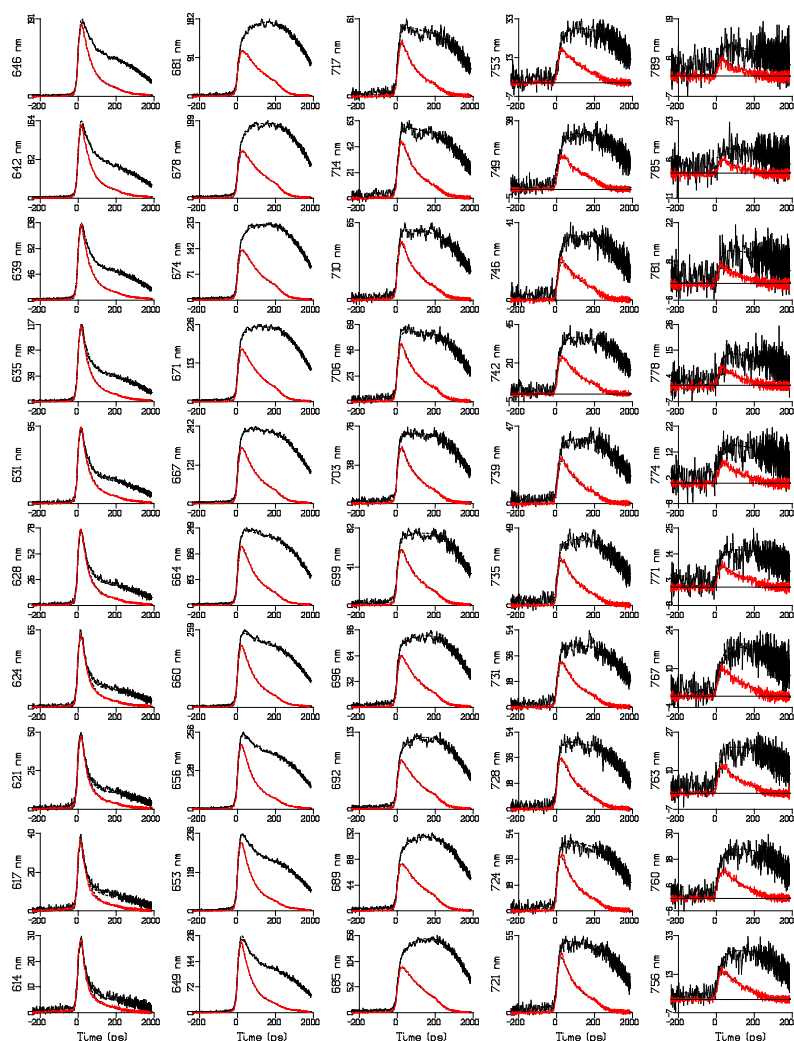


Figure.S4.3 Emission of CB_PB at 50 wavelengths after 590 nm excitation, as obtained from the streak images in Fig.4.2.b,e Key: unquenched (black), quenched (red). Dashed lines indicate the simultaneous target analysis fit. Note that the time axis is linear until 200 ps and logarithmic thereafter. Note also that each panel is scaled to its maximum. Overall rms error of the fit was 2.52.

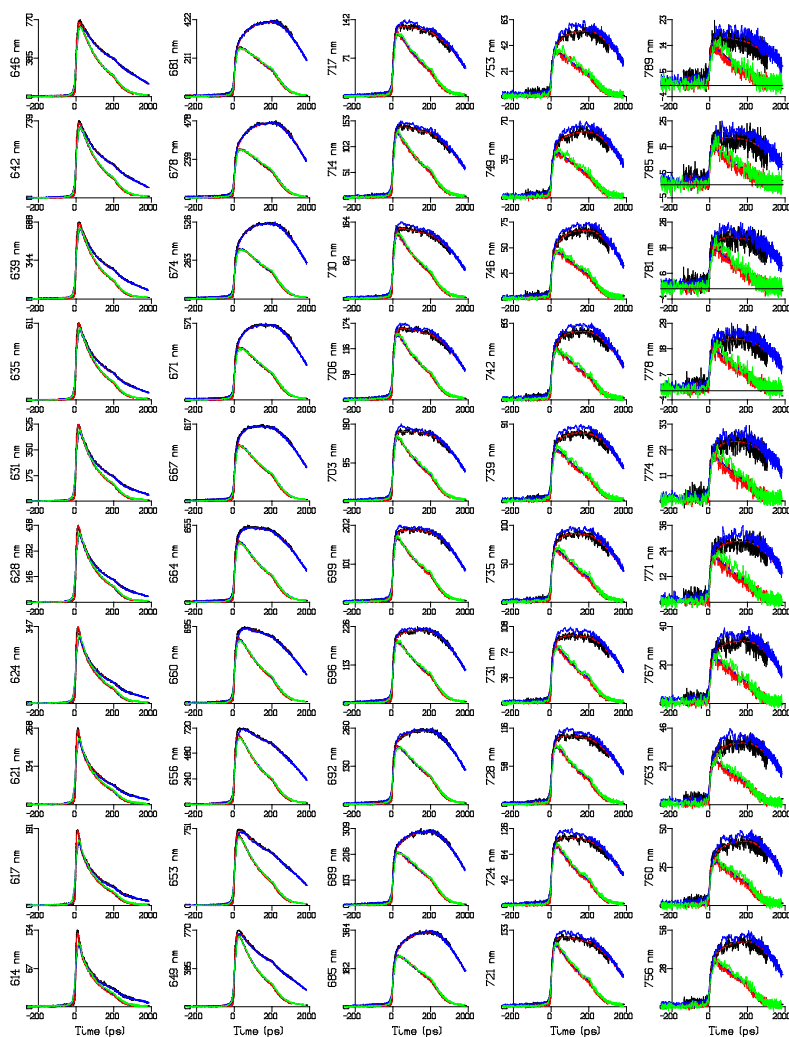


Fig.S4.4 Emission of WT_PB at 50 wavelengths after 590 nm excitation, as obtained from the streak images in Fig.4.2.cf. Key: unquenched time range 2 (black), quenched time range 2 (red), unquenched time range 4 (blue), quenched time range 4 (green). Dashed lines indicate the simultaneous target analysis fit. Note that the time axis is linear until 200 ps and logarithmic thereafter. Note also that each panel is scaled to its maximum. Overall rms error of the fit was 3.86.

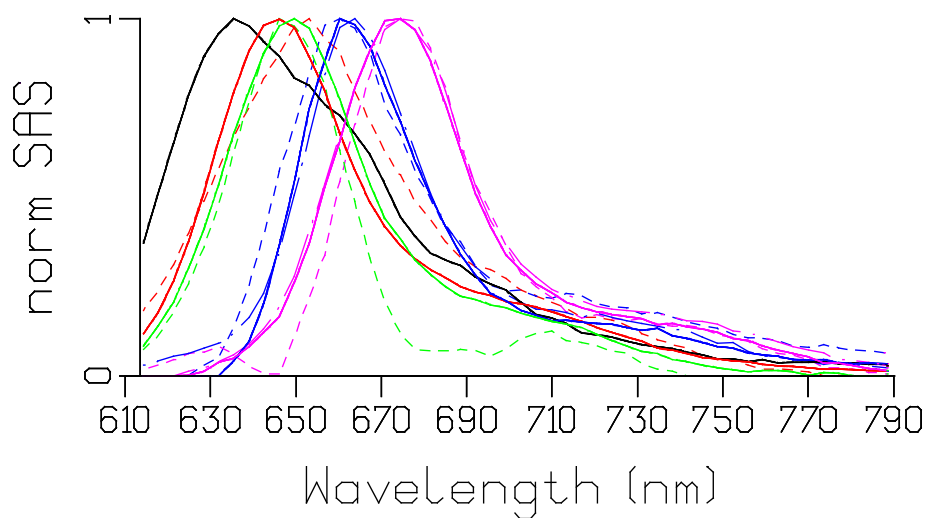


Figure.S4.5 Comparison of normalized SAS of WT_PB (solid), CB_PB (dashed) and CK_PB (dot dashed). Key: PC_S (black), PC_L (red), PC (of PB, red dash), loose PC (green), APC₆₆₀ (blue) and APC₆₈₀ (magenta).

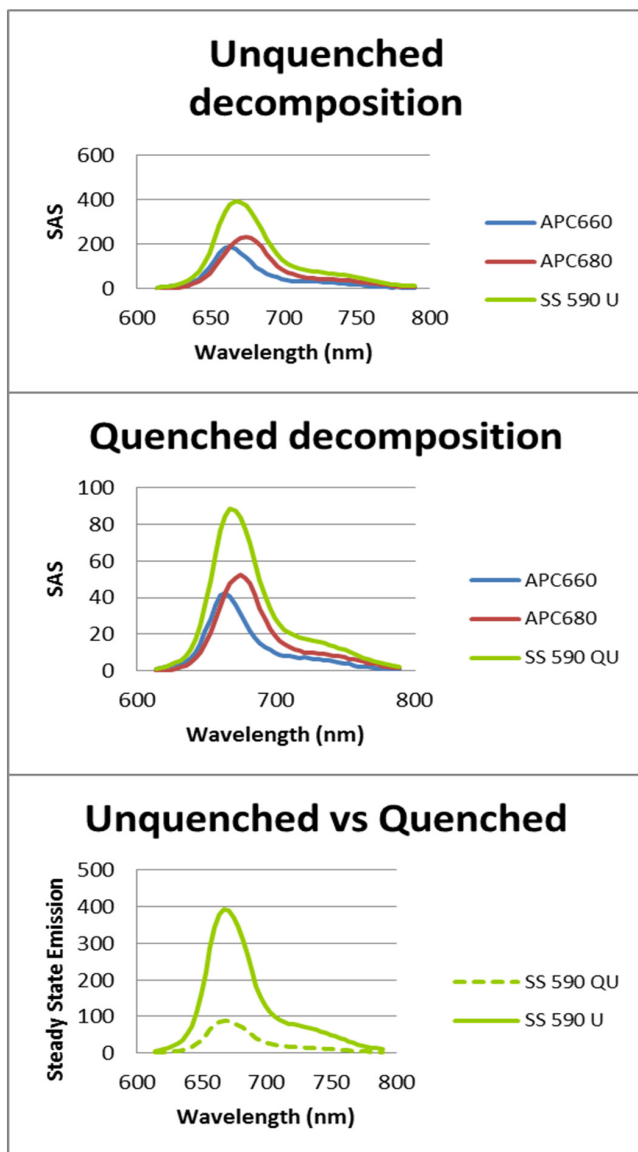


Figure.S4.6 Reconstructed steady-state spectra of CK_PB with 590 nm excitation in the unquenched and quenched state. In panels A and B, spectral contributions of each species are shown. In panel C, The green curves represent the sum of these for the unquenched (solid) and quenched (dash) states are shown again.

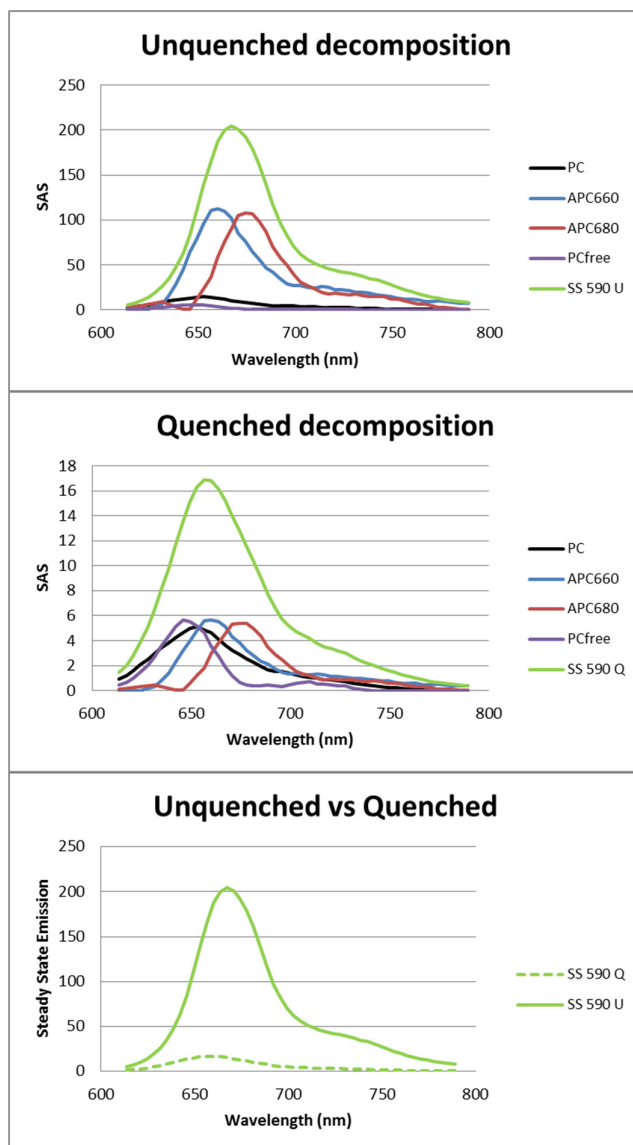


Figure.S4.7 Reconstructed steady-state spectra of CB_PB with 590 nm excitation in the unquenched and quenched state. Spectra are shown in the same layout as Fig. S4.6 .

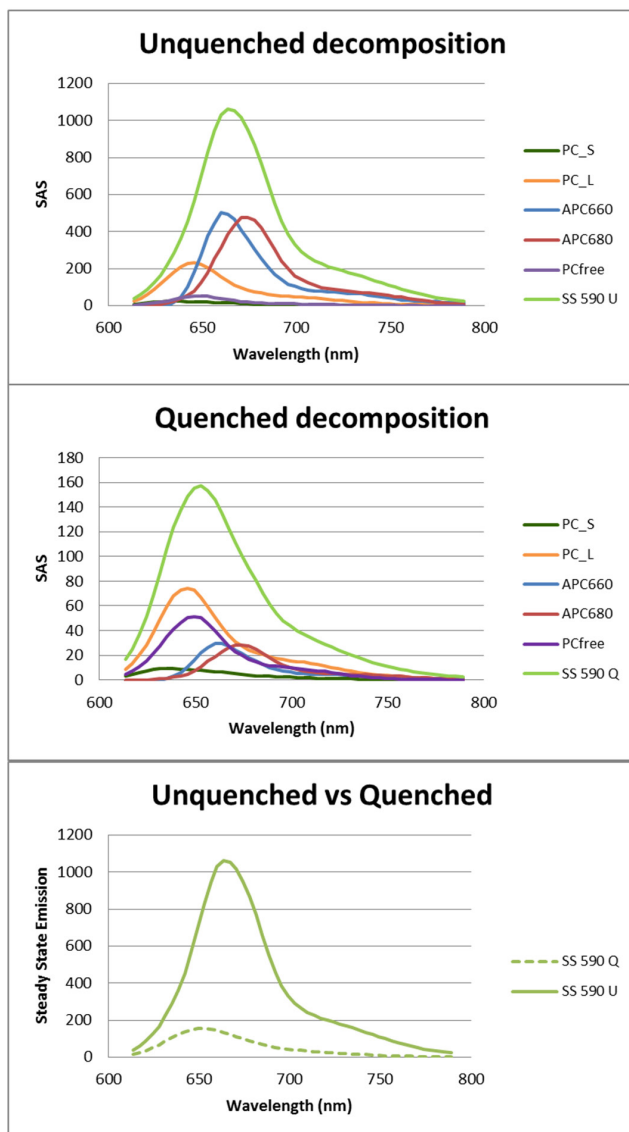


Figure.S4.8 Reconstructed steady-state spectra of WT_PB with 590 nm excitation in the unquenched and quenched state. Spectra are shown again in the layout of Fig. S4.6 and S4.7.

Chapter 5

Light Harvesting and Blue-green Light Induced Non-Photochemical Quenching in Two Different C-Phycocyanin Mutants of *Synechocystis* PCC 6803

This chapter is based on:

Lijin Tian, Ivo H.M. van Stokkum, Rob B.M. Koehorst and Herbert van Amerongen *The Journal of Physical Chemistry B*, 2012 in press

Abstract

Cyanobacteria are oxygen-evolving photosynthetic organisms that harvest sunlight and convert excitation energy into chemical energy. Most of the light is absorbed by large light-harvesting complexes called phycobilisomes (PBs). In high-light conditions cyanobacteria switch on a photoprotective mechanism called non-photochemical quenching (NPQ): During this process, absorption of blue-green light transforms the inactive orange form of the orange carotenoid protein OCP (OCPo) into the red active form OCPr that subsequently binds to the PB, resulting in a substantial loss of excitation energy and corresponding decrease of the fluorescence. In wild-type cells the quenching site is a bilin chromophore that fluoresces at 660 nm and is called APCQ660 but its exact location is still unknown. In the present work we studied NPQ in two different types of mutant cells (CB and CK) that possess significantly truncated PBs, using spectrally-resolved picosecond fluorescence spectroscopy. It is found that although the fraction of PBs that is being quenched seems somewhat smaller than in wild-type cells, both the site of quenching and the rate of quenching remain very similar and are apparently not dependent on the presence of the outer rods of the PBs that bind around 80% of the pigments.

Introduction

Cyanobacteria (also known as blue-green algae) are supposedly the earliest and one of the most successful species on earth to perform oxygenic photosynthesis. They play a key role in global carbon cycling and atmospheric oxygen accumulation. Due to their fast growth rate and facile genetic modification, cyanobacteria are thought to possess great potential for hydrogen and biofuel production in the future. Similar to algae and plants, cyanobacteria contain two large photosynthetic complexes in their thylakoid membranes, named photosystem I (PSI) and photosystem II (PSII), and here the light-dependent reactions of photosynthesis are taking place¹⁻⁴. Besides PSI and PSII, cyanobacteria contain giant light-harvesting or antenna systems, the so-called

phycobilisomes (PBs). They are located on the stromal side of the thylakoid membrane and they dramatically increase the cross section for light absorption. PBs have a complicated structure which also depends on species⁵. PBs of wild-type *Synechocystis* PCC 6803 (hereafter called *Synechocystis*) are composed of six C-Phycocyanin (C-PC) rods and three allophycocyanin (APC) core cylinders; one C-PC rod contains three hexameric disks, each containing 18 bilin pigments, and in addition a few linker proteins; one core cylinder contains four trimeric APC disks, each containing 6 pigments. One core cylinder is not directly in contact with the thylakoid membrane with the photosystems and it contains only APC trimers emitting at 660 nm, while both basal cylinders contain 3 chromophores that emit around 680 nm and serve as terminal energy acceptor of the PB^{6,7}. The whole PB is anchored by the core-membrane linker Lcm to the thylakoid membrane. Detailed PB structures are described by Arteni et al^{8,9}, whereas further information about the pigments and their spectroscopic properties can be found in refs^{5,10,11}. It is important to realize that the core contains 66 pigments that fluorescence around 660 nm, whereas only 6 fluoresce around 680 nm.

The presence of antenna systems on the one hand increases the capability of the photosystems to absorb sunlight, which is important in low-intensity sunlight, but on the other hand this also increases the probability that photodamage occurs in the presence of strong light. To overcome this problem, different kinds of self-protection mechanisms were developed during the long evolutionary history of the photosynthetic organisms, including cyanobacteria. One important protection mechanism, called blue-green light induced NPQ, was found in all cyanobacteria that contain the so-called orange carotenoid protein (OCP) and the phenomenon has been studied extensively during the past ten years¹¹⁻²⁹. This protection is realized *in vivo* by interactions between at least three different proteins, including OCP, the fluorescence recovery protein (FRP) and one of the core proteins of the PBs^{24,30}. In strong blue-green light, OCP changes from its inactive orange form (OCP⁰) into its red active (OCP^r) form, binds to APC and quenches to a large extent the electronic excitations in the PBs by dissipating the excitation energy as heat. In this way, most of the excitations are prevented from reaching the photosystems, thereby protecting them against photodamage. When the intensity

of the blue-green light is significantly decreased again, the binding between OCP^r and APC is released with the help of FRP, and the quenching process is stopped and thus the excitation energy can reach the reaction centers (RCs) again in a “normal” way²⁴.

In a recent study, we have performed time-resolved fluorescence measurements on isolated PBs from wild-type cells and from two different mutants. We found the same quenching site and a similar quenching rate *in vitro* as was reported before for wild-type cells *in vivo*¹¹. In order to investigate whether these conclusions are also true for blue-green light induced NPQ in the same two mutants *in vivo*, the present study was undertaken. Another reason to study these antenna size-truncated mutants is the increasing interest in the question to which extent the antenna size influences the production of biomass^{31,32}. Although this is not the main issue of the present work, a kinetic model including light harvesting and photo-protection as will proposed here can potentially be useful. One of the two studied mutants, called CK contains PSI and PSII as well as the APC core but it completely lacks the C_PC rods^{33,34}. The other one (CB) is lacking both the intermediary and the core-distal C_PC hexamers and only contains core-proximal C_PC besides the other photosynthetic complexes, PSI, PSII and APC core³⁵. Picosecond time-resolved fluorescence measurements were performed using a synchroscan streak-camera system. The obtained datasets were analyzed by using both global analysis and compartmental-based target analysis in a similar way as was done before for wild-type cells²⁶. It turns out that the blue-green light quenching takes place on APC₆₆₀ pigments in both mutants with a slightly smaller quenched fraction than in wild-type cells under similar conditions. The quenching rates cannot be determined very accurately due to the small fraction of quenched PBs for both mutants, but the quenching rates appear to be rather similar *in vivo* and *in vitro*.

Materials and methods

Growing conditions of *Synechocystis* cells and construction of mutants

For the construction of the CK and CB mutants we refer to ³³⁻³⁷. Two mutants were grown photoautotrophically in a modified BG11 medium ³⁸, with twice the concentration of sodium nitrate and with 10 mM NaHCO₃ added. Cells were grown in 250-ml flasks with 60 ml growing volume in a rotary shaker (45 rpm) at 30°C and illuminated by white light giving a total intensity of 40 $\mu\text{mol}\cdot\text{m}^{-2}\cdot\text{s}^{-1}$. All the cells were kept in the logarithmic growth phase by refreshing the medium every two or three days depending on growth rate.

Steady-state absorption

Absorption spectra were recorded on a Cary 5E spectrophotometer, equipped with an integrating diffuse reflectance sphere (DRA-CA-50, Labsphere) to minimize distortion of the absorption spectra by light scattering. The optical path length of the cell was 1 cm.

Time-resolved fluorescence

Time-resolved fluorescence measurements were performed on a picosecond streak-camera system ^{36,39}. Images were corrected for background signals and detector sensitivity, averaged, and sliced up into traces of 4 nm wide. The time window was 800 ps for all measurements. A laser power of 30 μW was used. The excitation spot size was typically $\sim 100\ \mu\text{m}$ in diameter and the laser repetition rate was 250 kHz. The instrument response function (IRF) was described with a double Gaussian, consisting of a dominating narrow Gaussian of ~ 8.0 ps FWHM on top of a minor broad Gaussian of ~ 40 -50 ps in case of 590 nm excitation. For the 400 nm excitation experiments, one Gaussian of ~ 9.2 ps FWHM was sufficient to describe/fit the data. The sample was stirred with a magnetic stirring bar (stirring rate ~ 10 Hz). All measurements were performed at 21°C and one measurement took 20 minutes. Cells were concentrated 3-5 times by low-speed centrifugation and dark adapted for 5 minutes before the time-resolved fluorescence measurements were started.

Conditions for measuring time-resolved fluorescence of cells during quenching have been described previously ²⁶; the same actinic blue-green light was used. All measurements were performed at room temperature (about 20°C).

Data analysis

Data obtained with the streak-camera setup were analyzed with the TIMP package for the “R project for Statistical Computing (R Development Core Team 2008)” and its graphical user interface (GUI) Glotaran; for details see ^{40,41}.

With global analysis the data were fitted globally as a sum of exponential decay functions convolved with an IRF and the amplitudes of each decay component as a function of wavelength constitute the so-called decay-associated spectra (DAS). Apart from providing an objective mathematical description of the datasets, this analysis provides global insight into the underlying excitation energy transfer and charge separation processes⁴².

For a more detailed analysis of the data use is made of target analysis where the datasets are fitted with different compartmental schemes (also called target models). The spectrum of each compartment and the energy transfer rates between them are estimated together with various decay rates, for instance corresponding to charge separation or nonphotochemical quenching. The methodology of global and target analysis is described in detail in ⁴³.

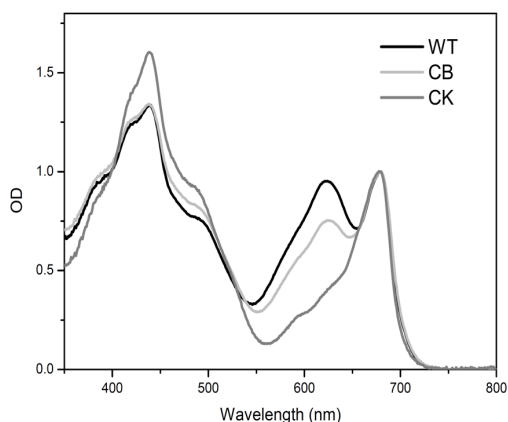
Results

Absorption spectra

The absorption spectra of WT *Synechocystis*, CK and CB mutants are shown in Fig.5.1. The spectra have been normalized at 680 nm. Although the spectra were recorded with an integrating sphere to minimize distortion due to scattering, the spectra are still deformed to some extent, partly by scattering and partly by sieving, especially on the blue side (i.e. at short wavelengths). The CK mutant shows absorption due to the APC core, which contributes substantially to the spectrum between 550 and 670 nm and both photosystems which are mainly responsible for the absorption below 500 nm and the large absorption band around 675 nm. The CB mutant shows extra absorption (mainly between 550 and 650 nm) due to the additional presence of C-PC, but the absorption is lower than that of the WT cells. It should be noted that at 400 nm the absorption is mainly due to Chls and Cars and the presence of APC and C-PC hardly alters the

absorption at this wavelength (the contribution is less than 10%³⁶). Therefore, in the time-resolved measurements with 400 nm excitation mainly PSI and PSII are excited. Excitation at 590 nm on the other hand, which was used for studying the CK, CB and WT cells, leads to a large fraction of directly excited PBs.

Figure 5.16: Room-temperature absorption spectra of wild-type and mutant *Synechocystis* cells. All spectra are normalized at 680 nm.



Time-resolved fluorescence

Time-resolved fluorescence spectra were recorded with a time resolution of several ps, using two different excitation wavelengths: 400 nm (see Fig.S5.1 in supplementary data), exciting mainly PSI and PSII and 590 nm (see Fig.S5.1), leading to increased excitation of the PBs. A time window of 800 ps was used for all experiments.

Global analysis

Excitation at 400 nm: In Fig.5.2 the DAS are shown that result from global analysis of the fluorescence kinetics of the two mutants upon 400 nm excitation. In both cases a fit with 4 lifetime components leads to a satisfactory description of the data. The corresponding lifetimes of the DAS are also given in Figure 5.2. The 5-ps component has a conservative spectrum, whereas the 27/28-ps component is all-positive and dominates the kinetics for both mutants. The 5-ps and 27/28 ps lifetimes and corresponding spectra are very similar to those observed in previous studies for isolated PSI and for BE cells, that contain PSI but no PSII and PBs^{36,44}. The 5-ps DAS corresponds to fast excitation-energy equilibration between pigments fluorescing below 700 nm and so-called red pigments fluorescing above 700 nm,. The 28-ps component mainly represents fluorescence decay due to charge separation from the equilibrated excited state of PSI. These results indicate that the PSI kinetics can be separated rather well from the kinetics of the

rest of the system. Note that, the 400 nm excitation light leads to some direct excitation of the PBs, about 7% as shown in table 5.1, and this has a small effect on the shape of the DAS of these two fastest components, especially for the CB mutant.

Besides these two DAS, two extra lifetime components are observed, with values of ~ 100 ps and ~ 600 ps, respectively. Although for the CK and CB cells the amplitudes of the 3rd and the 4th DAS are rather small, these components are responsible for a relatively large amount of the steady-state fluorescence below 680 nm due to the long fluorescence lifetimes. For the CK mutant the two slowest DAS components (137 and 629 ps) have similar shapes peaking at 680 nm, representing the emission of mainly Chls in PSII. The slowest DAS components (106 and 588 ps) of the CB cells show additional fluorescence due to the presence of C-PC. The additional fluorescence of APC with a peak around 660 nm in the 106-ps component is due to extra excitations that have arrived on APC from C-PC. The fluorescence around 640 nm in the slowest 588-ps DAS is due to part of the C-PC that apparently is not able to transfer its excitation energy. It is not due to Boltzmann-equilibrated excitations in intact PBs because it can easily be estimated that only $\sim 1\%$ of the excitations should reside on C-PC in that case, which should hardly be visible in this 588-ps DAS.

When the cells are brought into the quenched state by illumination by strong blue-green light, only a minor change in the DAS is obtained after 400-nm excitation, reflecting the fact that the Chls are not quenched directly, but quenching takes place in the PBs^{14,15,22,26}.

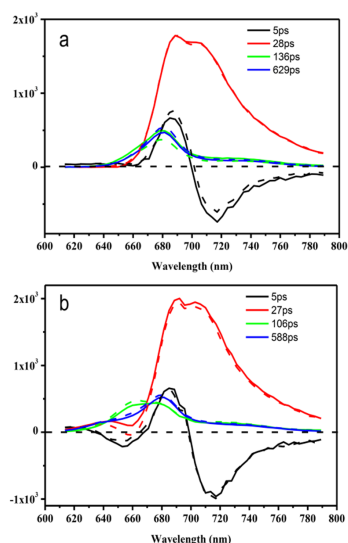
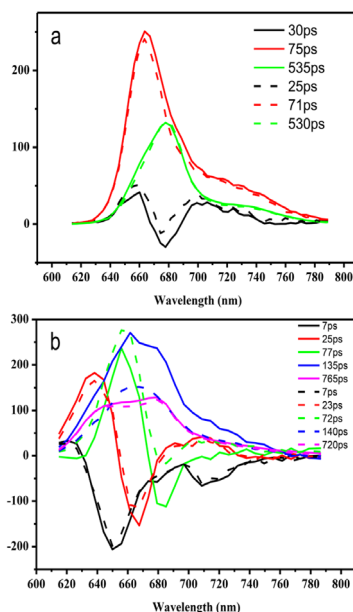


Figure 5.2: Fitting results (DAS) of the time-resolved fluorescence data obtained with the streak-camera setup using 400-nm excitation and a time window of 800 ps; a) CK and b) CB mutant cells. The corresponding lifetimes are listed in the figure. The solid lines correspond to unquenched cells and the dashed spectra correspond to quenched cells.

590-nm excitation: Time-resolved measurements were also performed on CK and CB cells with 590 nm excitation in order to “selectively” excite the outer antenna (APC/C-PC) and study excitation energy transfer (EET) to the RCs. The DAS and corresponding lifetimes for CK and CB cells are shown in Figs. 5.3a and 5.3b, respectively. For the CK mutant, the 30-ps DAS has a complicated shape. On the one hand it shows some EET characteristics reflecting transfer from APC (~660 nm) to PSII/PSI and at the same time there seems to be some contribution of PSI decay with fluorescence extending to the red. The 75-ps DAS, peaking at 660 nm, reflects mainly the fluorescence decay of APC. It is not accompanied by a negative component with similar area at longer wavelength, which would have been indicative of EET. However, this component is possibly due to EET to PSII followed by immediate charge separation in PSII with open RC’s in which case no negative component is expected. Also EET to PSI would lead to a similar spectrum. The DAS of the slowest component 535 ps is peaking at 678 nm, which is slightly blue-shifted from the DAS of the two slowest components upon 400 nm excitation (see Fig.S5.2 in the supplementary data) and shows a shoulder around 660 nm. These differences are mainly caused by the different excitation distributions over PBs and photosystems upon 590 nm and 400 nm excitation. At 590 nm mainly PBs are excited and the excitations equilibrate over the chromophores in the PBs and the Chls in the photosystems, while at 400 nm also many Chls are excited in uncoupled photosystems, that do not equilibrate with the blue-shifted chromophores of the PBs (for more details see target analysis below). Although the presence of unconnected APC cannot be excluded here, the fraction of unconnected APC must be rather small, if not negligible.

Figure 5.3: DAS of CK (a) and CB (b) mutants upon excitation of 590 nm. The corresponding lifetimes are listed in each figure. The solid lines correspond to unquenched cells and the dashed spectra correspond to quenched cells.



For the CB mutant five components are needed to get a satisfactory fit of the data at all wavelengths. From the DAS several clear EET steps can be observed (Fig.5.3b). The fastest component of 7-ps is almost entirely negative with a peak around 645 nm. It probably reflects EET within C-PC from blue pigments with relatively low dipole strength to somewhat more red-shifted pigments with higher dipole strength²⁶. The 25-ps component shows a positive peak at 640 nm and a negative one at 663 nm and is indicative of EET from C-PC to APC. The 77-ps component has a positive peak around 655 nm and a negative one at 680 nm, reflecting EET to both the lower energy pigments of the APC and Chls in PSII²⁶. The 135-ps component is rather similar to the 106-ps component that is obtained upon excitation at 400 nm as shown in Fig.S5.2 of the supplementary data. The 765-ps DAS has its main peak at 680 nm (PSII) but there is a substantial shoulder around 640 nm which is ascribed to some disconnected C-PC. The presence of some disconnected or badly connected C-PC was also seen upon excitation at 400 nm.

Target Analysis

To analyze in more detail EET between the different “pools” of pigments (compartments), target analysis was performed, leading to **Species Associated Spectra (SAS)** for the different compartments. A “pool” represents a group of pigments that shows fast internal excitation equilibration.

In our previous work a detailed model was built that was used to determine the quenching site of blue-green light induced NPQ in *Synechocystis*²⁶.

In the present analysis, no distinction was made between PSII with open and closed RCs and only average electron-transfer and recombination rates for open and closed RCs were considered.

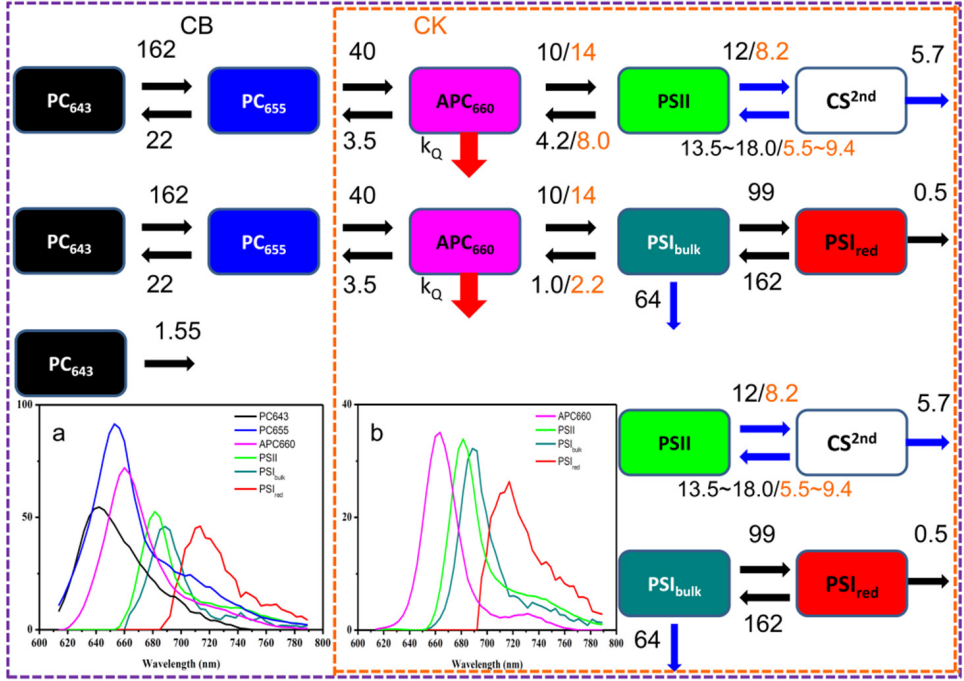


Figure 5.4: Compartmental schemes for target analysis. Compartments (colored boxes) represent pools of chromophores that are spectrally indistinguishable, and within which excitation energy is equilibrated on a time scale that cannot be resolved with the set up used. Forward and backward energy transfer processes between these compartments are indicated by the arrows, while rate constants of the individual transfer steps are indicated by the numbers. The orange and black dashed lines enclose compartments belonging to the CK and CB mutants, respectively. Insets a and b show species associated spectra of the various chromophores contained in compartments of the same color. In case the rates of particular energy or electron transfer steps are different in both mutants, the rates for the CK mutant are shown in orange.

Mutant	λ_{ex}	PSI_U	PSII_U	PSI_C	PSII_C	Total PSI	Total PS II	PS I/II _Chl	PS I/II _RC	PB_I	PB_II	C_PC _U	Total PB	Total Chl	Total exc
CK	400 nm	69	11	10	3	79	14	6	2	3	4	0	7	93	100
	590 nm	31	5	4	1	35	6	6	2	28	31	0	58	42	100
CB	400 nm	67	6	15	5	82	11	7	3	3	3	1	7	93	100
	590 nm	12	1	3	1	15	2	7	3	29	33	20	83	17	100

Table 5.1: Initial, relative absorbed energies (%) estimated from the target analysis. Energy is considered to be distributed over PSI and PSII coupled (PSI_C and PSII_C) and not coupled to PBs (PSI_U and PSII_U), PBs coupled to PSI and PSII (PB_I and PB_II) and

unattached C-PC (C-PC_U). The ratios PSI/II_ChI and PSI/II_RC are based on the number of chlorophylls and reaction centers, respectively. The total excitation was normalized to one.

The compartment scheme contains the following branches:

- Branch i), PBs transferring energy to PSI⁴⁵.
- Branch ii), PBs transferring energy to PSII⁴⁶;
- Branch iii), Part of C_PC that is not coupled to APC in the CB mutants³⁵.
- Branch iv), PSI, not coupled to PBs⁴⁷.
- Branch v), PSII, not coupled to PBs⁴⁷.

The relative numbers of excitations in the various branches were estimated in the target analysis and are listed in table 5.1. To enable the fitting, a number of constraints on the input parameters and the spectra are required, and they are listed and discussed in the supplementary data.

In order to take into account the fact that the amount of open and closed PSII RCs differs for the different samples and also can vary for different excitation wavelengths, the charge recombination rate was not globally fixed but was allowed to vary. On the other hand, the PSI kinetics hardly depends on the fact whether PSI is open or closed (see for instance Wientjes et al. 2011)⁴⁸. Compared to the kinetics of PSII, the PSI kinetics is relatively straightforward to model (see for instance also the 400 nm excitation results in Fig.5.2), and the same parameters were used as in our previous work²⁶.

For the CK mutant, the charge separation rate was determined to be 8.2 ns^{-1} , and it was forced to be same for the two different excitation wavelengths. For 400 nm excitation, the charge-recombination rate was $\sim 9.4 \text{ ns}^{-1}$, while it becomes $\sim 5.5 \text{ ns}^{-1}$ for 590 nm excitation, and the slower charge recombination rate in the second case is probably due to the presence of more open RCs. In addition to both photosystems, the CK mutant also contains the APC core complex. Its spectrum, as obtained from the target analysis, peaks around 660 nm as shown in green in Fig.5.4. Note that, the APC core also contains a small fraction of pigments that fluorescence around 680 nm^{6,9}, this fraction is not included here as a separate pool since equilibration between APC₆₈₀ and ChIs is probably reached within ps and their spectra are rather similar²⁶.

For the CB mutant we observe two additional pools of pigments, i.e. PC_S and PC_L, which lead to fluorescence peaking at 643 nm (orange spectrum) and 655 nm (magenta spectrum), respectively. Table 5.1 shows that $\sim 7\%$ of the excitations at 400 nm and $\sim 83\%$ at 590 nm excitation are on the PBs. It can be concluded from the results at 400 nm that the PSI/PSII ratio (relative number of RCs) is ~ 2.6 , which is higher than for the CK mutant where it is ~ 2.0 .

In the CB mutant, $\sim 25\%$ of the C-PC appears to be disconnected, giving rise to a long-lived fluorescence component peaking at 643 nm. To simplify the model, the corresponding spectrum was forced to be same as that of PC_s (the first pool in blue). The presence of some long-lived C-PC fluorescence is in agreement with previous sucrose-gradient results ³⁵, that show free PC bands at the top of the sucrose gradient.

With regard to the blue-green light induced quenching, the location of the quenching site was tested by adding an extra decay channel on one of the pools for the quenched samples. Each time, only one pool is allowed to be quenched. It turns out that APC₆₆₀ nm is the species that is directly quenched in both mutants but the fraction of quenched PBs differs and the same is true for the quenching rates. In case of the CK mutant, only 11% of the excited PBs was quenched with an overall quenching rate of $\sim 14 \text{ ns}^{-1}$, while in the CB mutant, $\sim 17\%$ of the excited PBs was quenched with a quenching rate of $\sim 26 \text{ ns}^{-1}$. Note that, probably somewhat fortuitously, for both mutants the *in-vivo* quenching rates are nearly the same as the corresponding rates *in vitro*, namely $\sim 26 \text{ ns}^{-1}$ and $\sim 26 \text{ ns}^{-1}$ respectively for CB and $\sim 15 \text{ ns}^{-1}$ and $\sim 14 \text{ ns}^{-1}$ for CK. However, as we have tested, different quenching rates combined with different quenching fractions of PBs can also fit the datasets equally well, thus each quenching rate can range from (12-50)/ns, which is the same for both mutants.

All the SAS that are obtained during the fitting procedure are shown in Fig.5.4 as insets. All of them show very reasonable spectral shapes and the correct positions of their maxima.

In summary, with the model shown in Fig.5.4 in combination with the input parameters listed in table 5.1, all datasets can be described satisfactorily. The target analysis of the time-resolved fluorescence measurements of the two

studied mutants provides a systematic and globally consistent description of the EET and charge-separation rates and pathways in *Synechocystis* and of the fluorescence spectra of the most prominent pigment pools. Moreover, also the quenching site, the quenched fraction of PBs and the quenching rate could be determined for both mutants.

Discussion

Energy harvesting kinetics of PBs in the CB and CK mutants *in vivo*

Energy absorbed by the PBs is transferred to either PSI or PSII. The DAS of the CK mutant reveals a 30 ps transfer process from the 660 nm pigments in APC to the pool of Chls (including the terminal emitter pigments in the APC core) fluorescing around 675-680 nm. The combination of this transfer process and the trapping process in PSI/PSII explains the strong positive peak in the DAS around 660 nm and the dip around 675-680 nm. The 75-ps DAS also shows emission around 660 nm but there is no negative peak present that reflects the emission of the acceptor pigments. The most likely explanation for the absence of such a negative peak is “immediate” charge separation after energy transfer, which is indeed expected to occur in PSI but not in PSII where charge separation occurs on a much slower time scale.

In the CB mutant, the 7 ps component is attributed to fast spectral equilibration within the PC rods of the cyanobacteria, which is also supported by previous work, where a 10 ps component was attributed to transfer within the hexameric subunits of the C_PC rods^{26,49}. Phycocyanobilins are covalently linked at three different positions in the phycobiliproteins and the pigments are called $\beta 155$, $\alpha 84$ and $\beta 84$. The DAS reflects energy transfer from $\beta 155$ to the pigment pair consisting of $\alpha 84$ and $\beta 84$ which are likely to be excitonically coupled^{50,51}.

Energy transfer from the rods to the core was reported to occur with a time constant of 90 ps for wild-type *Synechococcus* 6301^{52,53}, whereas it was found to take ~20 ps in wild-type *Synechocystis* 6803 as was also reported in another study on *Synechocystis*^{36,54}. Using picosecond fluorescence in combination with target analysis of wild type cells²⁶, it was possible to disentangle several processes that gave rise to an apparent 20 ps transfer process in previous studies and it was

concluded that the energy transfer from PC_L to APC occurs with a time constant of ~75 ps. In the present study, using the same procedure, the time constant is found to be 25 ps for the CB mutant. This is due to the fact that the pool size of C-PC in the CB mutant is only one third of that in WT cells. Assuming that the transfer time roughly scales with the number of pigments (see e.g. Broess et al., 2006)⁵⁵, indeed we find that the rate of this transfer step is approximately tripled in the CB mutant as compared to WT cells.

For isolated PBs of the CK mutant, energy transfer from APC₆₆₀ to APC₆₈₀ takes place with a time constant of 43 ps, while *in vivo* it seems to become somewhat faster, namely 30 ps (see DAS in Fig.5.3), but it should be realized that also the trapping process in PSI with time constant 27/28 ps, contributes to the 30-ps DAS. A comparison between results on isolated CB_PBs and *in vivo* results is less straightforward, because different models were used: *in vitro*, an overall transfer component with a lifetime of 34 ps was found whereas in the present study two subsequent steps of 6 and 25 ps are observed, relatively close to the 34 ps transfer time.

Quenching sites and quenching rates *in vivo*

In order to determine the rate of quenching and the type of chromophore that is being quenched, target analysis was performed. The analysis shows nearly identical spectra for the photosystems of the CB and the CK mutants and those of the WT cells (Fig.S5.5) and also the spectra of the APC₆₆₀ pools are very similar in all cell types. There is more variation in the spectra of the various chromophores in the C-PC rods. It is found in the present study for both mutants that the species that is directly quenched is APC₆₆₀ in agreement with the *in vitro* results on isolated PBs from these mutants. Only the quenched fraction of PBs is totally different. *In vivo*, ~11% of the PBs was quenched for the CK mutant and ~17% for the CB mutant for our growing and measuring conditions. On the contrary, 20 minutes of blue-green light illumination with similar intensity leads to 85% quenched PBs of isolated CK_PB and a full quenching of isolated CB_PB¹¹. However, two factors dramatically reduce the quenched fraction *in vivo*: firstly, less OCP is present in the intact cells than for isolated complexes, where the OCP

concentration was forty times as high as the PB concentration. Secondly, the cells contain FRP which enables the recovery process (disappearance of quenching) to take place in the cell. The presence of FRP reduces the amount of OCP^r bound to the PB, even though an equilibrium is achieved after the cells have been illuminated for a sufficiently long time. A smaller fraction of PBs was quenched in the CK mutant than in the CB mutant under the same light stress conditions. It cannot be concluded whether this is due to a difference in the relative amounts of OCP/FRP/PB or due to a difference in binding constants due to the lack of C-PC. The quenching rates cannot be determined with very high accuracy due to the relatively low amount of quenching for these in vivo systems but they are rather similar to those observed for isolated PBs and for intact WT cells. Therefore, our previous conclusion that the quenching is most likely caused by charge transfer between APC^Q₆₆₀ and the OCP carotenoid hECN in its activated form extends to the quenching in the CB and CK mutants.

Acknowledgements

We thank Dr. Ghada Ajlani for providing the mutant strains. We thank S. Laptanok (Ecole Polytechnique, 91128Palaiseau, France) and J. Snellenburg (VU Amsterdam University) for help with the use of the TIMP package and the software of Glotaran.

References

- (1) Nelson, N.; Ben-Shem, A. *Nat. Rev. Mol. Cell. Bio.* **2004**, *5*, 971-982.
- (2) Duysens, L. N.; Kamp, B. M.; Ames, J. *Nature* **1961**, *190*, 510-511.
- (3) van Amerongen, H.; Valkunas, L.; Grondelle, R. v. Exciton Dynamics in Different Antenna Complexes. Coherence and Incoherence. In *Photosynthetic excitons*; World Scientific Publishing Co. Pte. Ltd. Singapore, 2000.
- (4) Croce, R.; van Amerongen, H. *J. Photoch. Photobio. B.* **2011**, *104*, 142-153.
- (5) MacColl, R. *J. Struct. Biol.* **1998**, *124*, 311-334.
- (6) Glazer, A. N. *Biochim. Biophys. Acta* **1984**, *768*, 29-51.
- (7) Adir, N. *Photosynth. Res.* **2005**, *85*, 15-32.
- (8) Arteni, A. A.; Ajlani, G.; Boekema, E. J. *Biochimica. et. Biophysica. Acta-Bioenergetics* **2009**, *1787*, 272-279.
- (9) Jallet, D.; Gwizdala, M.; Kirilovsky, D. *Biochimica. et. Biophysica. Acta-Bioenergetics* **2011**, *1817*, 1418-1427.
- (10) Adir, N. *Photosynth. Res.* **2005**, *85*, 15-32.
- (11) Tian, L.; Gwizdala, M.; van Stokkum, Ivo H. M.; Koehorst, Rob B. M.; Kirilovsky, D.; van Amerongen, H. *Biophys. J.* **2012**, *102*, 1692-1700.
- (12) El Bissati, K.; Delphin, E.; Murata, N.; Etienne, A. L.; Kirilovsky, D. *Biochimica. et. Biophysica. Acta -Bioenergetics* **2000**, *1457*, 229-242.
- (13) Rakhimberdieva, M. G.; Stadnichuk, I. N.; Elanskaya, T. V.; Karapetyan, N. V. *FEBS Lett.* **2004**, *574*, 85-88.
- (14) Scott, M.; McCollum, C.; Vasil'ev, S.; Crozier, C.; Espie, G. S.; Krol, M.; Huner, N. P. A.; Bruce, D. *Biochemistry-Us* **2006**, *45*, 8952-8958.
- (15) Wilson, A.; Ajlani, G.; Verbavatz, J. M.; Vass, I.; Kerfeld, C. A.; Kirilovsky, D. *Plant. Cell.* **2006**, *18*, 992-1007.
- (16) Rakhimberdieva, M. G.; Bolychevtseva, Y. V.; Elanskaya, I. V.; Karapetyan, N. V. *FEBS Lett.* **2007**, *581*, 2429-2433.
- (17) Rakhimberdieva, M. G.; Vavilin, D. V.; Vermaas, W. F. J.; Elanskaya, I. V.; Karapetyan, N. V. *Biochimica Et Biophysica Acta-Bioenergetics* **2007**, *1767*, 757-765.
- (18) Wilson, A.; Boulay, C.; Wilde, A.; Kerfeld, C. A.; Kirilovsky, D. *Plant Cell* **2007**, *19*, 656-672.
- (19) Bailey, S.; Grossman, A. *Photochem. Photobiol.* **2008**, *84*, 1410-1420.
- (20) Kirilovsky, D.; Boulay, C.; Abasova, L.; Six, C.; Vass, I. *Biochimica. et. Biophysica. Acta-Bioenergetics* **2008**, *1777*, 1344-1354.
- (21) Wilson, A.; Punginelli, C.; Gall, A.; Bonetti, C.; Alexandre, M.; Routaboul, J. M.; Kerfeld, C. A.; van Grondelle, R.; Robert, B.; Kennis, J. T. M.; Kirilovsky, D. *Proc. Natl. Acad. Sci. U S A* **2008**, *105*, 12075-12080.
- (22) Rakhimberdieva, M. G.; Elanskaya, I. V.; Vermaas, W. F. J.; Karapetyan, N. V. *Biochimica. et. Biophysica. Acta-Bioenergetics* **2010**, *1797*, 241-249.
- (23) Wilson, A.; Kinney, J. N.; Zwart, P. H.; Punginelli, C.; D'Haene, S.; Perreau, F.; Klein, M. G.; Kirilovsky, D.; Kerfeld, C. A. *J. Biol. Chem.* **2010**, *285*, 18364-18375.

- (24) Gwizdala, M.; Wilson, A.; Kirilovsky, D. *Plant Cell* **2011**, *23*, 2631-2643.
- (25) Rakhimberdieva, M. G.; Kuzminov, F. I.; Elanskaya, I. V.; Karapetyan, N. V. *FEBS Lett.* **2011**, *585*, 585-589.
- (26) Tian, L. J.; van Stokkum, I. H. M.; Koehorst, R. B. M.; Jongerius, A.; Kirilovsky, D.; van Amerongen, H. *J. Am. Chem. Soc.* **2011**, *133*, 18304-18311.
- (27) Gorbunov, M. Y.; Kuzminov, F. I.; Fadeev, V. V.; Kim, J. D.; Falkowski, P. G. *Biochimica. et. Biophysica. Acta-Bioenergetics* **2011**, *1807*, 1591-1599.
- (28) Stadnichuk, I. N.; Yanyushin, M. F.; Maksimov, E. G.; Lukashev, E. P.; Zharmukhamedov, S. K.; Elanskaya, I. V.; Paschenko, V. Z. *Biochimica. et. Biophysica. Acta-Bioenergetics* **2012**, *1817*, 1436-1445.
- (29) Kuzminov, F. I.; Karapetyan, N. V.; Rakhimberdieva, M. G.; Elanskaya, I. V.; Gorbunov, M. Y.; Fadeev, V. V. *Biochimica. et. Biophysica. Acta-Bioenergetics* **2012**, *1817*, 1012-1021.
- (30) Boulay, C.; Wilson, A.; D'Haene, S.; Kirilovsky, D. *Proc. Natl. Acad. Sci. U S A* **2010**, *107*, 11620-11625.
- (31) Melis, A. *Plant Sci.* **2009**, *177*, 272-280.
- (32) Page, L. E.; Liberton, M.; Pakrasi, H. B. *Appl. Environ. Microbiol* **2012**, *78*, 6349-6351.
- (33) Elmorjani, K.; Thomas, J. C.; Sebban, P. *Arch. Micro.* **1986**, *146*, 186-191.
- (34) Ajlani, G.; Vernotte, C.; Dimagno, L.; Haselkorn, R. *Biochimica. et. Biophysica. Acta-Bioenergetics* **1995**, *1231*, 189-196.
- (35) Ughy, B.; Ajlani, G. *Microbiology-Sgm* **2004**, *150*, 4147-4156.
- (36) Krumova, S. B.; Laptinok, S. P.; Borst, J. W.; Ughy, B.; Gombos, Z.; Ajlani, G.; van Amerongen, H. *Biophys. J.* **2010**, *99*, 2006-2015.
- (37) Ajlani, G.; Vernotte, C. *Plant. Mol. Biol.* **1998**, *37*, 577-580.
- (38) Herdman, M.; Delaney, S. F.; Carr, N. G. *J. Gene. Microbiol.* **1973**, *79*, 233-237.
- (39) van Oort, B.; Murali, S.; Wientjes, E.; Koehorst, R. B. M.; Spruijt, R. B.; van Hoek, A.; Croce, R.; van Amerongen, H. *Chem. Physics* **2009**, *357*, 113-119.
- (40) Mullen, K. M.; van Stokkum, I. H. M. *J. Stat. Softw.* **2007**, *18*, 1-46.
- (41) Snellenburg, J. J.; Laptinok, S. P.; Seger, R.; Mullen, K. M.; Van Stokkum, I. H. M. *Journal of Statistical Software* **2011**, *43*, 1-22.
- (42) van Oort, B.; Amunts, A.; Borst, J. W.; van Hoek, A.; Nelson, N.; van Amerongen, H.; Croce, R. *Biophys. J.* **2008**, *95*, 5851-5861.
- (43) van Stokkum, I. H. M.; Larsen, D. S.; van Grondelle, R. *Biochimica. et. Biophysica. Acta-Bioenergetics* **2004**, *1657*, 82-104.
- (44) Gobets, B.; van Grondelle, R. *Biochimica. et. Biophysica. Acta-Bioenergetics* **2001**, *1507*, 80-99.
- (45) Ashby, M. K.; Mullineaux, C. W. *Photosynth. Res.* **1999**, *61*, 169-179.
- (46) Mullineaux, C. W. *Biochimica. et. Biophysica. Acta* **1992**, *1100*, 285-292.
- (47) Ohki, K.; Okabe, Y.; Murakami, A.; Fujita, Y. *Plant Cell Physiol.* **1987**, *28*, 1219-1226.
- (48) Wientjes, E.; Croce, R. *Photosynth. Res.* **2012**, *111*, 185-191.
- (49) Suter, G. W.; Holzwarth, A. R. *Biophys. J.* **1987**, *52*, 673-683.

Chapter 5

- (50) van Amerongen, H.; Struve, W. S. *J. Lumin.* **1992**, *51*, 29-38.
- (51) Demidov, A. A.; Borisov, A. Y. *Biophys. J.* **1993**, *64*, 1375-1384.
- (52) Gillbro, T.; Sandstrom, A.; Sundstrom, V.; Holzwarth, A. R. *Febs Letters* **1983**, *162*, 64-68.
- (53) Holzwarth, A. R. *Physiologia. Plantarum* **1991**, *83*, 518-528.
- (54) Bittersmann, E.; Vermaas, W. *Biochimica. et. Biophysica. Acta* **1991**, *1098*, 105-116.
- (55) Broess, K.; Trinkunas, G.; van der Weij-de Wit, C. D.; Dekker, J. P.; van Hoek, A.; van Amerongen, H. *Biophys. J.* **2006**, *91*, 3776-3786.

Supporting Materials

Streak images

Figure S5.17: Streak-camera images of the CK mutant (a and c) and the CB mutant (b and d). These images represent the fluorescence intensity (using a linear color gradient) as a function of time (vertical axis) and wavelength (horizontal axis); every vertical line represents a time trace of fluorescence at the corresponding wavelength, while every horizontal line reflects a fluorescence emission spectrum after a certain delay time. In panels a and b, C-Phycocyanin was selectively excited at 590 nm, and in panels c and d, Chls were selectively excited at 400 nm; all images presented here are background- and shading-corrected.

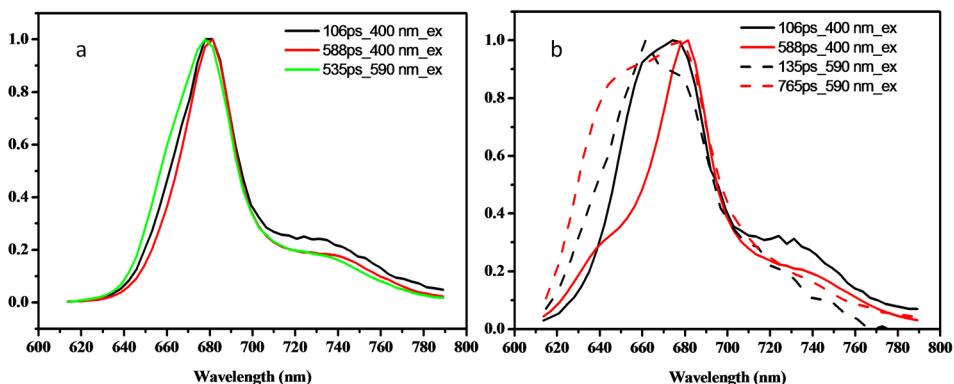
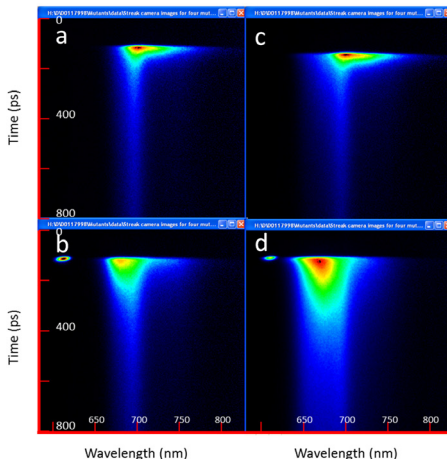


Figure S5.2: DAS of the slow components for excitation at 400 and 590 nm for the CK mutant (a) and for the CB mutant (b). All spectra are normalized at their maximum.

Target analysis

The target analysis presented in this work was performed in two steps: 1) a model was established without quenching to describe the non-quenched data, and ii) the

quenched data sets were fitting by using the model obtained in step 1) and including a quenching rate for one of the compartments.

In the first step, the two unquenched datasets obtained upon excitation at 400 nm and 590 nm were analysed globally. It was performed in almost the same way as was used for wild-type cells in our previous work (for details see (L. Tian et al 2011)) and its supporting information. In the present work, one extra restriction was made concerning the excitation input for branch i) and branch ii): the ratio R_{c1}/R_{c2} for these two values was considered to be the same for the two excitation wavelengths but was left free during the fitting. $C1$ and $C2$ represent the fractions of PBs that are linked to PSI and PSII, respectively. In the CK mutant, R_{c1}/R_{c2} is determined to be ~ 0.90 , while in the case of the CB mutant, it is about 0.87. Note that these values come with relatively big error bars which are not yet available in our fitting. Accurate values of R_{c1}/R_{c2} will require further experiments which are specially designed for this purpose.

During the second step, based on the results that were obtained in the first step data sets of quenched cells were analysed by adding an extra quenching rate to one of the pools. In this process, only a fraction of PBs was allowed to be

quenched, which is necessary for a good fitting. As an example, the full scheme of the model used for the CK mutant is shown in Figure S5.3. It is important to mention that the quenching site and quenching rate do not depend on R_{c1}/R_{c2} , since the quenching mainly occurs before reaching the photosystems as was also explained in (L. Tian et al 2012).

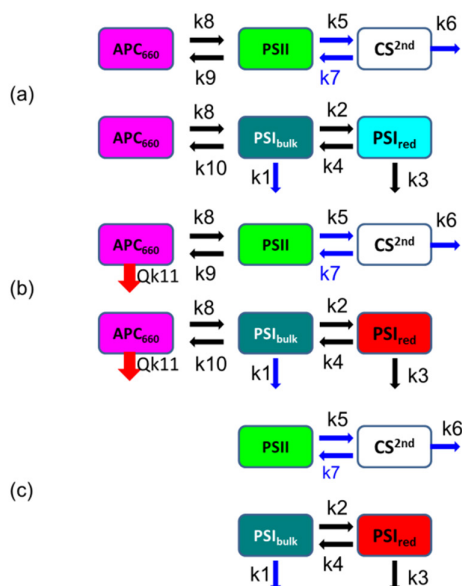


Figure S5.318: a full scheme for the CK mutant. Unquenched fraction of PBs (a), quenched fraction of PBs (b) and uncoupled Photosystems (c).

The fitting quality is visualized for selected decay traces at three different wavelengths in Figure S5.4.

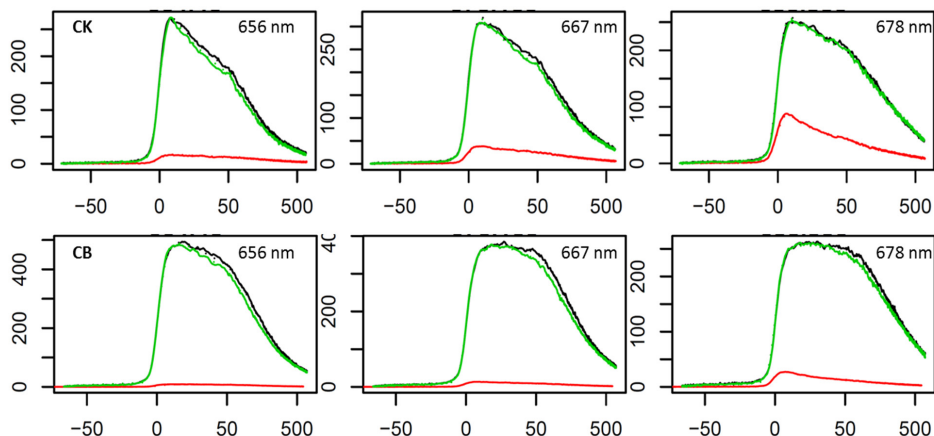


Figure S5.4: Decay traces at three different emission wavelengths are shown which are normalized to the amount of uncoupled PSI. Decay traces of unquenched cells upon 590 nm excitation (black), decay traces of quenched cells upon 590 nm excitation (green) and decay traces of unquenched cells upon 400 nm excitation (red). The target analysis fits are plotted in dots but are hardly visible because of the good fitting quality.

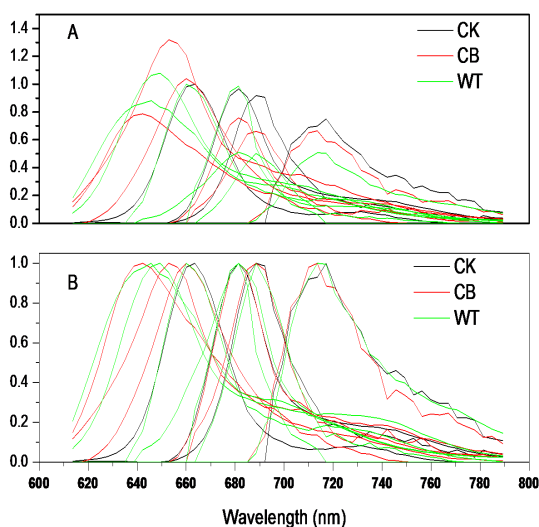


Figure S5.5: Three groups of SAS for CK and CB mutant cells (this work) and WT cells (L. Tian et al 2011); in A) each group of SAS was normalized in such a way that the APC660 spectrum had a value of one at 663 nm. In B) all spectra are normalized to one at their maxima, respectively. The two red-most groups of spectra, peaking around 690 and 715 nm are due to PSI and are nearly identical for the three types of cells. The same is true for the PSII SAS, peaking around 680 nm. More variation is obtained for the spectra corresponding to the chromophores in the PBs as discussed in the text.

Chapter 6

Summary and Discussion

General

The process of photosynthesis has been studied for centuries, but despite a large amount of progress, there are still many aspects that are not fully understood. An important part of the progress is the fact that many structures of photosynthetic complexes have been resolved ^{1,2} and these complexes have been studied separately in great detail, amongst other with ultrafast spectroscopic techniques. These studies allow to monitor excitation-energy transfer (EET) and charge separation (CS), the first crucial processes after the absorption of a photon. Many picosecond studies have also been performed *in vivo* in the past before the crystal structures were known, but due to an additional lack of knowledge about the organization and composition of the thylakoid membrane where most of the EET and CS processes take place, the obtained results were difficult to interpret. More recently, new interest has arisen in *in vivo* studies on photosynthetic organisms because a lot of molecular and organizational information has been obtained but also because the spectroscopic techniques have improved and mutants have become available that allow to study the effect of specific modifications in the organisms. This thesis focuses on the study of the light energy harvesting processes of photosynthetic complexes in cyanobacteria in general by using time-resolved fluorescence techniques, and with particular emphasis on the study of the protective process of non-photochemical quenching (NPQ) that is induced in the presence of high intensities of blue-green light. One of the important goals of researchers in the field of photosynthesis is to determine the photosynthetic efficiencies, to understand the underlying molecular mechanisms and to ultimately improve these efficiencies under certain conditions. In order to do so, one is forced to go down to the molecular level and to the picosecond time scale as is also pointed out in the introduction of this thesis. In the studies described in this thesis we have successfully combined spectrally-resolved, picosecond fluorescence measurements on wild-type and mutant cells of *Synechocystis* PCC 6803 with global and target data analysis, and a summary of the main findings is presented below.

PSII kinetics

Photosystem II (PSII) is considered to be the most important pigment-protein complex for oxygenic photosynthesis. It can use the sunlight energy as driving force to split water, to release oxygen and to transfer electrons to photosystem I (PSI). The excited-state kinetics of the core of PSII has frequently been studied over the past few decades but all studies were performed on the isolated PSII core complex, and it is not known how the PSII core performs *in vivo*. Moreover, a consensus on the interpretation of the fluorescence kinetics of PSII cores has not yet been reached. Some groups have claimed that the kinetics of PSII are trap-limited, which assumes excited-state equilibration between all chlorophylls to be much faster than the primary charge separation time, while others have reported that the kinetics are transfer-to-the-trap limited, which means that the energy transfer time from the antenna to the reaction center of Photosystem II where the charge separation takes place, dominates the overall trapping time.

In **Chapter 2**, we have performed *in vivo* picosecond time-resolved fluorescence measurements on the PAL mutant of *Synechocystis* PCC 6803 (a model cyanobacterium) that contains both PSI and PSII cores but no phycobilisomes (PBs), the natural light-harvesting complexes of cyanobacteria. By using the *in vivo* results on the BE mutant that is lacking both PSII and PBs it turns out to be possible to fully separate the PSI and PSII core kinetics for the PAL mutant *in vivo*. By performing target analysis, we can conclude that both the trap-limited model and the transfer-to-the-trap-limited model can describe the kinetics of the PSII core complex rather well whereas the kinetics turn out to be slightly slower *in vivo* as compared to the *in vitro* situation. We have also performed time-resolved fluorescence measurements on both mutants at 77K and the results confirm the results obtained at room temperature.

It is demonstrated that it is impossible to conclude which of the two models is correct, based on time-resolved fluorescence studies alone, but the results will help to remove existing controversies in future theoretical studies.

NPQ mechanism in cyanobacteria

As discussed by Melis et al³, the photosynthetic efficiency might be improved dramatically if the effect of the NPQ mechanism can be greatly reduced by truncating the antenna size. It is not clear to which extent this is also true for cyanobacteria because the amount of quenching that occurs due to NPQ seems to be independent of the amount absorption taking place in the photosynthetic system. Therefore, under certain growing conditions, the NPQ process might be overdone or maybe even redundant. In particular, this might be true in genetically modified versions of the cyanobacteria that are expected to be used in the future as new cellular plants for the production of chemicals and biofuels. In light of this aspect, a deep understanding of the NPQ mechanisms is important and will be useful for designing new organisms and growing conditions with optimal light-use efficiency. And there must certainly be space for improvement as already mentioned in the introduction of this thesis since the overall efficiency of photosynthesis is far below the theoretical maximum.

In **Chapter 3**, two of the most important questions regarding the photoprotective process of NPQ in cyanobacteria is being answered: What are the site and rate of NPQ in WT cells. Moreover, a partial answer is obtained for the question what the physical mechanism is, that is responsible for NPQ?

Different from plants and algae, the study on NPQ in cyanobacteria has only started recently. Kirilovsky and co-workers have demonstrated the importance of a PB-associated (i.e. not involving chlorophyll) thermal energy dissipation mechanism in the protection of cyanobacteria against light stress. This process is induced by the absorption of blue-green light by a soluble carotenoid protein, the orange-carotenoid protein OCP. In 2008, a very important step forward was made when it was shown that OCP can really act as the sensor of high light being a photoactive protein with an “active “red form⁴. The absorbance of light by OCP induces changes in the carotenoid and the protein, converting the dark stable OCP into a red unstable active form. The red form is accumulated and stabilized under conditions in which cyanobacteria need photoprotection: high light and cold.

However, the basic questions “where does the quenching exactly take place?”, “how fast/effective is the quenching?” and “what is the quenching mechanism?”

remained unanswered at that time. In this chapter, using spectrally-resolved, picosecond fluorescence we have studied intact cells of wild-type *Synechocystis sp. PCC 6803* and of mutants without and with extra OCP (Δ OCP and OverOCP) both in the unquenched and quenched state. With the use of target analysis we managed to spectrally resolve seven different pigment pools in the PBs and photosystems I and II, and to determine the rates of excitation energy transfer between them. In addition, the rates of charge separation and quenching could be resolved, all *in vivo*. It is revealed that upon OCP activation, one of the bilin chromophores in the APC core of the PB, here called APC_{660}^Q , becomes an effective quencher that prevents more than 80% of the excitations in the PB to reach Photosystems I and II. The quenching rate of its excited state turns out to be extremely fast, at least $(\sim 240 \pm 60 \text{ fs})^{-1}$. It is argued that the quenching is most likely caused by charge transfer between APC_{660}^Q and the OCP carotenoid hECN in its activated form, which is reminiscent of the quenching mechanism in *Arabidopsis* that was proposed by Prof. Graham R. Fleming and coworkers⁵. It can be excluded that the quenching is due to excitonic coupling between APC_{660}^Q and hECN, another mechanism that was proposed for non-photochemical quenching in plants⁶ and it is shown that it is unlikely that yet another quenching mechanism, excitation energy transfer to a carotenoid⁷ is responsible for the quenching in cyanobacteria.

In **Chapter 4**, two essential questions regarding the photoprotective process of non-photochemical quenching in cyanobacteria are answered: How does OCP-related non-photochemical quenching (site and rate) depend on the composition of the light-harvesting PBs of cyanobacteria and is the quenching mechanism of non-photochemical quenching for cyanobacteria *in vitro* the same as *in vivo*?

Interestingly, one important step in understanding the NPQ mechanism in cyanobacteria was made in 2011 by Gwizdala et al⁸. They showed that OCP, PBs and strong blue-green light are the only elements required to induce quenching by reconstitution of the NPQ process *in vitro*. In addition to our study as shown in **Chapter 3** the work in **Chapter 4** shows that the quenching takes place directly on the pigments of APC_{660} and the fast quenching rate indicates that the quenching is either caused by charge transfer between APC_{660}^Q and the OCP carotenoid or by

excitation energy transfer from APC_{660}^Q to the S_1 state of the carotenoid of OCP. Thus an important next step is to discriminate the latter two possibilities. However, experiments to answer this question are not easily feasible (if feasible at all) *in vivo*. Thus, *in vitro* studies seem to be a key approach to provide the answer to this question, preferably with PBs that are reduced in size in order to simplify the interpretation. However, it is mandatory to demonstrate that the quenching process is the same as *in vivo* for intact PBs. In this chapter, we managed to perform spectrally-resolved, picosecond fluorescence measurements on isolated PBs of different size, both in the quenched and the unquenched state. Two mutants were studied that both possess truncated light-harvesting antennae, PBs. One mutant called CK completely lacks the c_Phycocyanin (C_PC) rods. The other one (CB) is lacking both the intermediary and the core-distal C_PC hexamers. It is demonstrated that both the mechanism and the site of quenching are the same *in vitro* and *in vivo* in all systems, whereas the rate of quenching increases, going from the smallest *in vitro* system to the full-size *in vivo* system. The fastest rate seems to be essential to obtain optimal quenching *in vivo*.

In **Chapter 5**, we have studied the picosecond time-resolved fluorescence of two mutant cells of *Synechocystis*. PCC 6803 both with and without inducing NPQ. We successfully extend our previous conclusion about the NPQ mechanism to both CK and CB mutants *in vivo*. It is demonstrated that both the mechanism and the site of quenching remain the same in all systems studied.

Isolated PBs obtained from these mutant cells have been studied before and by using a large excess of the orange carotenoid protein (OCP) the quenching process was studied *in vitro* (Gwizdala et al. 2011 & **Chapter 4**)^{8,9}. Rates of EET and quenching were determined and it was found that the quenching occurs at the level of APC_{660} and not APC_{680} , identical to the situation for wild-type PBs. The amount of quenching for isolated PBs was very large, namely 85%. However, earlier *in vivo* studies on the CK mutant had shown that the amount of quenching was less than 10%. Despite this large “discrepancy”, it is demonstrated in this chapter that the *in vivo* and *in vitro* results on the quenched and unquenched PBs are fully consistent with each other. This is of relevance because it justifies studying isolated truncated PBs in the future in order to unravel the physical

mechanism that underlies NPQ *in vivo*. On the other hand it also provides valuable rate constants for EET and NPQ in whole cells that can be used to model photosynthesis in cyanobacteria (systems biology approach) and mutants thereof, like CK and CB.

Samenvatting

Algemeen

Het fotosynthese proces wordt al eeuwenlang onderzocht, maar ondanks een grote vooruitgang zijn er nog steeds vele aspecten die niet volledig worden begrepen. Een belangrijk deel van de vooruitgang heeft te maken met het feit dat veel structuren van fotosynthetische complexen opgelost zijn ^{1,2} en deze complexen afzonderlijk in detail werden onderzocht, onder andere met ultrasnelle spectroscopische technieken. Deze studies maken het mogelijk excitatie-energie-overdracht (EET) en ladingsscheiding (CS), de eerste cruciale processen na de absorptie van een foton, te volgen. Veel picoseconde studies zijn in het verleden *in vivo* uitgevoerd voordat de kristalstructuren bekend waren, maar door een additioneel gebrek aan kennis over de organisatie en de samenstelling van het thylakoïde membraan, waar de meeste EET en CS processen plaatsvinden, waren de verkregen resultaten moeilijk te interpreteren. Meer recent is nieuwe belangstelling ontstaan in *in vivo* studies van fotosynthetische organismen omdat veel moleculaire en organisatorische informatie beschikbaar is gekomen, maar ook omdat de spectroscopische technieken zijn verbeterd en mutanten beschikbaar zijn gekomen waarmee het mogelijk is geworden de effecten te bestuderen van specifieke wijzigingen in de organismen. In dit proefschrift ligt de focus op de bestudering met tijdsopgeloste fluorescentie technieken van processen waarbij licht ingevangen wordt door fotosynthetische complexen in cyanobacteriën met bijzondere nadruk op de bestudering van niet-fotochemische 'quenching' (NPQ), het beschermingsproces dat wordt geïnduceerd in aanwezigheid van een hoge intensiteit van blauw-groen licht. Één van de belangrijkste doelen van onderzoek op het gebied van fotosynthese is het bepalen van de efficiëntie van fotosynthetische processen, het begrijpen van de onderliggende moleculaire mechanismen, en uiteindelijk het verbeteren van die efficiëntie onder bepaalde condities. Om dit te kunnen doen, is men gedwongen in te zoomen tot het moleculaire niveau en tot de picoseconde tijdschaal zoals ook uiteen is gezet in de inleiding van dit proefschrift. In de studies beschreven in dit proefschrift hebben we met succes spectraal-opgeloste

picoseconde fluorescentie metingen aan wild-type en mutantcellen van *Synechocystis* PCC 6803 gecombineerd met zogeheten 'global' en 'target' data-analyse en een samenvatting van de belangrijkste bevindingen hieronder is weergegeven.

PSII kinetiek

Fotosysteem II (PSII) wordt beschouwd als het belangrijkste pigment-eiwitcomplex voor oxygene fotosynthese. Het kan de energie van het zonlicht gebruiken als drijvende kracht om water te splitsen, om zuurstof vrij te laten komen en elektronen over te dragen aan fotosysteem I (PSI). De kinetiek van de aangeslagen toestand van de PSII 'core' is vaak bestudeerd in de afgelopen decennia, maar alle studies werden uitgevoerd aan het geïsoleerde PSII core complex, en het is niet bekend hoe de PSII core *in vivo* functioneert. Bovendien is er nog geen consensus bereikt over de interpretatie van de fluorescentie kinetiek van de PSII core. Sommige groepen hebben beweerd dat de kinetiek van PSII 'trap'-gelimiteerd is ('trap' is ladingsgescheiden toestand), hetgeen veronderstelt dat de equilibratie van de aangeslagen toestand tussen alle chlorofyllen veel sneller is dan de tijdsduur van de primaire ladingsscheiding. Anderen daarentegen hebben gerapporteerd dat de kinetiek van PSII 'transfer-to-the-trap' gelimiteerd is, hetgeen betekent dat de energie-overdracht van de antenne naar het reactiecentrum van PSII, waar de ladingsscheiding plaatsvindt, de totale 'trapping'-tijd domineert.

In **hoofdstuk 2** hebben we *in vivo* picoseconde tijdsopgeloste fluorescentie metingen uitgevoerd aan de PAL-mutant van *Synechocystis* PCC 6803 (een model cyanobacterie) dat zowel de PSI als PSII core bevat, maar geen phycobilisomen (PBS), de natuurlijke licht-vergarende complexen van cyanobacteriën. Door de *in vivo* resultaten te gebruiken voor de BE mutant, waarin zowel PSII als PBS ontbreken, blijkt het mogelijk de kinetiek van de PSI en PSII cores van de PAL mutant *in vivo* volledig te scheiden van elkaar. Gebruikmakend van target-analyse, kunnen we concluderen dat zowel met het trap-gelimiteerde model als met het transfer-to-the-trap-gelimiteerde model de kinetiek van de PSII core vrij goed beschreven kan worden, terwijl de kinetiek *in vivo* iets trager blijkt te zijn in

vergelijking met de *in vitro* situatie. Wij hebben eveneens tijdsopgeloste fluorescentie metingen uitgevoerd aan beide mutanten bij 77K en de resultaten bevestigen de resultaten verkregen bij kamertemperatuur.

Het is aangetoond dat het onmogelijk is om te concluderen welke van de twee modellen correct is, op basis van tijdsopgeloste fluorescentie studies alleen, maar de resultaten zullen helpen om de bestaande controverses weg te nemen in toekomstige theoretische studies.

NPQ mechanisme in cyanobacteriën

Zoals bediscussieerd door Melis et al.³, zou de fotosynthetische efficiëntie aanzienlijk kunnen worden verbeterd wanneer het effect van het NPQ mechanisme sterk kan worden verminderd door het reduceren van de antennegrootte. Het is niet duidelijk in hoeverre dit ook geldt voor cyanobacteriën omdat de hoeveelheid “quenching” die ontstaat ten gevolge van NPQ onafhankelijk lijkt van de hoeveelheid absorptie die plaatsvindt in het fotosynthesesysteem. Daarom zou, onder bepaalde groeiomstandigheden, het NPQ-proces ‘overdreven’ kunnen zijn of misschien zelfs overbodig. Met name kan dit het geval zijn in genetisch gemodificeerde exemplaren van de cyanobacteriën die naar verwachting zullen worden gebruikt in de toekomst als nieuwe cellulaire ‘fabriekjes’ voor de productie van chemicaliën en biobrandstoffen. In het licht van dit aspect, is een volledig begrip van de NPQ-mechanismen belangrijk en zal ‘t nuttig zijn voor het ontwerpen van nieuwe organismen en groeiomstandigheden waarbij een optimale efficiëntie van het lichtgebruik bereikt wordt. Er moet zeker ruimte zijn voor verbetering, zoals reeds vermeld in de inleiding van dit proefschrift, aangezien de algehele efficiëntie van fotosynthese ver onder het theoretisch maximum ligt.

In **hoofdstuk 3** worden twee van de belangrijkste vragen met betrekking tot het fotobeschermingsproces NPQ in cyanobacteriën beantwoord: Wat zijn de locatie en de snelheid van NPQ in WT cellen? Een gedeeltelijk antwoord wordt verkregen op de vraag wat het fysisch mechanisme is, dat verantwoordelijk is voor NPQ?

In tegenstelling tot wat het geval is voor planten en algen, is de studie naar NPQ in cyanobacteriën pas kort geleden begonnen. Kirilovsky en medewerkers hebben

het belang aangetoond van een PB-geassocieerd (dat wil zeggen geen betrokkenheid van chlorofyl) thermische energiedissipatie mechanisme bij de bescherming van cyanobacteriën tegen lichtstress. Dit proces wordt veroorzaakt door de absorptie van blauw-groen licht door een oplosbaar carotenoïde-eiwit, het oranje-carotenoïde eiwit (OCP). In 2008 werd een zeer belangrijke stap voorwaarts gezet toen werd aangetoond dat OCP werkelijk kan optreden als de sensor van hoge lichtintensiteit, zijnde een fotoactief eiwit met een "actieve" rode vorm⁴. De absorptie van licht door OCP induceert veranderingen in de carotenoïde en het eiwit, waarbij het in het donker stabiele OCP omgezet wordt in een rode, instabiele actieve vorm. De rode vorm wordt geaccumuleerd en gestabiliseerd onder omstandigheden waarbij voor cyanobacteriën fotoprotectie noodzakelijk is: hoge lichtintensiteit en lage temperatuur.

Echter, de fundamentele vragen "waar vindt de quenching precies plaats?", "hoe snel/effectief is de quenching?", en "wat is het quenching-mechanisme?" bleven onbeantwoord op dat moment. In dit hoofdstuk hebben we, met behulp van spectraal-opgeloste picoseconde fluorescentie intacte cellen bestudeerd van wild-type *Synechocystis sp. PCC 6803* en van mutanten zonder en met extra OCP (Δ OCP en OverOCP) zowel in de niet-gequenchte als in de gequenchte toestand. Met gebruikmaking van target-analyse zijn we erin geslaagd om zeven verschillende pigment 'pools' in de PBS, PSI en PSII spectraal op te lossen, en de snelheden van excitatie-energie-overdracht tussen hen vast te stellen. Bovendien konden de snelheden van ladingsscheiding en quenching worden opgelost, alle *in vivo*. Het is aangetoond dat bij activatie van OCP, een van de bilin chromoforen in de APC core van PBs, hier APC_{660}^Q genoemd, een effectieve quencher is die voor meer dan 80% van de excitaties in de phycobilisoom voorkomt PSI en II te bereiken. De snelheid van quenching van de aangeslagen toestand blijkt zeer hoog, ten minste $(\sim 240 \pm 60\text{fs})^{-1}$. De oorzaak achter de quenching wordt de ladingsoverdracht tussen APC_{660}^Q en het OCP carotenoïde hECN in zijn geactiveerde vorm verondersteld te zijn, hetgeen doet denken aan het quenchingmechanisme in het plantje *Arabidopsis* hetgeen is voorgesteld door Prof. Graham R. Fleming en medewerkers⁵. Het kan worden uitgesloten dat quenching wordt veroorzaakt door exciton-koppeling tussen APC_{660}^Q en hECN, een ander mechanisme dat voor

NPQ in planten werd voorgesteld⁶ en het is aangetoond dat het onwaarschijnlijk is dat nog een ander quenchingmechanisme, excitatie-energie-overdracht naar een carotenoïde⁷ verantwoordelijk is voor de quenching in cyanobacteriën.

In **hoofdstuk 4** worden twee essentiële vragen over het NPQ-proces in cyanobacteriën beantwoord: Hoe hangt de OCP-gerelateerde NPQ (locatie en snelheid) af van de samenstelling van de licht-vergarende PBs van cyanobacteriën, en is het quenchingmechanisme van NPQ voor cyanobacteriën *in vitro* hetzelfde als *in vivo*?

Een belangrijke stap in het begrijpen van het NPQ-mechanisme in cyanobacteriën is gemaakt in 2011 door Gwizdala en medewerkers⁸. Middels reconstitutie van het NPQ-proces *in vitro* toonden zij aan dat OCP, PBs en sterk blauw-groen licht de enige noodzakelijke elementen zijn om quenching te induceren. Naast onze studie beschreven in **hoofdstuk 3** laat het werk in **hoofdstuk 4** zien dat de quenching direct plaatsvindt op de pigmenten van APC₆₆₀ en de hoge quenchingssnelheid geeft aan dat de quenching ofwel door ladingsoverdracht tussen APC₆₆₀^Q en de OCP-carotenoïde, of excitatie-energie-overdracht van APC₆₆₀^Q naar de S₁ toestand van de OCP-carotenoïde wordt veroorzaakt. Dus een belangrijke volgende stap is om de laatste twee mogelijkheden te onderscheiden. Echter, experimenten om deze vraag te beantwoorden zijn niet makkelijk haalbaar (zo niet helemaal onhaalbaar) *in vivo*. Dus lijken *in vitro* studies een sleutelbenadering om een antwoord te krijgen op deze vraag, bij voorkeur met PBs die qua afmeting verkleind zijn om zo de interpretatie te vereenvoudigen. Het is echter een eerste vereiste aan te tonen dat het quenchingsproces hetzelfde is als *in vivo* voor intacte PBs. In dit hoofdstuk zijn we erin geslaagd om spectraal-opgeloste, picoseconde fluorescentie metingen uit te voeren aan geïsoleerde PBs van verschillende grootte, zowel in de gequenchte als in de niet-gequenchte toestand. Beide mutanten hebben verkleinde licht-vergarende antennes, PBs. Één mutant, CK genoemd, mist volledig de staafvormige c_Phycocyanin (C_PC) eiwitcomplexen. In de andere mutant (CB) ontbreekt naast de middelste ook de meest van de APC-core verwijderde C_PC hexameer. Het is aangetoond dat zowel het mechanisme als de locatie van de quenching dezelfde zijn *in vitro* en *in vivo* in alle bestudeerde systemen, terwijl de quenchingssnelheid toeneemt, gaande van het kleinste *in*

vitro systeem naar het volledige *in vivo* systeem. De hoge snelheid lijkt essentieel ten einde optimale quenching te verkrijgen *in vivo*.

In **hoofdstuk 5** hebben we de picoseconde fluorescentie bestudeerd van twee mutantcellen van *Synechocystis. PCC 6803* zowel met als zonder het induceren van NPQ. Wij hebben met succes onze eerdere conclusie over het NPQ-mechanisme weten uit te breiden richting CK en CB mutanten *in vivo*. Het is aangetoond dat zowel het mechanisme als de locatie van quenching gelijk blijven in alle onderzochte systemen.

Geïsoleerde PBs verkregen uit deze mutantcellen zijn al eerder onderzocht, en gebruikmakend van een grote overmaat OCP werd het quenchingsproces bestudeerd *in vitro* (Gwizdala et al., 2011 en hoofdstuk 4)^{8,9}. Snelheden van EET en quenching werden bepaald en het bleek dat de quenching plaatsvindt op het niveau van APC₆₆₀ en niet APC₆₈₀, identiek aan de situatie voor wild-type PBs. De hoeveelheid quenching voor geïsoleerde PBs was erg groot, namelijk 85%. Echter, eerdere *in vivo* studies van de CK mutant hadden aangetoond dat de hoeveelheid quenching minder dan 10% was. Ondanks deze grote "discrepantie" wordt in dit hoofdstuk aangetoond dat de *in vivo* en *in vitro* resultaten van de gequenchte en niet-gequenchte PBs volledig met elkaar in overeenstemming zijn. Dit is relevant omdat het toekomstige studies van verkleinde PBs rechtvaardigt teneinde het fysische mechanisme te ontrafelen dat ten grondslag ligt aan NPQ *in vivo*. Anderzijds biedt het ook waardevolle snelheidsconstanten voor EET en NPQ in intacte cellen die kunnen worden gebruikt om een model te ontwikkelen voor de fotosynthese in cyanobacteriën (systeembioologische benadering) en mutanten daarvan, zoals CK en CB.

Reverences

- (1) Jordan, P.; Fromme, P.; Witt, H. T.; Klukas, O.; Saenger, W.; Krauss, N. *Nature* **2001**, *411*, 909-917.
- (2) Umena, Y.; Kawakami, K.; Shen, J. R.; Kamiya, N. *Nature* **2011**, *473*, 55-60.
- (3) Melis, A. *Plant Sci* **2009**, *177*, 272-280.
- (4) Wilson, A.; Punginelli, C.; Gall, A.; Bonetti, C.; Alexandre, M.; Routaboul, J. M.; Kerfeld, C. A.; van Grondelle, R.; Robert, B.; Kennis, J. T.; Kirilovsky, D. *Proceedings of the National Academy of Sciences of the United States of America* **2008**, *105*, 12075-12080.

- (5) Holt, N. E.; Zigmantas, D.; Valkunas, L.; Li, X. P.; Niyogi, K. K.; Fleming, G. R. *Science* **2005**, *307*, 433-436.
- (6) Bode, S.; Quentmeier, C. C.; Liao, P. N.; Hafi, N.; Barros, T.; Wilk, L.; Bittner, F.; Walla, P. J. *Proceedings of the National Academy of Sciences of the United States of America* **2009**, *106*, 12311-12316.
- (7) Ruban, A. V.; Berera, R.; Iliaia, C.; van Stokkum, I. H.; Kennis, J. T.; Pascal, A. A.; van Amerongen, H.; Robert, B.; Horton, P.; van Grondelle, R. *Nature* **2007**, *450*, 575-578.
- (8) Gwizdala, M.; Wilson, A.; Kirilovsky, D. *Plant Cell* **2011**, *23*, 2631-2643.
- (9) Tian, L.; Gwizdala, M.; van Stokkum, Ivo H. M.; Koehorst, Rob B. M.; Kirilovsky, D.; van Amerongen, H. *Biophysical Journal* **2012**, *102*, 1692-1700.

Publications

Volha. V. Chukhutsina, [Lijin Tian](#), Ghada. Ajlani, and H. van Amerongen (2010). Time-Resolved Fluorescence of Photosystem I in vivo: Global and Target Analysis. Proceedings of the 15th International Congress on Photosynthesis August 22-27, 2010 Beijing, China

[Lijin Tian](#), Ivo H. M. van Stokkum, Rob B. M. Koehorst, Aniek Jongerius, Diana Kirilovsky, and Herbert van Amerongen (2011). Site, Rate, and Mechanism of Photoprotective Quenching in Cyanobacteria. *Journal of the American Chemical Society* 133 (45), 18304-18311.

[Lijin Tian](#), Michal Gwizdala, Ivo H. M. van Stokkum, Rob B. M. Koehorst, Diana Kirilovsky, and Herbert van Amerongen (2012). Picosecond Kinetics of Light Harvesting and Photoprotective Quenching in Wild-Type and Mutant Phycobilisomes Isolated from the Cyanobacterium *Synechocystis* PCC 6803. *Biophysical Journal*. 102(7), 1692-1700.

Ron Gill, [Lijin Tian](#), Walter R. C. Somerville, Eric C. Le Ru, Herbert van Amerongen, and Vinod Subramaniam (2012). Silver Nanoparticle Aggregates as Highly Efficient Plasmonic Antennas for Fluorescence Enhancement. *The Journal of Physical Chemistry C* 116 (31), 16687-16693

[Lijin Tian](#), Shazia Farooq and Herbert van Amerongen (2012). Probing the Picosecond kinetics of the Photosystem II Core Complex in vivo. *Phys. Chem. Chem. Phys.*, 2013, **15**, 3146-3154.

[Lijin Tian](#), Ivo H.M. van Stokkum, Rob B.M. Koehorst and Herbert van Amerongen (2012). Light Harvesting and Blue-green Light Induced Non-Photochemical Quenching in Two Different c-Phycocyanin Mutants of *Synechocystis* PCC 6803. *Journal of the Physical Chemistry B*, Article ASAP.

Ron Gill*, [Lijin Tian](#) , Herbert van Amerongen, Vinod Subramaniam (2013), Emission enhancement and lifetime modification of phosphorescence on silver nanoparticle aggregates, Submitted.

Others:

Yajuan Sun, Yue Chen, [Lijin Tian](#) ,Yi. Yu, Xianggui Kong, Qinghui. Zeng, Youlin Zhang, and Hong Zhang (2007). Morphology Dependent Upconversion Luminescence of ZnO:Er³⁺ Nanocrystals. *J. Luminescence* 128 (15)

[Lijin Tian](#), Yajuan Sun, Yi Yu, Xianggui Kong, and Hong Zhang (2008). Surface effect of nano-phosphors studied by time-resolved spectroscopy of Ce³⁺. *Chemical Physics Letters*, 452(1-3), 188-192.

Junwei Zhao, Yajuan Sun, Xianggui Kong, [Lijin Tian](#), Yu Wang, Langping Tu and Hong Zhang (2008). Controlled Synthesis, Formation Mechanism and Great Enhancement of Red Upconversion Luminescence of NaYF₄:Yb³⁺, Er³⁺ Nanocrystals/Sub-microplates at Low Doping Level, *J. Phys. Chem. B* 112 15666-15672.

Yajuan Sun, Yue Chen, [Lijin Tian](#) , Yi Yu , Xianggui Kong , Junwei Zhao, and Hong Zhang(2008). Controlled Synthesis and Morphology Dependent Upconversion Luminescence of NaYF₄:Yb, Er nanocrystals (2008). *NANOTECHNOLOGY* 18 (27)

Kai Song, [Lijin Tian](#), Xianggui Kong, Kai Liu, Qinbin Zhang, Chuang Du, Yajuan Sun, Xiaomin Liu (2010). Preparation, Characterization and Specific Biological Labeling of Silica Coated Up-conversion Fluorescent Nanocrystals[J]. *Spectroscopy and Spectral Analysis*, 30 (1): 133-136.

Acknowledgements

At the end of this thesis it is my great pleasure to express my sincere thanks to the following people for their teaching, their encouragement, their massive help and their sincere friendships.

To my supervisor, Herbert, an excellent supervisor. When I look back, I am surprised that almost all of your ideas and opinions turned out to be great and correct. That makes a PhD study a lot easier. Thank you very much for directing me to walk around many difficulties that I have encountered during the research and thank you very much for your great patience in correcting or modifying my manuscripts and this thesis many times. It was a great pleasure to work with you.

To my coworkers, Dr. Diana Krilovsky, Dr. Michal Gwizdala, Dr. Ghada Ajlani, thank you very much for providing me with the beautiful cells and nice samples, and thank you for the fruitful discussions. I feel very proud that I had the pleasure of working with you.

To Ivo, Joris and Sergey, thanks to all of you for teaching me how to perform the data analysis by using the software developed by you; without your help it would not have been possible to build the models in this thesis. Thank you very much.

To Rob, you have always been the first one I came to if there was any problem with the setups, with the data, and you were always willing to help, to share your experience and to provide solutions. You helped me a lot in designing the measurements, in performing data analysis and in drawing the publishable figures and in writing. Thank you very much.

To Arie, Jan Willem and Arjen, thanks for all your great technical support in the laser lab.

To Cor, for your help in culturing the cells and many useful discussions.

To Caner, Olga, Tünde, Shazia, Fugui, Evgenia, Daan, Alena, and Shanthi, it is my great pleasure to work with you guys, thank you very much for all the help that you have provided. I really miss the time that we had together in Wageningen.

To Netty, thank you very much for all your help.

To Johannes, John, Henk, Frank, Elena, Folket, Elena, Ruud, Dane, Pieter and Edo, Thank you for sharing your nice stories during the coffee break, and thank you for your help.

谢谢众多的中国朋友，包括在瓦村的，郭军利&王俊有;秦音&肖英华;宋颜如;程旭;李鹤群;王思;杨婷&刘庆;化辰雷;宋春旭,覃伟,孙研研,李涛等。在荷兰的,卢希峰&苏爱春,黄慧艳&刘怀峰,徐朋奇,朱井义&孙晓蕾等;在中国的,芦晶,李媛,聂海胜,曹庆琴,宁雷,莫海珍,杨冬英,卢玉,刘畅,等。还有在国外的,罗静&高然,张楠,等。“海内存知己,天涯若比邻”,感谢大家,愿我们的友谊长存。

And in the end,

To my families, 感谢爸爸妈妈给予的无私的支持.

感谢我亲爱的妻子,肇颖,谢谢你在艰苦日子中的默默付出和不间断的鼓励,让我们永远相伴.

Curriculum Vitae

My name is Lijin Tian. I was born on the 8th of June in 1983, in a small but beautiful village in Shandong province, China. From 2001 to 2005, I studied Applied Physics at the Shandong University of Science and Technology. In 2005, I went to the Changchun Institute of Optics, Fine Mechanics and Physics, Chinese Academy of Sciences, “the cradle of China’s Optics”. I have spent there about four years and studied solid state physics. During the four years, I have worked on upconverting nanophosphors, and started to get familiar with spectroscopic techniques. In 2007, I went to the Van ’t Hoff institute in Amsterdam as a visiting student, and after that I decided to come to the Netherlands to continue my PhD study. In 2009, back in the Netherlands at the University of Wageningen, I started my PhD project under the supervision of Prof. Herbert van Amerongen, and stepped into the fascinating research field of photosynthesis. In 2013, I have finished my thesis and I defend my thesis on 8th May in the same year.

Education Statement of the Graduate School		The Graduate School
Experimental Plant Sciences		EXPERIMENTAL PLANT SCIENCES
Issued to: Lijin Tian Date: 8 May 2013 Group: Biophysics, Wageningen University and Research Centre		
1) Start-up phase	<u>date</u>	
► First presentation of your project		
"Blue light induced NPQ in cyanobacteria"	Nov 02, 2009	
► Writing or rewriting a project proposal		
The primary events in photosynthesis studied with picosecond (micro)spectroscopy. In vitro and in vivo measurements in the presence and absence of abiotic stress	Apr 02, 2009	
► Writing a review or book chapter		
► MSc courses		
Spectroscopy	Sep 2009	
► Laboratory use of isotopes		
Subtotal Start-up Phase	9.5 credits*	
2) Scientific Exposure	<u>date</u>	
► EPS PhD Student Days		
EPS PhD student day, Utrecht University	Jun 01, 2010	
EPS PhD student day, Wageningen University	May 20, 2011	
► EPS Theme Symposia		
Annual EPS Theme Meeting Theme 3: Metabolism and Adaptation, Wageningen University	Feb 10, 2011	
Annual EPS Theme Meeting Theme 3: Metabolism and Adaptation, University of Amsterdam	Mar 22, 2013	
► NWO Lunteren days and other National Platforms		
Dutch Meeting on Molecular and Cellular Biophysics, Veldhoven	Sep 28-29, 2009	
Scientific meeting on chemistry related to physics & Material sciences	Feb 15-16, 2010	
Dutch Meeting on Molecular and Cellular Biophysics, Veldhoven	Oct 04-05, 2010	
Dutch Meeting on Molecular and Cellular Biophysics, Veldhoven	Oct 01-02, 2012	
► Seminars (series), workshops and symposia		
The more you see: spectroscopy in molecular biophysics, farewell symposium Marcus Hemminga	Sep 24, 2009	
Symposium 'Photosynthesis: from Femto to Peta and from Nano to Global'	Nov 05, 2009	
Laser life and biophotonics, VU University, Amsterdam	Oct 10, 2010	
workshop Photosynthesis in Venice (Italy)	Sep 20-21, 2010	
workshop Photosynthesis in Passau (Austria)	Apr 06-10, 2011	
► Seminar plus		
► International symposia and congresses		
Harvest EU meeting - Kick off, Naantali (Finland)	Nov 29-Dec 01, 2009	
Non-photochemical quenching, Tianjin (China)	Aug 18-22, 2010	
The 15th international photosynthesis conference, Beijing (China)	Aug 22-27, 2010	
Harvest EU meeting, Venice (Italy)	Sep 22-24, 2010	
The 17th International Biophysics Congress (IUPAB)	Oct 30-Nov 03, 2011	
► Presentations		
Poster: Dutch Meeting on Molecular and Cellular Biophysics, Veldhoven	Sep 28-29, 2009	
Poster: 15th international photosynthesis conference, Beijing (China)	Aug 22-27, 2010	
Poster: Dutch Meeting on Molecular and Cellular Biophysics	Oct 04-05, 2010	
Oral: Harvest EU meeting, Venice (Italy)	Sep 22-24, 2010	
Oral: Harvest EU meeting, Passau	Apr 06-10, 2011	
Oral: The 17th International Biophysics Congress (IUPAB)	Oct 30-Nov 03, 2011	
Poster: Dutch Meeting on Molecular and Cellular Biophysics, Veldhoven	Oct 01-02, 2012	
► IAB interview	Feb 18, 2011	
► Excursions		
Subtotal Scientific Exposure	20.2 credits*	
3) In-Depth Studies	<u>date</u>	
► EPS courses or other PhD courses		
BioSolarCells Winter School-The Artificial Leaf	Jan 30-Feb 02, 2012	
Tulip course_Holland Research School of Molecular Chemistry	Apr 10-13, 2012	
► Journal club		
member of a literature discussion group at Biophysics	2009 - 2013	
► Individual research training		
Subtotal In-Depth Studies	6.0 credits*	
4) Personal development	<u>date</u>	
► Skill training courses		
Scientific Writing	Jul 2010	
Scientific publishing	Nov 19, 2010	
Dutch language I	Apr 2010	
► Organisation of PhD students day, course or conference		
► Membership of Board, Committee or PhD council		
Subtotal Personal Development	4.5 credits*	
TOTAL NUMBER OF CREDIT POINTS*		40.2